Doctoral Dissertation

博士論文

Identification of a neural circuit controlling locomotion speed by regulating the phase delay between the movement of head and tail in Drosophila larvae

(ショウジョウバエ幼虫において頭尾の位相差の調節による運動速度制御を担う神経回路機構の解明)

A Dissertation Submitted for Degree of Doctor of Philosophy

December 2021

博士（理学）申請

令和 3 年 12 月

Department of Physics, Graduate School of Science,

The University of Tokyo

東京大学大学院理学系研究科物理学専攻

LIU, Yingtao

劉　英濤

Abstract

Locomotion speed is essential for animals' survival. To achieve the desired speed, animals regulate the locomotor cycle called stride by its duration and amplitude in terrestrial animals. It has been widely observed in terrestrial animals that a stride can be separated into two phases: a "variable phase" and an "invariable phase" in terms of their duration. The duration of the "variable phase" is mainly varied with speed while the duration of the "invariable phase" remains almost unchanged (e.g., in pedestrian animals, the duration of the stance phase varies primarily with changing speeds, while the duration of the swing phase is not much varied). However, how the central nervous system generates the variable motor output is less understood. This gap is due to the basic technical difficulty in recording and manipulating the component neurons in most animals. In this thesis, I investigated the neural mechanisms to modulate the motor output for the desired speed using *Drosophila melanogaster* larvae, a model animal with powerful genetic tools to target and manipulate the central neurons.

Larvae move by peristalsis, a type of movement widely used by legless animals defined as a sequential wave-like movement from one end to the other. Though the tools for neuroscience study have been well established in *Drosophila* larvae, it remains not well understood how the movement dynamics are changed with speed. This study aims: (1) to identify the kinematic parameters varied with speeds and the key muscular groups; (2) to identify the neural circuit that modulates the speed-dependent rhythm.

First, I analyzed the kinematics in larval locomotion to reveal the key parameters adapted to locomotion speed. I defined a stride as the period between consecutive unhooking moments and then divided each stride into two phases: the first portion named tail lag phase is a period from unhooking to the initiation of the peristaltic wave, and the second portion named wave phase is a period from the initiation of the wave to unhooking. I found that the tail lag and the wave duration vary differently with the speeds and the tail lag varies more. To reveal the muscular mechanism to control the tail lag, I analyzed the dynamics of muscle contraction during locomotion. As a result, a group of muscles perpendicular to the crawling direction, the lateral transverse muscles (LTM), were identified to contract together before a forward wave is initiated, with the relaxation of these muscles coinciding with the start of the wave. The greater the duration of the contraction of the LTM, the more the tail lags the initiation of the wave.

Next, I investigated the upstream central mechanisms and found that the interneurons A26f and A31c have significant functional roles in regulating the activity of LTM and the locomotion speed. A26f neurons, which are GABAergic premotor neurons providing most output to LTM, are coactivated across the segments of the ventral nerve cord at the initiation of the fictive forward locomotion to inhibit the LTM. A31c neurons, which are GABAergic second-order premotor neurons presynaptic with A26f neurons locally, burst synchronously at an earlier phase of the initiation of the fictive forward locomotion and are activated again when the wave-like pattern is initiated. Using perturbational analysis by optogenetic tools, I revealed that A31c and A26 neurons are required to regulate the activity of LTM during peristalsis. A31c neurons upregulate the contraction of LTM while A26f neurons downregulate. Furthermore,

A26f neurons play a significant function in regulating the appropriate tail lag as well as the locomotion speed.

In summary, this study revealed that: (1) by analyzing the kinematics of peristalsis and dividing a stride into tail lag phase and wave phase, the tail lag varies more with speed than the wave duration varies, (2) by analyzing the muscular contraction pattern, the lateral transverse muscular group contract together during the tail lag and their duration of contraction naturally depends on the tail lag thus the speed, and (3) by analyzing the upstream neural circuit, A31c-A26f system modulates the inhibitory input to LTM to regulate the tail lag and thereby the speed. These results suggest that *Drosophila* larvae use a speed control strategy shared in the animal kingdom that the duration is adjusted preferably in one phase but less in the other. The LTM is similar to the extensor muscles in pedestrian animals regarding their adaption to the variation of the "variable phase" (stance phase/tail lag phase). Because of the basic similarity in the structure of the kinematics and the adaption of muscular activity underlying the speed control in the animal kingdom, the revealed central mechanism that the modulation of inhibitory output regulates the duration of the "variable phase" may be generally identical across animals. Further work may be required to target and analyze the descending neuronal pathways to unravel the higher central mechanism of speed control, which is difficult to be accessed in most animals. In addition, as the co-contraction of transverse muscles and their role in speed regulation is first reported, this work advances the understanding of the mechanism behind the peristaltic movement.

List of Main Abbreviations

Abbreviation	Meaning
A	Anterior
A1-A9	Abdominal segment 1 – abdominal segment 9
AD	Activation domain
A-P	Anterior-posterior
BDSC	Bloomington Drosophila Stock Center
cho	Chordotonal
Chr2	Channelrhodopsin 2
CsCh	CsChrimson
CATMAID	Collaborative Annotation Toolkit for Massive Amounts of Image Data
CD4	Cluster of Differentiation 4
CNS	Central nervous system
CoM	Central of Mass
CPG	Central pattern generator
D	Dorsal

DBD	DNA binding domain
DL	Dorsal lateral
es	external sensory
EM	Electron microscopy
FAS2	Fasciclin 2
FLP	Flippase
FRT	Flippase recognition site
GFP	Green fluorescent protein
L	Lateral
LTM	Lateral transverse muscle
M	Medial
MCFO	MultiColor FlpOut
md	multidendritic
MN	Motor neuron
P	Posterior
PBS	Phosphate-buffered saline
Pcc	Pearson’s correlation coefficient
Psync	Posterior synchronous activity
ROI	Region of interest
SEG	Subesophageal ganglion
THRX	Thorax

T1-T3	Thoracic segment 1 – thoracic segment 3
UAS	Upstream activating sequence
V	Ventral
VL	Ventral lateral
VNC	Ventral nerve cord
yw	*yellow white*

Table of Contents

Chapter 1. Introduction

Locomotion speed is adapted to animals' requirements in the changing environment. To achieve the required speed, animals modulate the rhythm of motor output. Peristalsis, the sequential wave-like movement of body parts from one end to the other, is widely used by soft-bodied terrestrial animals for locomotion (Trimmer and Lin, 2014; Wigglesworth, 2012). However, little is known about how the rhythmic motor output is modulated in peristalsis for the required speed. I used *Drosophila* larvae, a model animal with powerful manipulation tools for studying neural circuits, to investigate the central neural control of the motor output at different speeds. In this chapter, I first review the studies regarding the speed-dependent modulation of motor output. Then I introduce the current understanding of speed control and the approaches to studying the neural circuit in *Drosophila* larvae. Finally, I present the purpose and the arrangement of this thesis.

1-1. Speed-dependent modulation of motor output

Changing speed is an essential skill for an animal's survival. Speed varies as a function of both the amplitude and the duration of a locomotor cycle, also known as a stride in terrestrial animals. When speeded up, the movement of body parts is not accelerated equally like playing a video in fast mode but is flexibly modulated. The locomotion rhythm changes as a function of speed. The underlying neural mechanism is still understudied.

A well-studied case is the change of kinematics with speeds in the locomotion of pedestrian animals. These animals move by means of alternating movement of opposing legs (Hooper, 2017), which naturally leads to the division of a locomotor cycle into stance and swing phases (Figure 1.1 A, B). It was well understood in human walking that the duration of the stance phase varies primarily with the changed speeds, while the duration of the swing phase varies less (Grillner et al., 1979). The variations can be quantified by analyzing the relationship between the speed and the stance duty factor, the proportion of the time spent in the stance phase in a stride. It was shown in a wide range of species, including insects, birds, mammals, and humans, that the stance duty factor decreased through the range of walking speed (DeAngelis et al., 2019; Frigon et al., 2014; Jacobson and Hollyday, 1982; Nirody et al., 2021). The stance duty factor can be changed abruptly when gait transition emerges. For example, the stance duty factor decreases slowly through the range of walking speed while dropping abruptly at the initiation of running in humans (Alexander, 1989). Gait transition is widely used by mammals (Maes and Abourachid, 2013). However, in insects, it was proposed that the variability of the stepping pattern lies on a continuous manifold without the abrupt change to a preferred locomotion gait (Ayali et al., 2015; DeAngelis et al., 2019).

The modulation of motor patterns is controlled by the central pattern generator (CPG), which is defined as an ensemble of neurons that can produce rhythmic outputs in the absence of rhythmic input (Marder and Bucher, 2001). The existence of CPG to generate the locomotion patterns was first identified in the insect ventral nerve cord (VNC) (Wilson, 1961), the analogous functional structure of the spinal cord in invertebrates, which was then identified in

the spinal cord of lamprey, amphibians, and cat (Squire, 2009). Currently, CPG is a core concept to explain the generation of rhythmic patterns.

Previous studies have revealed that some neural mechanisms modulate the speed-dependent motor outputs, though linking the flexible behavior with specific interneurons is still a difficult task. In insects, the understanding of the walking CPG is derived chiefly from the study of stick insects and cockroaches (Mantziaris et al., 2020). The non-spiking interneurons show an essential role in regulating the frequency of the rhythmic activity in leg motor neurons in the stick insects (Büschges, 1995). In vertebrates, the organization of the spinal neurons is conserved, which allows classifying the spinal neurons into several classes. Among those classes, dI6, V0, V1, V2, and V3 neurons are shown to control locomotion (Bellardita and Kiehn, 2015; Crone et al., 2009; Talpalar and Kiehn, 2010), where V1 and V2a interneurons are shown to be required for the regulation of the speed-specific locomotion patterns (Betley et al., 2009; Crone et al., 2009). For example, V2a interneuron subclasses are shown to be activated selectively to recruit different classes of motor neurons for the desired speeds in zebrafish (Ampatzis et al., 2014).

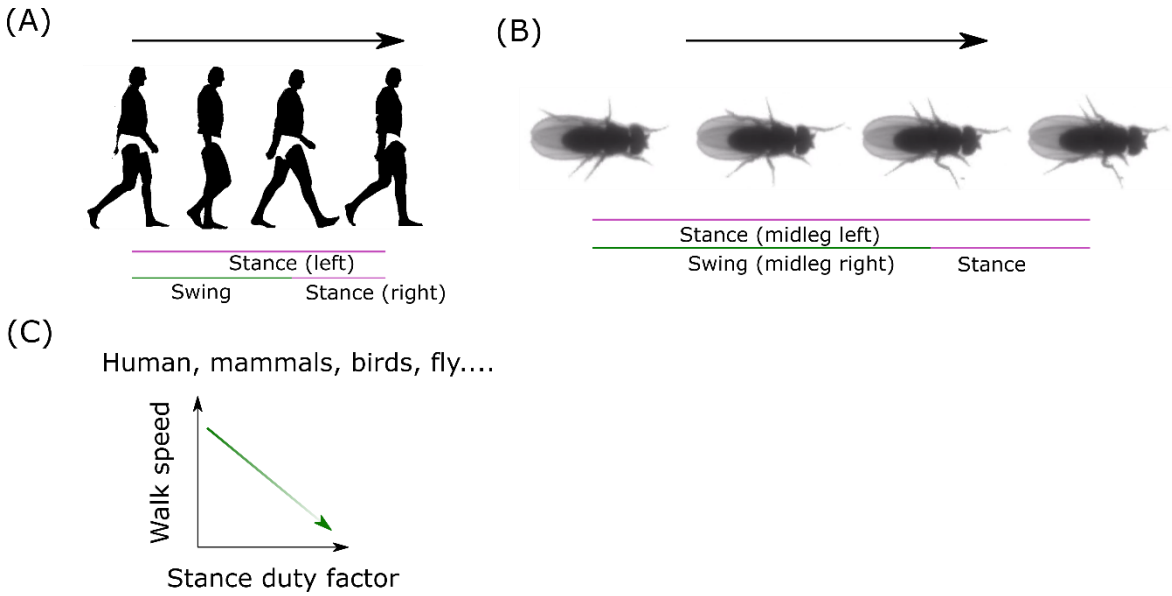

Figure 1.1 Speed-dependent modulation of the duration of stance phase.

(**A**) Schematic diagram of stance and swing phase in the human walk. (**B**) Schematic diagram of stance and swing phase in *Drosophila* walk. (**C**) The stance duty factor is increased with decreasing speed in pedestrian animals (DeAngelis et al., 2019; Frigon et al., 2014; Grillner et al., 1979; Jacobson and Hollyday, 1982; Nirody et al., 2021).

1-2. Behavioral and neural basis concerning speed modulation in *Drosophila* larvae

Considering the complexity of the nervous system and the difficulty in accessing the interneurons, it is a reasonable choice to use the model animal *Drosophila* to investigate the neural mechanism of the speed modulation since this animal has a small nervous system but a large collection of well-established genetic tools to target, record, and manipulate interneurons. In this section, I will introduce the behavioral and neural basis concerning speed modulation in the peristaltic movement of *Drosophila* larvae.

Locomotion is one of the most robust and quantifiable behaviors in *Drosophila* larvae. When locomotes on a flat surface, the larva executes a typical motor program that it crawls forward continuously for several locomotor cycles (strides) when switches to another behavior including turning, roaring, stopping, or backward crawling from time to time (Lahiri et al., 2011). The larva travels the most distance during the continuous forward crawling. For each forward stride, a contraction is initiated from the tail, and sequentially wave-like contraction is executed from posterior to anterior segments. This type of movement is called peristalsis (Figure 1.2 A). Though it is important to consider how the surrounding environment acts on the larval body during locomotion, there were few investigations of the mechanics of larval crawling, especially regarding the force between the larva and the interacting substrate due to the system being too small to be measured. In bigger soft-bodied animal caterpillars which show a similar anterior peristaltic wave for locomotion, investigations of the crawling mechanics have been carried out. Direct measurements of the reaction force from the ground to the caterpillar have shown that most positive reaction forces come from the stretching of anterior prolegs but

not the pushing from posterior prolegs during crawling (Lin and Trimmer, 2010). Their finding suggests that the substrate functions as the "external skeleton" to keep the body in tension to generate the stretching force for the movement of posterior prolegs.

Concerning the behavior consequences of varied speed in *Drosophila* larvae, previous studies have analyzed the kinematics at the organism or segment levels. At the organism level, the speed is dependent on the time and distance of a stride. Previous studies have reached different conclusions regarding the relationship between speed and the stride parameters (Aleman-Meza et al., 2015; Berrigan and Pepin, 1995; Heckscher et al., 2012). The speed has been found to be more correlated with stride length by Berrigan and Pepin, to be more correlated with stride duration by Heckscher et al., and to have a similar correlation with stride length and stride duration by Aleman-Meza et al. (Aleman-Meza et al., 2015; Berrigan and Pepin, 1995; Heckscher et al., 2012). As they used different experimental conditions, these inconsistent results may reflect that the distinct strategies were used to modulate the motor output for the desired speed according to the larval stage and the environment. The segmental kinematics have been characterized by Heckscher et al. in the first instar larvae (Heckscher et al., 2012). The intersegmental phase lag does not vary over arrange of stride period, which suggests that the larvae maintained a similar body form for different speeds (Heckscher et al., 2012). However, as their results were obtained from the crawling of the first instar larvae in a linear channel, it is unclear if their conclusion can be applied to the wandering third instar.

The muscular configuration and the anatomy of the nervous system have been analyzed in detail in *Drosophila* larvae. The animal has a body plan of three thoracic (T1 - T3) and nine abdominal segments (A1 - A9). Thirty somatic muscles are arranged in a stereotyped

pattern in most hemisegments (Sink, 2006). Somatic muscles can be named by the position (dorsal, ventral, lateral, or segmental boundary) and the orientation (longitudinal, transverse, oblique, or acute). Most dorsal and ventral muscles orient longitudinally or acutely/obliquely, whereas most lateral muscles orient transversely (Figure 1.2 B, C). Each hemisegment has about 43 somatic sensory neurons classified into external sensory (es) neurons, chordotonal (cho) neurons, and multidendritic (md) neurons (Bate and Arias, 1993). The ventral nerve cord (VNC, the analogous functional structure of the spinal cord in invertebrates) has a similar segmented structure corresponding to the body wall (neuromeres T1 - T3, A1 - A9). Each hemineuromere has about 40 motor neurons (Landgraf and Thor, 2006). Each motor neuron's morphology and muscular projection were characterized (Landgraf and Thor, 2006). Although the sensory neurons, the motor neurons, and the muscles have been targeted and analyzed at a single cell level, the interneurons of the VNC are less understood. Each hemineuromere has about 270 interneurons in the first instar (Rickert et al., 2011).

The muscular and motor neuron's activity have been analyzed during the forward peristalsis (Heckscher et al., 2012; Zarin et al., 2019). Heckscher et al. have analyzed the length change of dorsal longitudinal (DL) muscles, ventral longitudinal (VL) muscles, and lateral transverse (LT) muscles. When the first instar larva crawls forward in a linear channel, despite slight time differences between the activity of different muscle groups, the muscles are activated in a wave-like sequence from the posterior to anterior segments. A time lag about the duration of one intersegmental time lag of the wave-like sequence has been found between the contraction of the LT muscles and that of the longitudinal muscles of the same segment, which leads to the LT muscles and the longitudinal muscles of the adjacent anterior segment are contracted at a

similar time as a unit (Heckscher et al., 2012; Kohsaka et al., 2019). This motor pattern has been also identified in the isolated nerve cord of third instar larvae (Pulver et al., 2015). By expressing calcium sensors in the body wall muscles of second instar larvae restricted in a gel chamber to stabilize the larva during the peristalsis, it has been found that the 30 muscles of a hemisegment formed four coactivated muscular groups during the forward peristalsis (Figure 1.3 A; Zarin et al., 2019).

Regarding the neural control of locomotion speed, previous studies have analyzed the role of sensory feedback (Caldwell et al., 2003; Hughes and Thomas, 2007; Song et al., 2007; Vaadia et al., 2019), neuromodulation (Schützler et al., 2019), and interneurons (Kohsaka et al., 2014). Several sensory neurons (cho neurons and multiple subtypes of md neurons) have been identified as proprioceptors to be crucial for the generation of the normal rhythm of peristalses. Impairing their function can cause the slower rhythm of forward locomotion (Caldwell et al., 2003; Hughes and Thomas, 2007; Song et al., 2007). The activity of several proprioceptors have been characterized in crawling (Vaadia et al. 2019), which shows distinct dynamics (Figure 1.3 B). How the proprioceptive information is integrated to generate the desired locomotion rhythm remains unknown. It has been proposed that when a segment is contracted, the sensory feedback sends a “mission accomplished” signal to promote the relaxation for rapid movement (Hughes and Thomas, 2007). Regarding the role of neuromodulators, the amine neuromodulators octopamine/tyramine regulate the locomotion speed in the context of the nutritional state (Koon et al., 2010; Schützler et al., 2019). The octopaminergic motor neurons globally innervate somatic muscles (Monastirioti et al., 1995). They regulate the growth of the excitatory neuromuscular arbors to promote the electrical activity globally in somatic muscles in the

starvation state (Koon et al., 2010). On the other hand, when satiated, tyramine globally decreases the excitability of motor neurons to achieve a slower speed. For most interneurons, the functional role is still mysterious. A group of inhibitory neurons, Period-positive Median Segmental Interneurons (PMSIs), have been proposed to control locomotion speed by adjusting the intersegmental delay of peristaltic waves (Kohsaka et al., 2014). PMSIs are primarily inhibitory premotor neurons, which are activated after the motor neuronal activity. The inhibitory outputs are required to promote rapid movement by relaxing the muscles at the proper timing following the contraction. Their work reveals that the phase duration can be controlled by modulating the inhibitory input to the motor neurons, which might be a general principle for the generation of desired stride duration.

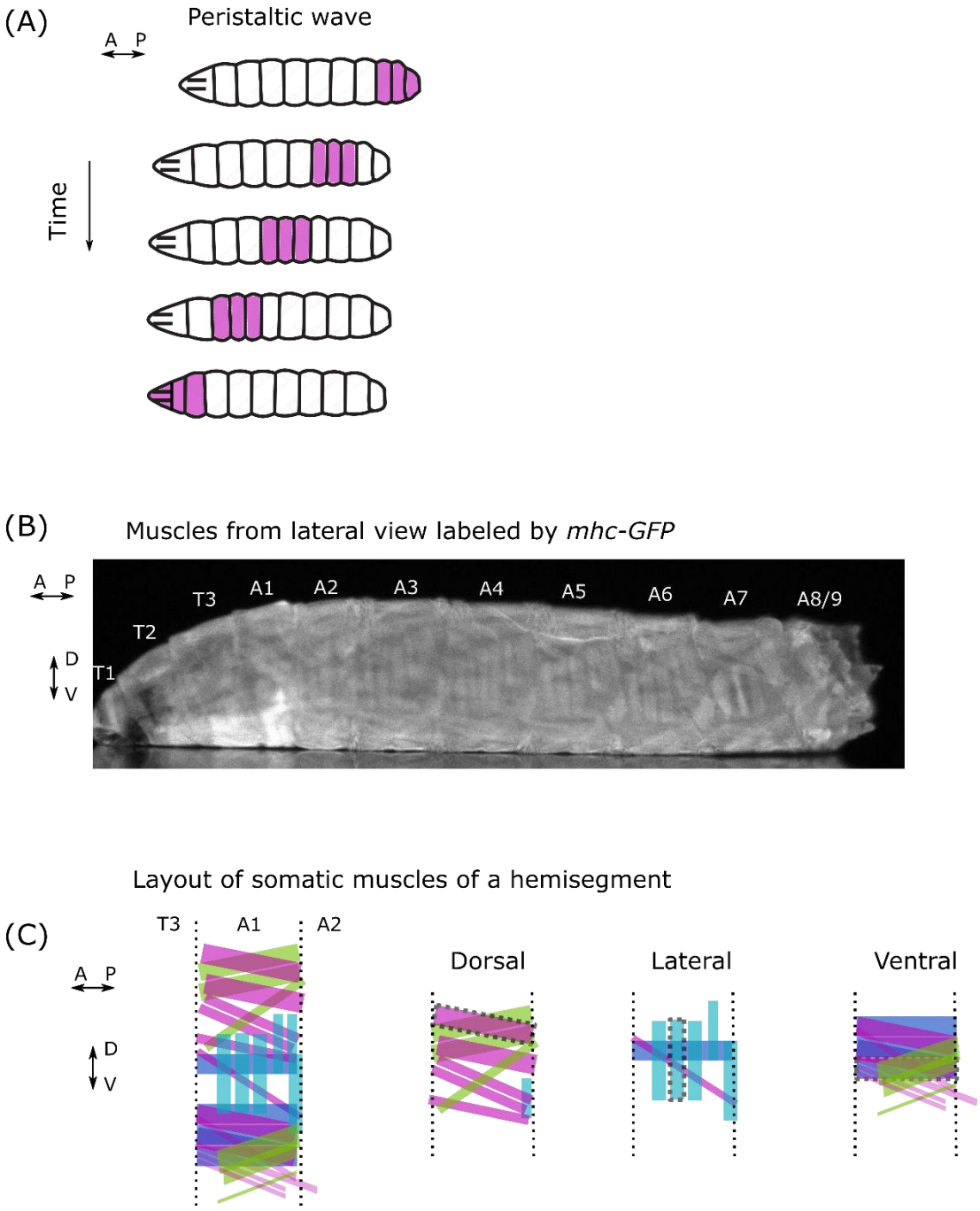

Figure 1.2 Forward peristaltic movement of larva and the anatomy of muscles

(**A**) Schematic drawing of a crawling larva. (**B**) Lateral view of a larva during crawling. Muscles are labeled by *mhc-GFP*. (**C**) Schematic diagram of muscles from external view in A1 hemisegment. Colors represent the muscular orientation (magenta: oblique; green: acute; blue: longitudinal; cyan: transverse). Thin dashed lines represent the segmental boundary. Muscles whose dynamics are characterized in this study are outlined with thick dashed lines.

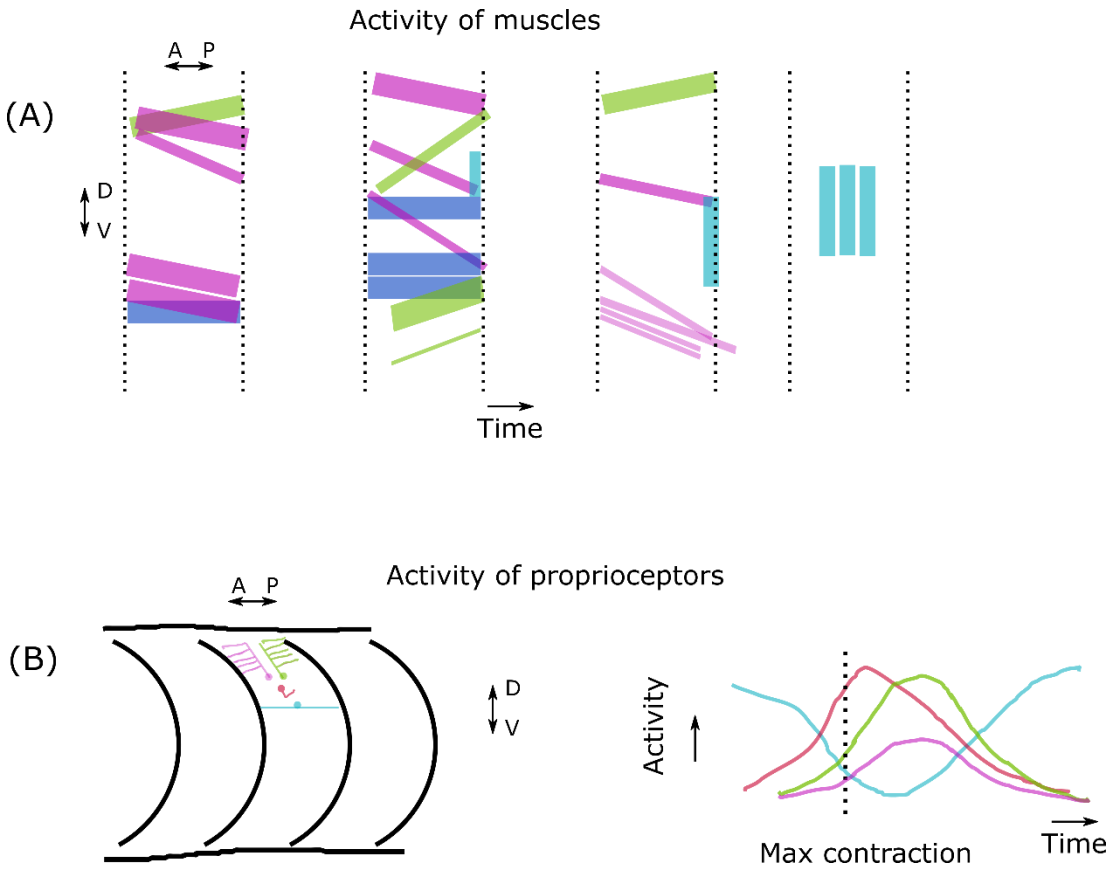

Figure 1.3 Activity of muscles and dorsal proprioceptors during forward peristalsis.

(**A**) Schematic diagram of the four muscular groups activated sequentially during forward peristalsis (Zarin et al., 2019). Dashed line: segmental boundary. (**B**) Schematic diagram of the morphology and activity profile of dorsal proprioceptors during a forward wave. Magenta: ddaE sensory neuron; green: ddaD sensory neuron; red: dmd sensory neuron; cyan: dbd sensory neuron (Modified from Vaadia et al., 2019). **Left**: Morphology. **Right**: Calcium fluorescence when the contraction wave passes the segment. Max contraction indicates the time when the segment is most contracted.

1-3. General approaches for motor circuit study in *Drosophila melanogaster*

To dissect the motor circuit in *Drosophila*, neurons are targeted by the genetic tool and analyzed. In this section, I review the general approaches for motor circuit study with special attention to those approaches used in this study.

1-3-1. Genetic systems for targeted gene expression

Several versatile binary transcriptional systems, including the GAL/UAS system, the LexA/LexAop system, and the QF/QUAS system, have been established to target the gene expression in specific cells in *Drosophila melanogaster* (Brand and Perrimon, 1993; Lai and Lee, 2006; Potter et al., 2010). These systems have been devised to divide the task of targeting the gene expression by the first component (e.g., GAL4) and expressing the transgene of interest by the second component (e.g., upstream activation sequence, UAS). The GAL4/UAS system is the most ubiquitous binary transcriptional system in *Drosophila melanogaster* (Figure 1.4 A). The GAL4 protein has been identified in yeast *Saccharomyces cerevisiae* as a gene regulator, which binds to a specific genome sequence (e.g., UAS) to activate the transcription of the downstream transgene (Guarente et al., 1982). The sequences encoding GAL4 and UAS have been cloned and integrated into the genome of *Drosophila melanogaster* as a gene expression system to target tissues of interest (Brand and Perrimon, 1993). Generation of the cell-type-specific GAL4 lines leads to the specific expression of the UAS element. The advent of this binary system further has boosted the generation of GAL4 and UAS lines to study the nervous system. The LexA/LexAop system and the QF/QUAS systems have been designed later, with

similar working mechanisms (Lai and Lee, 2006; Potter et al., 2010). The multiple binary systems enable one to target gene expressions in different cells in the same animal independently.

Several genetic systems have been developed based on the existing binary systems to refine the expression to smaller subsets of cells. The GAL80 protein suppresses the activation of transcription by GAL4 (Figure 1.4 A; Guarente et al., 1982). Multiple GAL80 lines have been generated to suppress the GAL4 transcription according to the neurotransmitter or the location (Simpson, 2016). Another approach splits the AD domain and DBD domain of the GAL4 protein and drives their expression in different cell groups (Figure 1.4 A; Luan et al., 2006). The UAS-downstream expression is refined in the cells of the interception of the cells targeted by the GAL4.AD and GAL4.DBD.

1-3-2. Visualization of neuronal morphology by genetic systems and antibody labeling

Neurons show diverse and unique shapes. The morphology of single neurons can be revealed by light microscopy when the expression of a marker is confined to a few neurons. To confine the GAL4- or LexA-driven expression, one can use MultiColor FlpOut (MCFO) system for stochastic labeling (Figure 1.4 B; Nern et al., 2015). In this system, multiple small-molecule tags are expressed in a subset of cells stochastically. Different labeling possibilities can be achieved by using the different MCFO systems.

To map the structure of interest into a standard coordinate system in the CNS, one can use an antibody to label specific structures as landmarks. Antibody labeling of fasciclin2 (FAS2)

is widely used to map the coordinates of neurites in the neuropil (Landgraf et al., 2003). By comparing the position of FAS2 landmarks and the neuronal expression of interest in the neuropil, one can determine the neuron's segmental identity and projection pattern. It also allows one to compare neurons that have been published or reconstructed in the EM database (section 1.3.3) to determine the neuron's identity (Ohyama et al., 2015; Saalfeld et al., 2009).

Engineered GFP or molecular markers are used to visualize subcellular compartments. For example, the molecular markers fused with the membrane-fused proteins cluster of differentiation 4 (CD4) or myristoylation (myr) are widely used to mark the neuronal membrane (Han et al., 2011), enabling the visualization of the small neuronal processes. Syt::GFP an engineered GFP by fusing GFP with synaptotagmin 1, is used to label neuronal presynaptic sites (Zhang et al., 2002). DenMark, an engineered red fluorescent protein by fusing mCherry with Icam5, is used to label the postsynaptic sites (Nicolaï et al., 2010).

1-3-3. Reconstructing connectivity by EM methods and trans-synaptic tracing

Analyzing the connectivity of component neurons is one of the main steps to understanding the function of the circuit. Currently, only EM-based methods can distinguish synaptic connections between neurons in the dense CNS volume. To reconstruct the synapses in *Drosophila* larvae, a whole first instar larval CNS was sliced and imaged with transmission electron microscopy (Ohyama et al., 2015). Annotation of synapses and tracing of neurons have been manually performed by neuroanatomists collaboratively in a web-based image server Collaborative Annotation Toolkit for Massive Amounts of Image Data (CATMAID; Saalfeld et al., 2009). As

recent progress, all the upstream neurons of the motor neurons in a full segment had been reconstructed (Zarin et al., 2019).

Another approach uses genetic tools to trace the upstream/downstream neuronal partners targeted by GAL4 or LexA driver. A recently developed tool, *trans*-Tango, labels downstream neurons by expressing a ligand in the presynaptic site to trigger the receptor on the postsynaptic membrane to activate the transcription in the downstream neurons (Talay et al., 2017). These tools enable fly neuroscientists to reveal the circuit diagram at the single-cell level.

1-3-4. Calcium imaging

To monitor the activity of targeted neurons, genetically encoded calcium indicators (GECIs) are widely used. GCaMP, a calcium sensor engineered from GFP, is the archetype of current GECIs (Figure 1.4 C; Nakai et al., 2001). The GCaMP is a complex created by permutating an enhanced GFP (EGFP) circularly and connecting the N terminus and C terminus to the M13 fragment of myosin light chain kinase (M13) and calmodulin (CaM), respectively. When Ca^{2+} binds to the CaM, fluorescence intensity is increased due to the conformational change of the protein (Figure 1.4 C). Current versions of calcium sensors have been invented to be brighter, faster, and have multiple colors to simultaneously image different calcium activities (Chen et al., 2013; Inoue et al., 2019). As the calcium activity cannot reflect the electrical activity in fine time scale, genetically encoded voltage indicators (GEVIs) have been invented to measure the electrical activity directly (Knöpfel and Song, 2019). The expanding genetic

sensors for measuring neuronal activity enable one to monitor the activity of multiple neurons from microscopes.

In *Drosophila* larvae, calcium imaging in the CNS dissected out (isolated preparation) is widely used. The activity pattern resembles that in the intact animals as the CPG can generate rhythmic motor output without sensory feedback, which is called the "fictive" locomotion. Specifically, wave-like activity shows in the isolated CNS of *Drosophila* larvae, which is called "fictive wave".

1-3-5. Optogenetics

Perturbational technologies are essential for testing the function of the component neurons. To manipulate the electrical activity in targeted neurons, genetic activators/silencers have been derived from known ion channels/pumps or toxins. Among them, the optogenetic tools enable one to manipulate neuronal activity with high temporal precision (Nagel et al., 2003). Channelrhodopsin, a light-gated cation channel, is widely used to activate neurons. As the wavelength of light to activate the channelrhodopsin is visible by *Drosophila* larvae, a red-shifted channelrhodopsin, CsChrimson (Figure 1.4 D), is widely used since it induces a minimal response in behaving *Drosophila* larvae (Klapoetke et al., 2014). Optogenetic silencers prevent action potential generation during illumination. Multiple optogenetic silencer constructions have been generated and tested in *Drosophila*, including light-gated chloride pumps (e.g., NpHR), proton pumps (e.g., ArCh), and anion channels (e.g., GtACR1, Figure 1.4 D) (Mohammad et al., 2017; Wiegert et al., 2017). The utility of these tools is still limited by their electrophysiological

property (Wiegert et al., 2017). For example, the chloride reversal potential led by activating anion channels might cause depolarized spiking in some neurons (Price and Trussell, 2006).

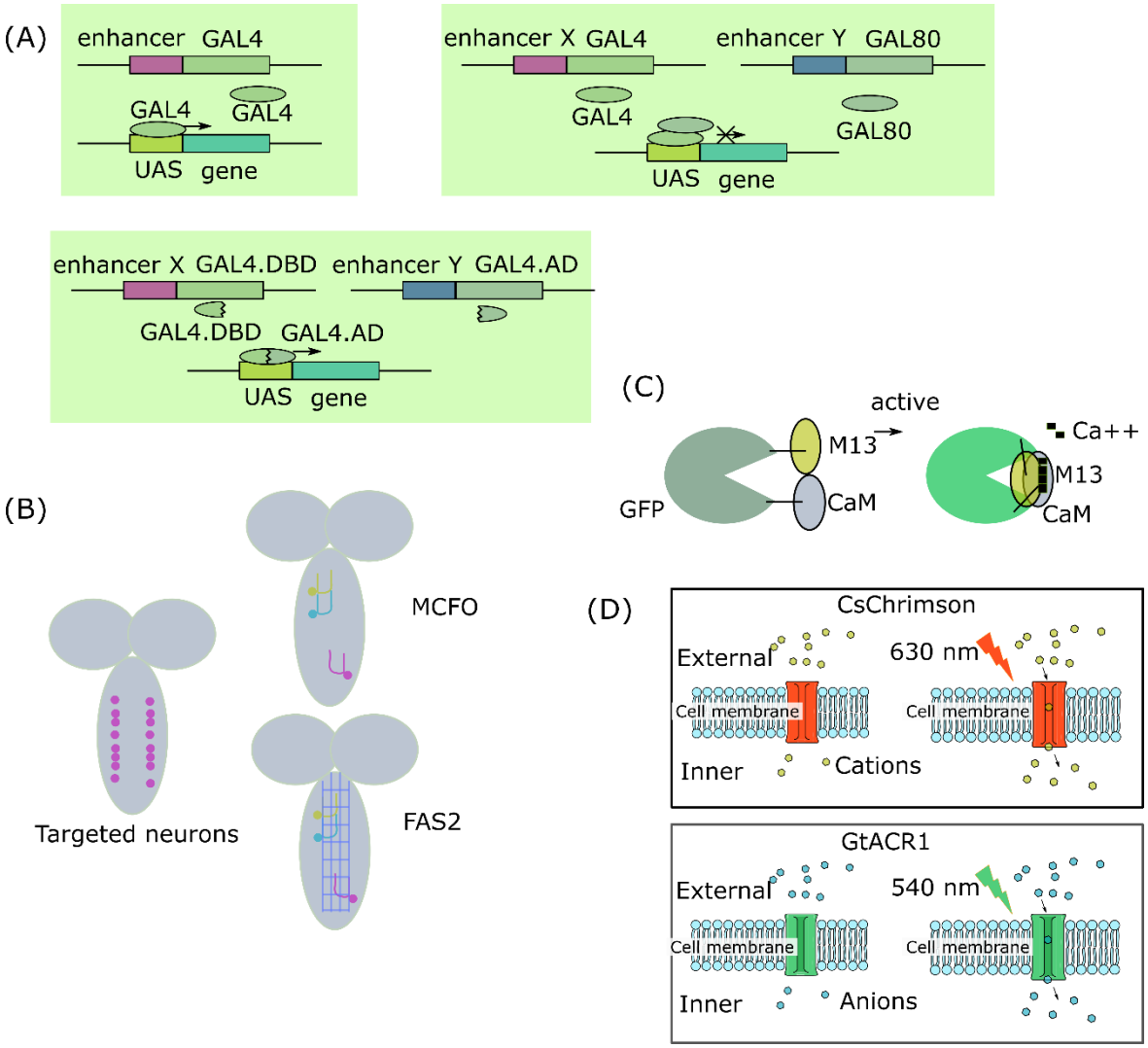

Figure 1.4 Genetic tools for motor circuit study in *Drosophila*

(**A**) Schematic diagram of the genetic targeting system GAL4/UAS and its derivates of GAL80 and split-GAL4 to refine expression. **Upper left**: a driver sequence (up) carries a promoter/enhancer and the gene encoding the GAL4. GAL4 proteins (oval) are expressed and activate the transcription of the gene under the control of the UAS. **Upper right**: The GAL4

protein is expressed by a driver sequence of enhancer A (upper left). The GAL80 protein is expressed by a driver sequence of enhancer B (upper right). Transcription is suppressed by GAL80 (lower). (**B**) Schematic diagram of the stochastic labeling by MCFO system and the FAS2 staining to generate a reference coordinate. Grey area: CNS. Circles: neurons. Blue mesh: FAS2. (**C**) Schematic diagram of activation of GCaMP by calcium ion. CaM: Calmodulin. M13: M13 fragment of myosin light chain kinase. (**D**) Schematic diagram of the opening of cation or anion channels by light stimulation of the optogenetic tool. **Upper**: Light stimulation of CsChrimson causes the opening of the cation channel and the influx of cations. **Lower**: Light stimulation of GtACR1 causes the opening of the anion channel and the influx of anions.

1-4. Purpose and organization of this thesis

From the reviews of the previous study in section 1.1, the duration of the component phases of a locomotor cycle can be modulated differently for the required speed. However, the neural control mechanisms to achieve the flexible motor output are less understood. In this study, I investigated the neural mechanisms to modulate the rhythm of motor output for the desired speed in *Drosophila* larvae. As the kinematics at different locomotion speeds were not well understood in this animal, I attempted (1) to identify the kinematic parameters varied with speeds and the key muscular groups (Figure 1.5 A, B); and (2) to identify the upstream central neurons that modulate the rhythm of motor output (Figure 1.5 C). For this purpose, I break this thesis into the following chapters:

(1) Materials and methods (Chapter 2).

(2) Investigation in the behavior and muscular pattern: adaption in behavior and muscular contraction for different speeds (Chapter 3).

First, I analyzed the kinematics in larval locomotion to reveal the key parameters related to locomotion speed. I defined a stride as the period between consecutive unhooking moments and then divided each stride into two phases: the first portion named tail lag before the peristaltic wave is initiated, and the second portion after, which is named wave phase. I found the tail lag varied differently with the wave duration. I analyzed the relationship between the speed and the duration of the two phases. I found that the tail lag and wave duration vary differently with the speeds, while the tail lag plays a significant role in speed regulation.

Next, I analyzed the kinematics of muscular contraction in abdominal segments. A group of muscles perpendicular to the crawling direction, the lateral transverse muscular group (LTM), were identified to be contracting together before a wave is initiated, with the relaxation of these muscles coinciding with the start of the wave. Furthermore, the tail lag scales with the amplitude and duration of LTM contractions. These results collectively suggest that the LTM is a key muscular group whose contraction duration is crucially coupled with the tail lag and locomotion speed.

(4) Investigation in the upstream neural circuit: identification of neural circuits underlying speed regulation by modulating inhibitory inputs to LTM (Chapter 4).

To reveal the central control of the generation of speed-dependent motor output, I investigated the upstream neural circuit of the LTM. An upstream interneuron A26f, a local GABAergic neuron presynaptic to the motor neurons innervating LTM, is coactivated at the initiation of the fictive forward locomotion. A31c, a GABAergic neuron presynaptic to the A26f neuron, bursts synchronously at an earlier phase of the initiation of the fictive forward locomotion and is activated again when the wave-like pattern is initiated. These neurons work together to regulate the activity of the LTM at the initiation of a forward movement. The activity of A26f neurons is required for the desired level of activity of LTM to generate the tail lag. Furthermore, the A31c neuron synapses in significant proportion with the descending and ascending neurons. These results collectively suggest that the activity of inhibitory premotor neurons is modulated to regulate the duration of contraction of LTM to generate the required speed.

(5) Conclusion and Discussion (Chapter 5).

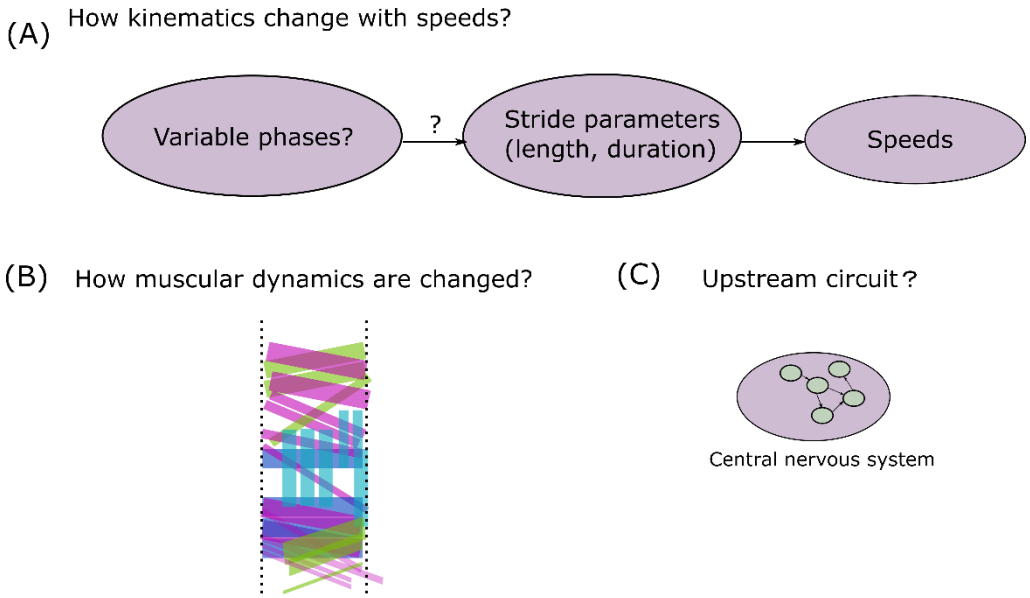

Figure 1.5 Questions investigated in this thesis

(**A**) How kinematics are changed regarding the locomotion speeds? (**B**) How muscular dynamics are adapted to the kinematic parameters? Colored blocks: muscles in a segment (see figure 1.2). (**C**) How do the upstream interneurons regulate the activity of the key muscular group and thereby the speed? Green circles represent the central neurons.

Chapter 2. Materials and methods

2-1. Materials

2-1-1. Fly strains

Genotype	Source or reference	Additional information
yw	BDSC #6598	
GMR24H08-GAL4.AD	BDSC #68300	*A31c-a8-sp-AD*
GMR45F08-GAL4.DBD	BDSC #70239	*A31c-a8-sp-DBD*
GMR44F09-GAL4.DBD	BDSC #71061	*A31c-sp-DBD*
GMR41F02-GAL4.AD	BDSC #75660	*A31c-sp-AD*
R76E09-LexA	BDSC #54951	*A26f-LexA*
VT050223-GAL4.AD	BDSC #72931	*A26f-sp-AD*
R15E05-GAL4.DBD	BDSC #68731	*A26f-sp-DBD*
GMR45F08-GAL4	BDSC #49565	*A31c-a8-GAL4*
GMR76E09-GAL4	BDSC #39931	*A26f-GAL4*
GMR41F02-LexA	BDSC #54794	*A31c-LexA*
nSyb-LexA_VK00027	This study	Pan-neuronal LexA
eve[RRa-F]-GAL4	gift from Dr. Miki Fujioka	Motor neuron aCC and RP2 GAL4

Sr-GAL4	BDSC #26663	Tendon cell GAL4
UAS-CD4::GCaMP6f_attp40	(Kohsaka et al., 2014)	
LexAop2-RGECO1_VK00005	(Kohsaka et al., 2014)	
LexAop-jRCaMP1b	BDSC #64428	
20XUAS-6XGFP	BDSC #52262	
trans-Tango	BDSC #77124	
MCFO-4	BDSC #64088	
Mhc-GFP	gift from Dr. Cynthia L. Hughes	Muscle GFP
UAS-CsChrimson::mVenus	BDSC #55136	
UAS-GtACR1_attp2	gift from Dr. Chris Doe	
UAS-VNC-CsChrimson	gift from Dr. Stephan Pulver	

2-1-2. Antibodies

Designation	**Source or reference**	**Concentration**
rabbit anti-GFP	Af2020, Frontier Institute	1:1000
mouse anti-FAS2	1D4, DSHB	1:10
guinea pig anti-GFP	Af1180, Frontier Institute	1:1000
rabbit anti-HA	C29F4, Cell Signaling Technology	1:1000
mouse anti-ChAT	4B1, DSHB	1:50
rabbit anti-GABA	A2052, Sigma;	1:100
mouse anti-VGluT	Gift from Dr. Hermann Aberle	1:1000
rabbit anti-DsRed	#632496, Clontech	1:500
goat Alexa Fluor 488-conjugated anti-rabbit IgG	A-11034, Invitrogen Molecular Probes	1:300
goat Alexa Fluor 555-conjugated anti-mouse IgG	A-21424, Invitrogen Molecular Probes	1:300
goat Alexa Fluor 488-conjugated anti-guinea pig IgG	A-11073, Invitrogen Molecular Probes	1:300

2-2. Methods

2-2-1. Fly strains

Except specifically mentioned, larvae were raised in standard cornmeal-based food at room temperature (25 °C), and third instar larvae were used for experiments. *trans*-Tango larvae were incubated at 30 °C for one day before the experiment (Talay et al., 2017). I used the following ATR feeding conditions for optogenetics: 10 mM ATR yeast from 18 to 36 hours in CsChrimson and Chr2.T159C groups, 3mM ATR yeast from 24 to 48 hours in GtACR1 groups. Fly strains are listed in section 2.1. I used the split GAL4 drivers *A31c-a8-sp* (*R24H08-GAL4.AD*, *R45F08-GAL4.DBD*), *A31c-sp* (*R41F02-GAL4.AD*, *R44F09-GAL4.DBD*), *A26f-sp* (*VT050223-GAL4.AD*, *R15E05-GAL4.DBD*). Transgenic flies *nSyb-LexA* were generated in the lab. The enhancer sequence of *neuronal Synaptobrevin (nSyb)* (*R57C10*, Pfeiffer et al., 2012) was cloned into pBPLexA::p65Uw plasmid (Pfeiffer et al., 2010). The transgenic line was generated in the *VK00027* locus (BestGene Inc., USA).

2-2-2. Immunostaining

I used a standard immunostaining procedure (Kohsaka et al., 2014). First, I dissected the larvae in fillet preparation, fixed it in 4% formaldehyde for 30 min at room temperature, washed twice with 0.2% Triton X-100 in PBS (PBT) for 15 min at room temperature, blocked with 5% normal goat serum in PBT for 30 min at room temperature, and stained with the first antibody at 4 °C

for 24 to 48 hours. After that, I washed twice with PBT for 15 min and stained with the second antibody at 4 °C for 24 to 48 hours.

2-2-3. Calcium imaging

In the calcium imaging of the isolated CNS, I dissected out the CNS of third instar larvae (Kohsaka et al., 2014), transferred the CNS to a drop of TES buffer (TES 5 mM, NaCl 135 mM, KCl 5 mM, $MgCl_2$ 4 mM, $CaCl_2$ 2 mM, sucrose 36 mM; pH = 7.15), and attached it dorsal-up on MAS-coated slide glass for imaging (Matsunami Glass, Japan). The fluorescence of GCaMP6f was detected by a spin-disk confocal unit (CSU21, Yokogawa, Japan) and an EMCCD camera (iXon, Andor Technology, Germany) with an upright microscope, Axioskop2 FS (Zeiss, Germany). I used a dual-view system (CSU-DV, Solution Systems, Japan) to perform dual-color calcium imaging for GCaMP and R-GECO1.

2-2-4. Top-view crawling assay and analysis

The third instar wandering larvae of *Sr-GAL4 > GFP* (about 0 - 4 hrs after wandering) were used. I transferred a larva onto an agarose plate of a standard concentration (1.5%), waited for about 1 minute, and took a video for 5 minutes. An Olympus stereotyped microscope and a 0.7x lens were used for magnification. A CMOS camera (Hamamatsu C11440-22CU) was used for video recording. A square of 1.6 x 1.6 cm of 1024 x 1024 pixels was recorded. The frame rate was set at 30 Hz. A mercury lamp of about 5 $\mu W/mm^2$ blue light was used for illumination.

I reviewed the videos to extract all the episodes of straight runs of more than three strides. I then randomly selected three episodes for each larva and analyzed the stride parameters. An ImageJ script was used for manual annotation. I first manually annotated the planting position of the prominent ventral denticle at a8 at one lateral side to calculate the stride length and the moment that the mouth hook is unhooking to calculate stride duration. Then I manually annotated when the A8 prominent denticle traveled to half a segment length to determine the time of wave initiation, where the segment length was manually determined by clicking the prominent ventral denticle of segments A7 and A8 when they were planted.

To model the relationship between the stride duration and the duration of the two constituent phases, I tested the piecewise linear model with two pieces and polynomial models. I then compared the Bayesian information criterion (BIC) between these models (Burnham and Anderson, 2004). The BIC is defined as:

$$\mathrm{BIC} = K\ln(n) - 2\ln(\hat{L}).$$

K is the number of estimated parameters in the model. n is the number of data. $\hat{L}$ is the maximum value of the likelihood function for the model. In the case of least squares estimation with normally distributed errors, BIC can be expressed as:

$$\mathrm{BIC} = K\ln(n) + n\ln(\hat{\sigma}^2),$$

where $\hat{\sigma}^2$ is the average of the squares of residuals. I calculated the BIC for the linear piecewise model of two pieces and the polynomial models of degrees from 2 to 10. The BIC has a minimum value with the cubic polynomial model.

2-2-5. Side-view imaging of the muscular ends and analysis

The third instar wandering larvae (about 0 to 12 hours after wandering) were used. An agarose plate of a standard concentration (1.5%) with black ink (0.2%) was used as the substrate. I oriented a CMOS camera (Hamamatsu C11440-22CU) and its zoom lens (Computar MLM3X-MP) with a 2x extender (RICOH FP-EX2) horizontally for recording. Each time one larva was transferred to the agarose plate for recording. I manually moved the plate to let the camera focus on the larval body wall. The top-view imaging was simultaneously recorded with the same instrument described in the previous method section. I shined blue light (about 20 μW/mm2) by a mercury lamp and an Olympus stereotyped microscope to illuminate the GFP-tagged tendon cells. I recorded in 30 Hz for about 3 minutes and typically collected 3-5 episodes on focus. Each episode includes 2-5 straight crawls.

To analyze the kinematics of the muscular movement, I used DeepLabCut (Mathis et al., 2018) to track the muscular ends. I labeled the muscular ends for 40-50 frames in each video and trained the network by all the labeled frames. The resnet50 network was used for training. The neural network was trained 1,000,000 times. To understand the relationship between LTM contraction and the head and tail movement, an ImageJ script was used to obtain the minimum/maximum length of LTM, the maximum thoracic length, the tail traveling distance, and the tail lag. To obtain the minimum/maximum length of LTM, I annotated the position of the muscular ends of the LTM in segments A2-A7 when they were mostly contracted and extended and calculated the distance of the muscular ending pairs. To obtain the maximum thoracic length, I annotated the anterior end of the head and the central point of the A1/T3 segmental boundary at the dorsal side and calculated the distance between them. To obtain the

tail traveling distance, I annotated the planting positions of the tail and calculated the distance. The tail lag was obtained as the previous section described.

2-2-6. Optogenetics for free-crawling larvae and larvae in the fillet preparation and Cartesian preparation

I used the same imaging system and analysis method of the top-view-imaging assay in the optogenetics of free-crawling larvae. According to the optogenetic tool, the background light and the light for the optogenetic stimulation were set as the following. In the GtACR1 groups, I used a 660 nm LED (Thorlabs M660L3) to shine the background light of 0.6 μW/mm2 and used a 590 nm LED to shine the light for the optogenetic stimulation light of about 150 μW/mm2. In the CsChrimson groups, I used an 850 nm infrared light (CCS LDQ-150IR2-850) of 40 μW/mm2 for background light and used the 660 nm LED to apply the optogenetic stimuli of about 60 μW/mm2.

In the muscular imaging, I used fillet preparation and Cartesian preparation. In the fillet preparation, I used a previously described procedure to dissect the body wall in the dorsal midline and to expose the muscles (Kohsaka et al., 2014). In the Cartesian preparation, I prepared a PDMS plate with a standing PDMS island filled with 4°C TES buffer, transferred a larva to the PDMS plate, and used two pins to fix the head and tail of the third instar larvae (Figure 4.6 A). The tail was pinned to the bottom PDMS substrate to make it perpendicular to the larval sagittal plane with two pricking points close to the two prominent lateral denticles in the A8 segment. The head was pinned to the PDMS island to make it perpendicular to the larval

frontal plane. After pinning, the PDMS island was attached with the tail pin and supported the ventral larval body. 4 °C TES buffer was used to reduce the larval motion during the preparation. I changed the buffer to 25 °C before imaging.

After the preparation, I used a local stimulation microscope for muscular imaging and optogenetic stimulation (Takagi et al., 2017). The microscope (FV1000, Olympus) have two separate optical paths for the muscular imaging and optical stimulation: blue light from a Xeon lamp (X-light, Japan), which is used to image the muscles in the abdominal segments A3/A4-A7/A8, and a scanning laser of blue (488 nm) or green (559nm) light (FV1000, STIM function), which is used to stimulate the CNS optogenetically. A dichroic mirror separates the two optical paths. I used a 4x Olympus lens and a 1 x adapter for the fillet preparation or a 0.63 x adapter for the Cartesian preparation. The muscular imaging was recorded by an EMCCD camera (iXon, Andor Technology, Germany). In the Cartesian preparation, a rectangular scanning of about 0.85 mm x 0.4 mm by a 559nm laser was used for optogenetic stimulation (about 20 μW/mm2 for the CsChrimson groups and about 40 μW/mm2 for the GtACR1 groups), while a blue light from Xe lamp was used for muscular illumination (about 10 μW/mm2 at center). In the fillet preparation, a tornado scanning of a radius of about 0.3mm by a 488 nm laser was used to activate the Chr2 (about 400 mW/mm2), while the blue light was used for muscular illumination (about 50 μW/mm2).

I used DeepLabCut (Mathis et al., 2018) to track the muscular ends. I labeled the muscular ends 40-50 frames in each video and trained them together. The resnet50 network was used for training. The neural network was trained 1,000,000 times.

I used paired Student's t-tests to compare the values between before and after the optogenetic stimulation. All data points are used for the statistical test.

Chapter 3. Adaption in behavior and muscular contraction for different speeds

3-1. Larvae crawl faster by increasing stride frequency and/or stride length

The locomotion behavior has been extensively studied in *Drosophila* larvae. In a typical behavioral assay, a larva is placed on the substrate of an agarose gel plate. On this kind of soft substrate, the larva shows stereotyped exploration behavior of a combination of successive cycles of forward crawling (forward cycles) and reorientation (Berni, 2015; Lahiri et al., 2011). The exploration range is suggested to be mainly dependent on the crawling speed during the forward cycles but not the fraction of time spent out of the forward cycles (Aleman-Meza et al., 2015).

To better understand the underlying kinematics for different speeds, I assayed the free crawling on the agarose plate of larvae expressing GFP in the tendon cells (Figure 3.1 A and section 2.2.4 for detail). I measured the stride length, stride frequency, and speed and analyzed their relationship. The stride length was measured by the traveling distance of the most posterior segment in a stride. The stride duration was measured by the time interval between unhooking moments. The stride frequency was calculated from the averaged stride duration in forward cycles before the larva stopped forward cycles or crawled out of the field of view. The speed

was calculated from the stride length and stride frequency. I found that the speed correlates with both the stride frequency and the averaged stride length (Figure 3.1 B, C). However, Pearson's correlation coefficient (Pcc) between the speed and the stride frequency ($r = 0.92$) is higher than the Pcc between the speed and the stride length ($r = 0.64$). The stride frequency also has a larger dynamic range, with a maximum value of about three times the minimum (the maximum stride length is about 1.7 times the minimum). I also found that the stride length is weakly correlated with the stride frequency ($r = 0.32$; Figure 3.1 D). These results suggest that the animal tunes both the stride length and the stride frequency for speed regulation, but the stride frequency is the main parameter to be regulated.

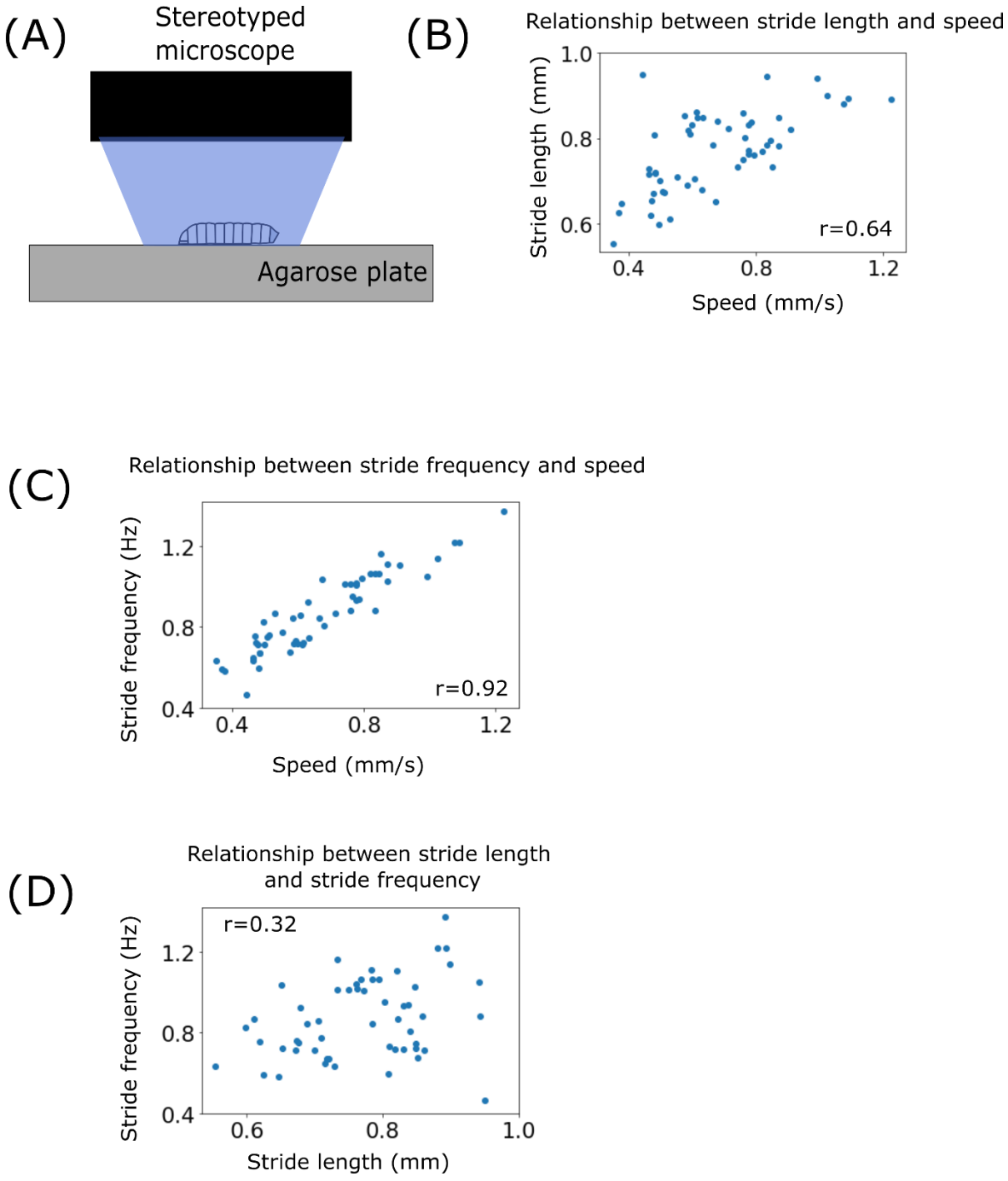

Figure 3.1 Measurement of the stride parameters in free crawling assay

(**A**) Schematic drawing of the free crawling assay. (**B**) Relationship between the averaged stride length and speed. *r* represents Pearson's correlation coefficient. (**C**) Relationship between the stride frequency and speed. (**D**) Relationship between the stride frequency and stride length.

3-2. Definition of the tail lag and wave phase in a stride during successive forward crawling

Drosophila larvae extend the head and contract the tail at the initiation of a forward crawl, which is called telescoping. Though the telescoping can be seen as a part of the peristaltic wave, it is poorly understood how it relates to the wave and how it varies as a function of speed. From some previous literature, it can be noticed that the body length is varied during crawling (Berrigan and Pepin, 1995). Furthermore, the amplitude of the variation can be unstable (Berrigan and Pepin, 1995). It suggests that the relative movement of the head and tail could be non-stereotyped. If so, the locomotion speed might be affected by the phase delay between the movement of the head and tail. To better understand this phenomenon, I defined a stride as the period between consecutive unhooking moments and divided each stride into two portions: the first portion before the peristaltic wave is initiated and the second portion after (Figure 3.2 A). The resulting two phases were named the tail lag phase and wave phase. The wave phase approximates the whole duration of a contraction wave since I defined its initiation by the initiation of the contraction wave and defined its completion by the initiation of head extension, which marks the ending of the contraction.

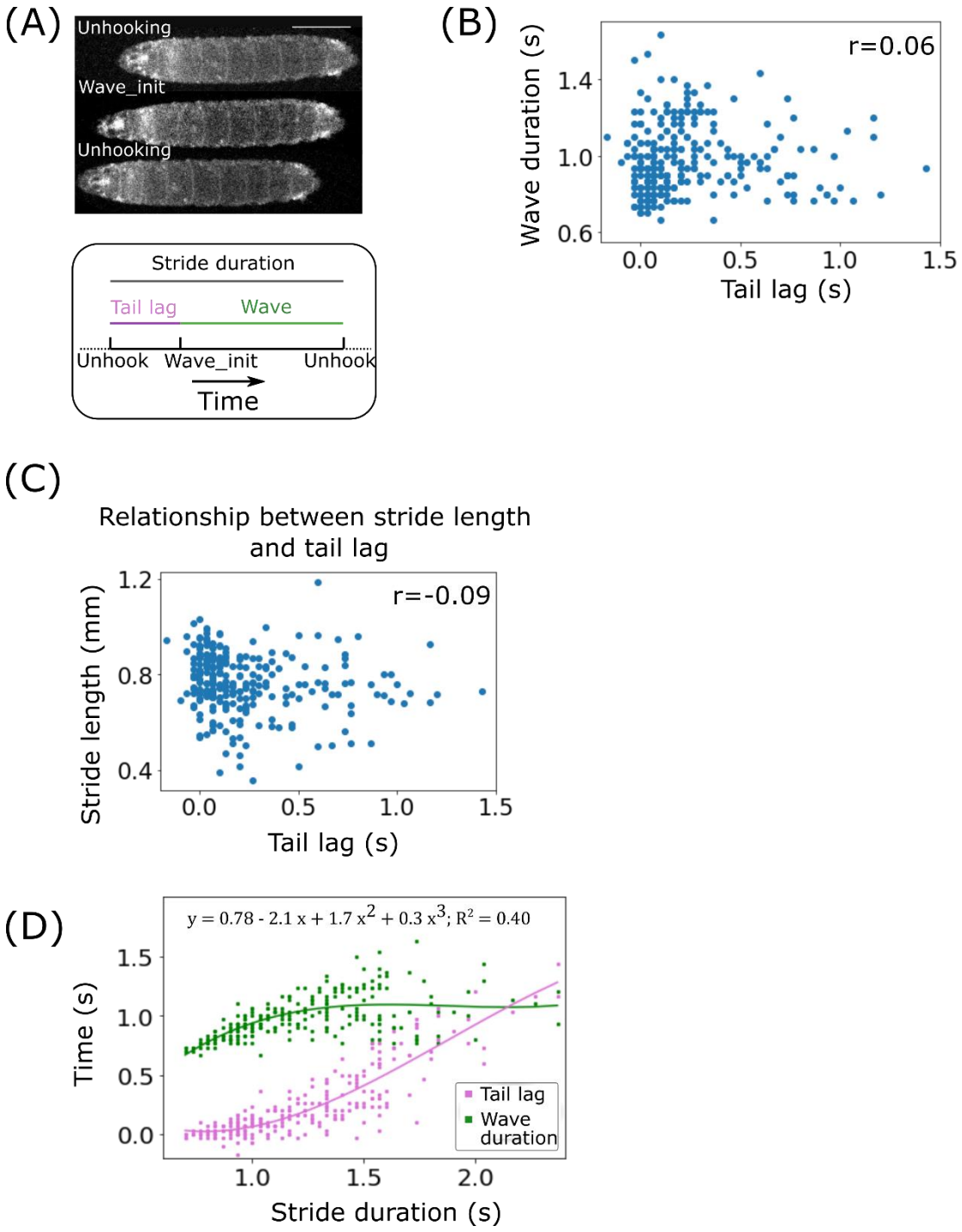

Figure 3.2 Tail lag phase and wave phase are two independent phases

(**A**) Schematic drawing of the definition of the two phases. Scale bar: 1 mm. (**B**) Relationship between the stride length and tail lag. (**C**) Relationship between the stride duration and the two durations, tail lag, and wave duration. (**D**) Relationship between stride duration and duration of component phases (wave duration and tail lag). Pcc between stride duration and tail lag is 0.86. Pcc between stride duration and wave duration is 0.56. Lines: cubic regressions. The function at the upper side denotes the regression function of the tail lag. As the stride duration equals the sum of the tail lag and the wave duration, the terms of regression function of the wave duration are [0.78, 3.1, -1.7, -0.3]. The R squared shares the same value of 0.40.

3-3. Crawling speed is correlated with the tail lag

Based on the previous definition, I measured the duration of the tail lag and wave duration in successive bouts of forward crawling, where the wave-initiation moment was manually annotated at the time when the ventral-posterior end moves half a segmental length (see section 2.2.4 for detail). I first compared the variation of the tail lag and the wave duration. The two values are not correlated (r = 0.06; Figure 3.2 B), which suggests the duration of the two phases are varied independently. It raised the question of which parameter mainly decided the stride duration. To answer this, I analyzed the relationship between the stride duration and the two constituent durations. Both the tail lag and wave duration are correlated, but the tail lag has a higher correlation (r = 0.86) than the wave duration (r = 0.56) (Figure 3.2 D). Notably, the two durations varied differently through the range of stride duration. I tested multiple models and found that the cubic polynomial model best represents the dataset based on an information-theoretical approach BIC (see section 2.2.4 for detail; Figure 3.2 D; Burnham and Anderson, 2004). The tail lag has an increased gradient with stride duration. By comparing the gradient of the two durations, I found that the main contributor to the variation of stride duration transits from wave duration to tail lag at about 1.08s. The tail lag is also not correlated with the stride length (r = -0.09; Figure 3.2 C). I then analyzed the relationship between the speed and the two temporal parameters. I found the speed is both correlated with the wave duration and the tail lag. The Pcc is -0.62 for the wave duration and -0.74 for the tail lag (p-value = 0.127 by Fisher-z transformation, Figure 3.3 B). I then defined a duty factor parameter by the proportion of the tail

lag in stride duration. The duty factor decreased with the increased speed. The gradient of linear regression is -0.47 (Figure 3.3 C).

These results suggest that the larva can control the delay between the initiation timing of the wave-like contraction at the tail and the completion of the wave at the head for speed regulation. The shortening of the tail lag decreases the stride duration for faster crawling. This mechanism is independent of the regulation of stride length and wave duration.

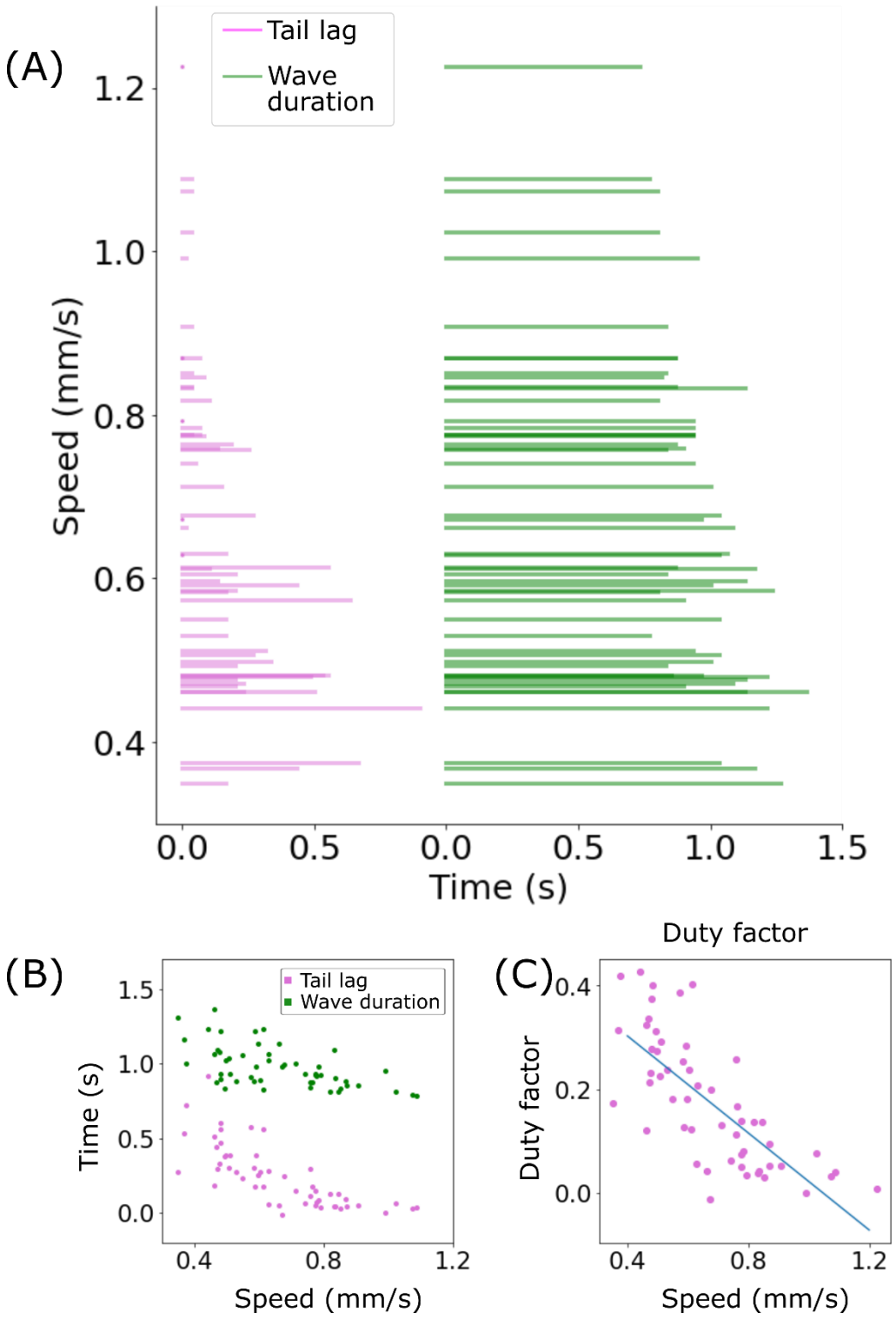
(A)
Tail lag
Wave duration
Speed (mm/s)
1.2
1.0
0.8
0.6
0.4
0.0
0.5
0.0
0.5
1.0
1.5
Time (s)
(B)
Tail lag
Wave duration
Time (s)
1.5
1.0
0.5
0.0
0.4
0.8
1.2
Speed (mm/s)
(C)
Duty factor
Duty factor
0.4
0.2
0.0
0.4
0.8
1.2
Speed (mm/s)

Figure 3.3 Tail lag increased with decreasing speeds

(**A-B**) The relationship between tail lag and wave duration. (**C**) Relationship between speed and the fraction of the two durations in a stride. Blue line: linear regression. The slope is -0.47.

3-4. The LTM has a larger amplitude and duration of contraction with increased tail lag

To examine how the motor output is modulated as a function of speed, I measured the muscular length in abdominal segments during crawling. The muscular attachment sites are targeted by a tendon-cell-specific GAL4 driver, which drives the expression of a bright GFP (*20 × UAS – 6 × GFP*). I then imaged the free crawling larvae from the lateral side (Figure 3.4 A). The movement of muscular ends of the LT2, DL, and VL muscles were tracked in segments A2-A7 during straight crawling by DeepLabCut (see section 2.2.5 for detail).

I found that most longitudinal muscles were not contracted during the tail lag phase (Figure 3.4 B). However, the LT2 muscles, a representative muscle in the lateral transverse muscle group (LTM), were contracted together with a variant amplitude and duration across segments during this period (Figure 3.4 B). To understand the biological meaning of the variable contraction of LTM, I first examined if the stride length was tuned by the amplitude of contraction. However, the correlation is weak between the minimum length of LTM (LTM_min) and the stride length (r = -0.24; Figure 3.4 C). The correlation is also weak between the LTM_min and the maximum length of thoracic segments (r = -0.33; Figure 3.4 D). I then analyzed if the temporal parameters were affected by the amplitude of LTM contraction. I found that the stride duration is correlated with the minimum length of LTM (r = -0.65; Figure 3.5 A). By dividing a stride duration, I found that the tail lag is strongly correlated with the LTM_min (r = -0.77; Figure 3.5 B), whereas the wave duration is not correlated with the LTM_min (r = -0.05; Figure 3.5 B). Similarly, the duration of the LTM contraction is correlated with the tail lag (r = 0.84) but not correlated with the wave duration (r = 0.20) (Figure 3.5 C). Finally, I also

found the speed is correlated with the contraction duration of LTM but not with the minimum length of LTM (Figure 3.5 D, E).

These results suggest that the stronger contraction of LTM increases the stride duration by increasing the tail lag but not wave duration. The stride length is less affected by the increased recruitment of LTM.

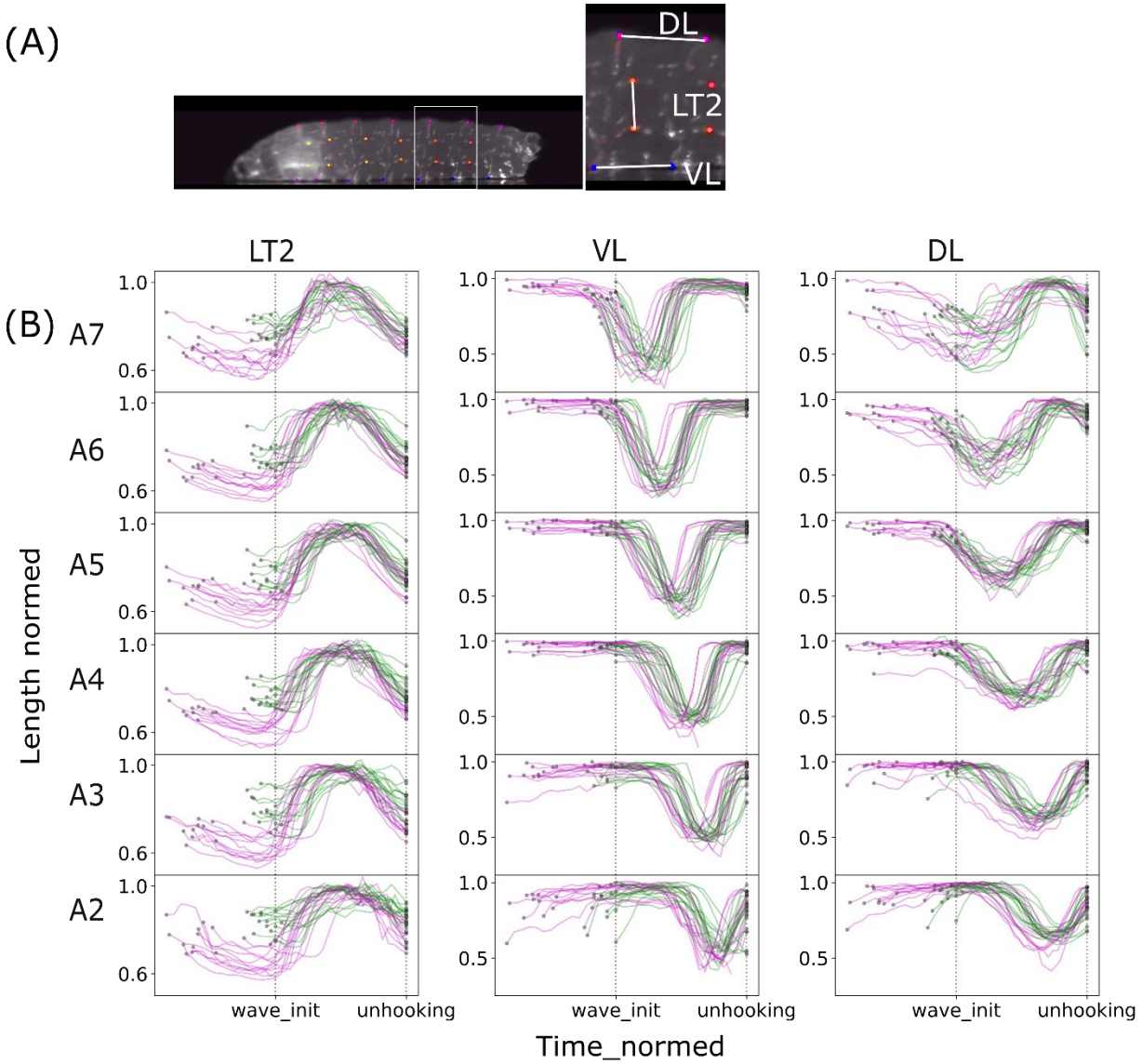

(C) Relationship between stride length and the minimum length of LTM

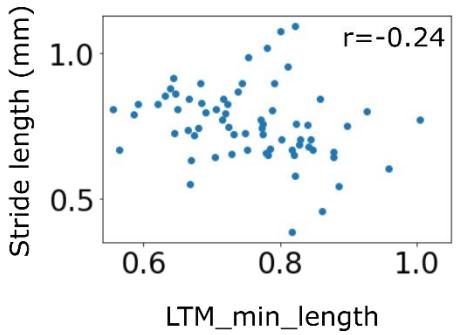

(D) Relationship between max length of thrx segments and the minimum length of LTM

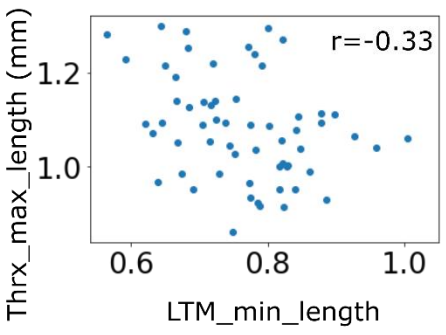

Figure 3.4 Kinematics of the muscular length by automatic tracking

(A) An example frame of the side-view imaging with DeepLabCut tracking in free crawling larvae. The colored spots correspond to the automated tracking of the tendon cells of the LT2, DL, and VL muscles. **(B)** Tracking results of the muscular length of the LT2 muscles in all the 25 FWs of 6 larvae in forward strides. Magenta: 11 FWs with tail lag more than 0.2 s. Green: 14 FWs with tail lags less than 0.2 s. Time is aligned with the wave_init and unhooking moment. **(C)** Relationship between the minimum length of LTM and the stride length. (**D)** Relationship between the minimum length of LTM and the maximum length of thoracic segments T1-T3.

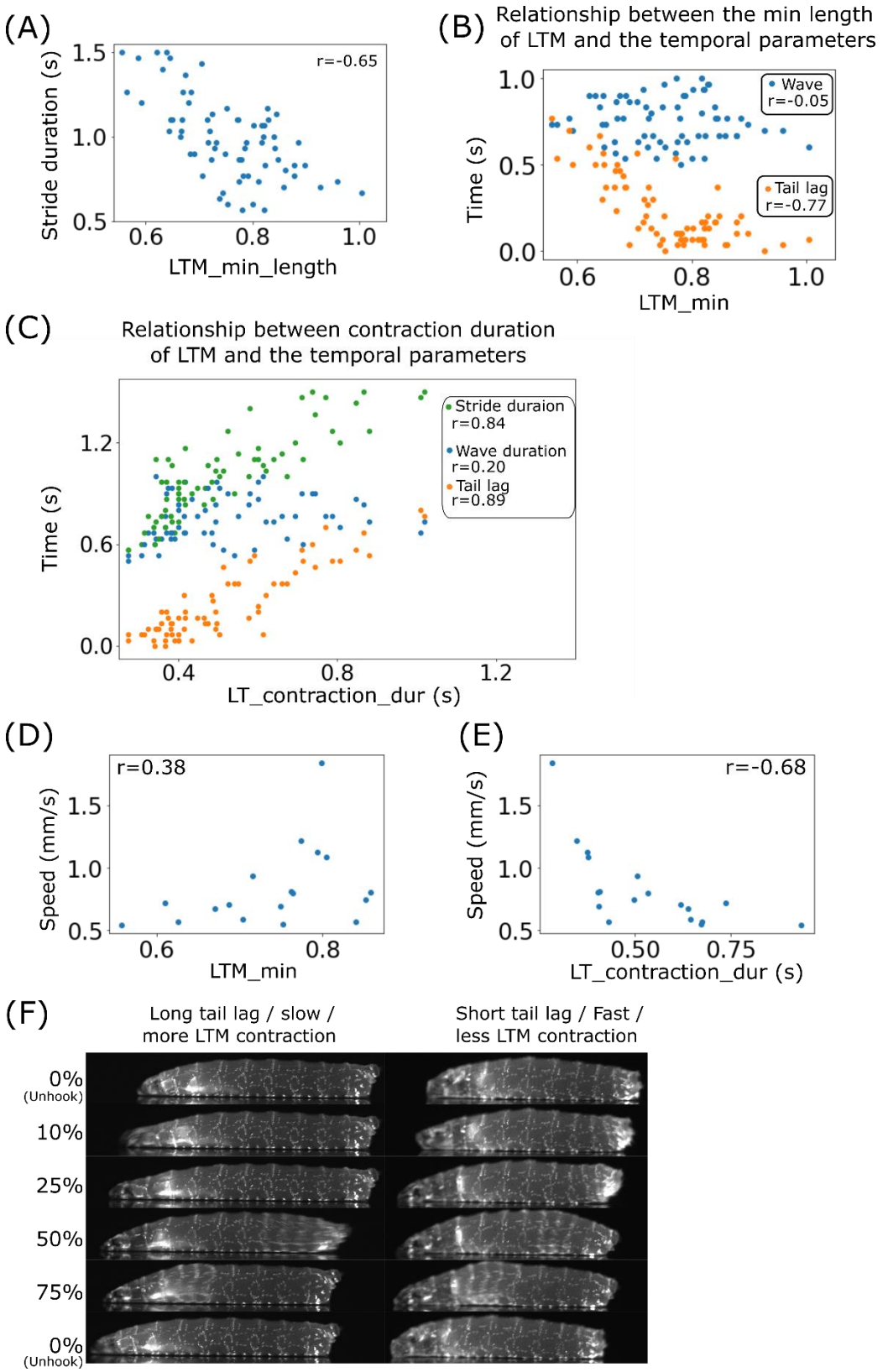
(A)
Stride duration (s)
LTM_min_length
r=-0.65
(B)
Relationship between the min length of LTM and the temporal parameters
Time (s)
LTM_min
Wave r=-0.05
Tail lag r=-0.77
(C)
Relationship between contraction duration of LTM and the temporal parameters
Time (s)
LT_contraction_dur (s)
Stride duraion r=0.84
Wave duration r=0.20
Tail lag r=0.89
(D)
Speed (mm/s)
LTM_min
r=0.38
(E)
Speed (mm/s)
LT_contraction_dur (s)
r=-0.68
(F)
Long tail lag / slow / more LTM contraction
Short tail lag / Fast / less LTM contraction
0% (Unhook)
10%
25%
50%
75%
0% (Unhook)

Figure 3.5 LTM contracts more with a longer duration as the tail lag increases

(A) The relationship between the minimum length of LTM and the stride duration. **(B)** The relationship between the minimum length of LTM and the duration of component phases (wave duration and tail lag). (**C)** Relationship between the contraction duration and the temporal parameters (stride duration, wave duration, and tail lag). **(D)** Relationship between the minimum length of LTM and the locomotion speed. **I** Relationship between the duration of contraction of LTM and locomotion speed. **(F)** Example frames of the side-view imaging in free crawling larvae. Left: a stride with a long tail lag. Right: a stride with a short tail lag.

3-5. Summary

In this chapter, I divided a stride into two phases: the tail lag and the wave phase. I reported that the speed variation was more coupled with the time spent in the tail lag phase than in the wave phase. I identified the LTM as a recruited muscular group during the tail lag phase. The amplitude and duration of the LTM contraction are crucially coupled with the duration of tail lag (Figure 3.6). Furthermore, the contraction and relaxation of the LT muscles are not wave-like but highly synchronized. It leads to two hypotheses: (1) A rhythm generator determines the timing of initiation and completion of LTM contraction, which is highly coupled with the pattern generator of the peristaltic wave. (2) A central module modulates the output to LTM whose communication with the wave pattern generator is not required.

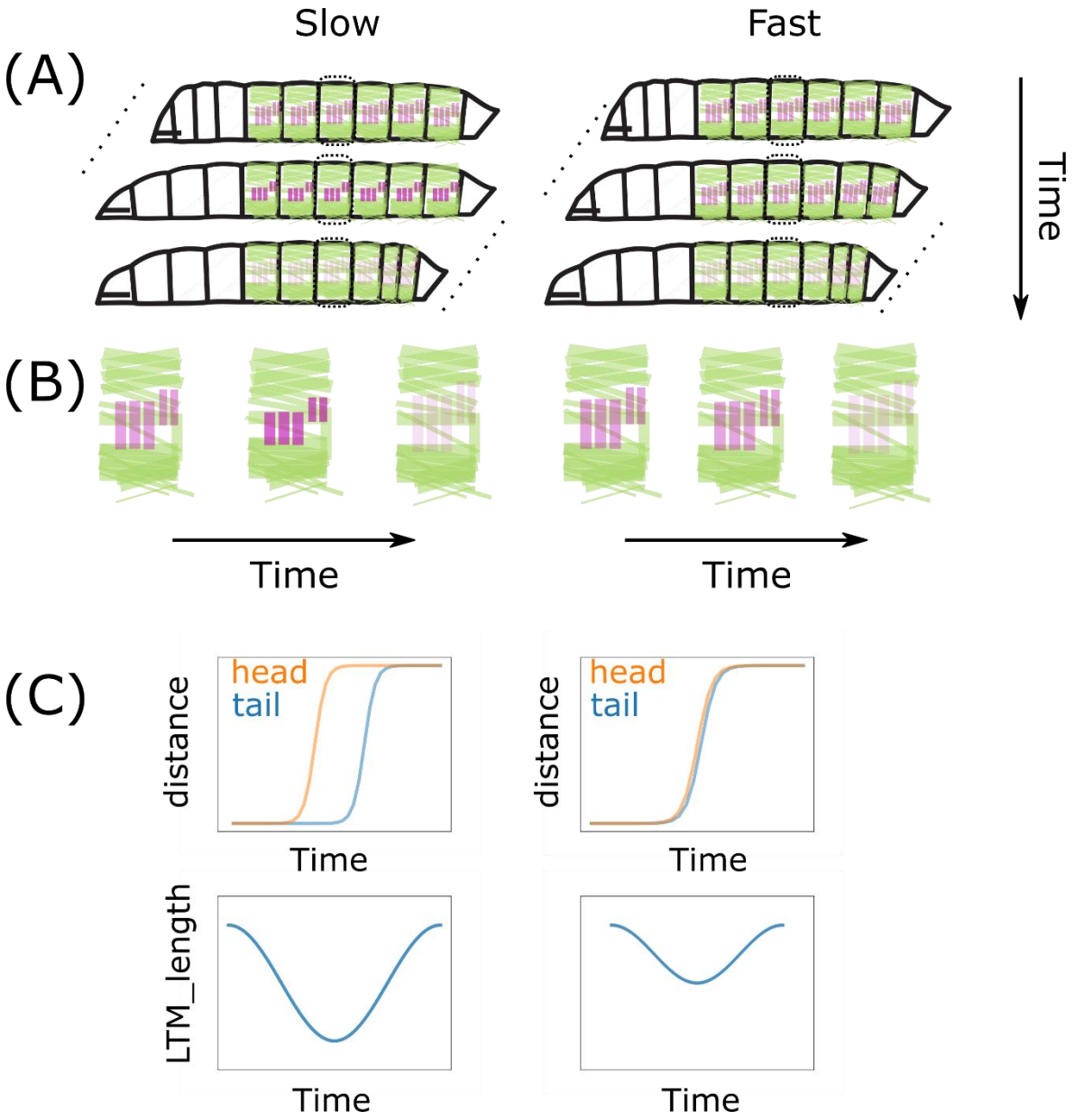

Figure 3.6 Summary

(A) Schematic drawing of the time sequence of LT muscles and the corresponding larval movement. The darker purple color represents more contraction. **(B)** Schematic drawing of the LT muscles. **(C)** Schematic diagram of the activity of LT muscles.

Chapter 4. Identification of neural circuits underlying speed regulation by modulating inhibitory inputs to LTM

As described in chapter 3, LT muscles are recruited together and contracted most during the tail lag phase. The amplitude and duration of the contraction of LT muscles are highly coupled with the duration of tail lag. These results imply the existence of a neural circuit controlling the synchronized output to the LT muscles. It also leads to the hypothesis that the central module for speed control should modulate the output to the LT muscles. In this chapter, I investigated the upstream central neurons of the LT muscular group. The chapter is divided into two parts. In part I, I will introduce the anatomy, calcium activity, and genetic tracing of two interneurons as candidate interneurons concerning the modulation of tail lag. Part II will introduce the perturbational analysis based on the optogenetic tools.

PART I: Anatomy, calcium imaging, and genetic tracing

4-1. A26f neurons are inhibitory premotor neurons innervating motor neurons of LTM

To understand the neural mechanism underlying the generation of tail lag, I searched for the premotor neurons synapsed with the MNs innervating LTM, where A26f neurons turned out as a candidate. Zarin et al. used the EM database to reconstruct all the premotor neurons in the A1 segment (Zarin et al., 2019). Among the premotor neurons specifically innervating the MNs for LTM, I found that A26f neurons and A19l neurons have a long range of extension of their axons across several segments, which is an uncommon feature for premotor neurons. The long axonal projection is possibly necessary for the control of synchronized activity of LT muscles. Both A26f neurons and A19l neurons innervated all the MNs for LTM and the MN for VA and DO (Zarin et al. 2019).

I targeted A26f neurons by a split GAL4 driver (termed "*A26f-sp*"), which drove expression in A26f neurons in neuromeres A3-A5 (Figure 4.2 A). To identify the neurotransmitter, I co-stained *A26f-sp > GFP* with anti-GABA, anti-ChAT, and anti-VGlut and found that the A26f neurons are GABAergic neurons (Figure 4.1 B). The A26f neurons were reported to be corazoninergic (Zarin et al., 2019). However, by comparing the morphology with the corazoninergic neurons (Santos et al., 2007), it was clear that A26f neurons are not the putative corazoninergic neurons.

To reveal its morphology, I targeted the expression of a single A26f neuron in segment A5 by a LexA driver (*A26f-LexA*). I co-stained the *A26f-LexA > LexAop-CD4::GCAMP6f*

samples with anti-GFP and anti-FAS2 that labels neuronal bundles to provide a reference coordinate system (see section 1.3.2, Figure 4.1 A). The cell body locates in the dorsal cortex. The axon projects to the contralateral DL neuropil via a distant path that travels along the neuropil boundary ventrally. After reaching the contralateral DL neuropil, it branches to ascend along the DL fascicle for two neuromeres to reach the segmental boundary of neuromere A2/A3 and to descend into the A6 neuromere. The dendritic-like processes are arborized from the axon at the ventralmost medial neuropil, extend dorsally, and are arborized to dense processes near the DM fascicle and near the dorsalmost neuropil bilaterally. The A26f neuron is projected across four neuromeres. EM reconstruction has revealed that the A26f neuron innervates the MNs for LT muscles in multiple neuromeres (Figure 4.1 C). The morphology implied the potential of the A26f neurons to control the activity of LT muscles broadly in multiple segments.

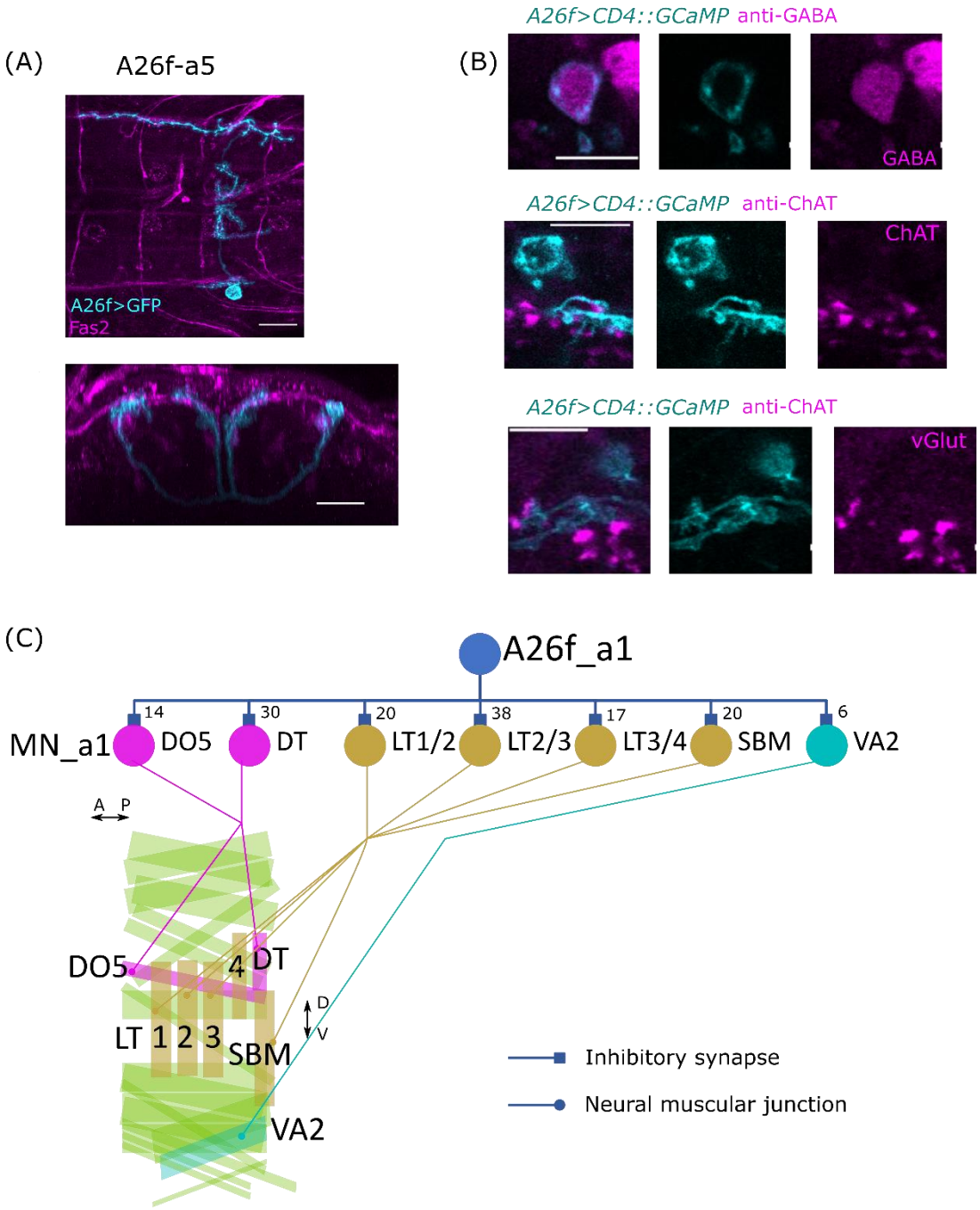

Figure 4.1 A26f neuron is a GABAergic premotor synapsed with motor neurons innervating LT muscles

(A) Confocal images of the co-staining of the A26f neuron in neuromere A5 targeted by the *A26f-LexA* and the FAS2 bundles. Upper: dorsal view. Lower: frontal view. Scale bars: 20 μm. **(B)** Confocal images of immunostaining of A26f neurons and the antibodies to identify the neurotransmitters. Scale bars: 10 μm. **(C)** Schematic diagram shows the connectivity between the pair of A26f neurons in A1 neuromere and the downstream MNs in neuromere A1 innervating the muscles. **Upper**: The connectivity between the A26f neurons and the motor neurons. The number between the A26f-a1 neuron and the MNs shows the synaptic output number reconstructed in CATMAID (Zarin et al., 2019). Magenta: MNs projecting via intersegmental nerves (ISN). Orange: MNs projecting via segmental nerve a branch (SNa). Cyan: MNs projecting via segmental nerve c branch (SNc). **Lower:** Schematic diagram shows the muscles innervated by the motor neurons.

4-2. A26f neurons are coactivated at the initiation of FW

Next, I analyzed the activity of A26f neurons to understand their activity pattern and the relationship with the motor state. I then used a dual-color imaging system to monitor the activity of A26f neurons and the pan-neuronal activity by using *A26f-sp* driving the expression of GCaMP and a pan-neuronal driver *nSyb-LexA* driving the expression of red fluorescent calcium indicator RGECO1. I performed calcium imaging in the isolated CNS (see section 2.2.3 for detail). I manually circled the ROIs at the medial dendritic sites to analyze fluorescence since the expression was not overlapped with the segmental homologs. Unlike most neurons exhibiting the fictive wave-like activity, the calcium activity of the A26f neurons is synchronized in neuromeres A3-A5 (Figure 4.2 B, C). I compared the correlation between the activity of the A26f neurons and neurons labeled by the pan-neuronal line (nSyb-neurons**)**. The correlation of the A26f segmental homologs is much higher than that of the neurons labeled by the pan-neuronal line (Figure 4.2 D). I then analyzed the fluorescence of the A26f neurons at the initiation of FWs (Figure 4.2 C). I aligned the time series at two time points when the ΔF/F of nSyb_a4 maximized and the ΔF/F of nSyb_a1 maximized. A26f neurons can exhibit one or several peaks at the initiation phase of the FW. The averaged profile of the activity of the A26f neurons shows a peak that is earlier than the peak of nSyb_a4 of about 2.5 times the intersegmental delay, though the time of the peak of the A26f neurons is not strictly defined by the intersegmental delay. Finally, I analyzed the time lag of the ΔF/F between A26f neurons of different segments during forward waves and compared it with that between nSyb-neurons. Despite the nSyb-neurons having a significant time lag across segments, the tail lag is close to

zero in A26f neurons (Figure 4.2 E).

These results suggest that A26f neurons have the potential functional role in controlling the activity of the LTM at the initiation of the FW.

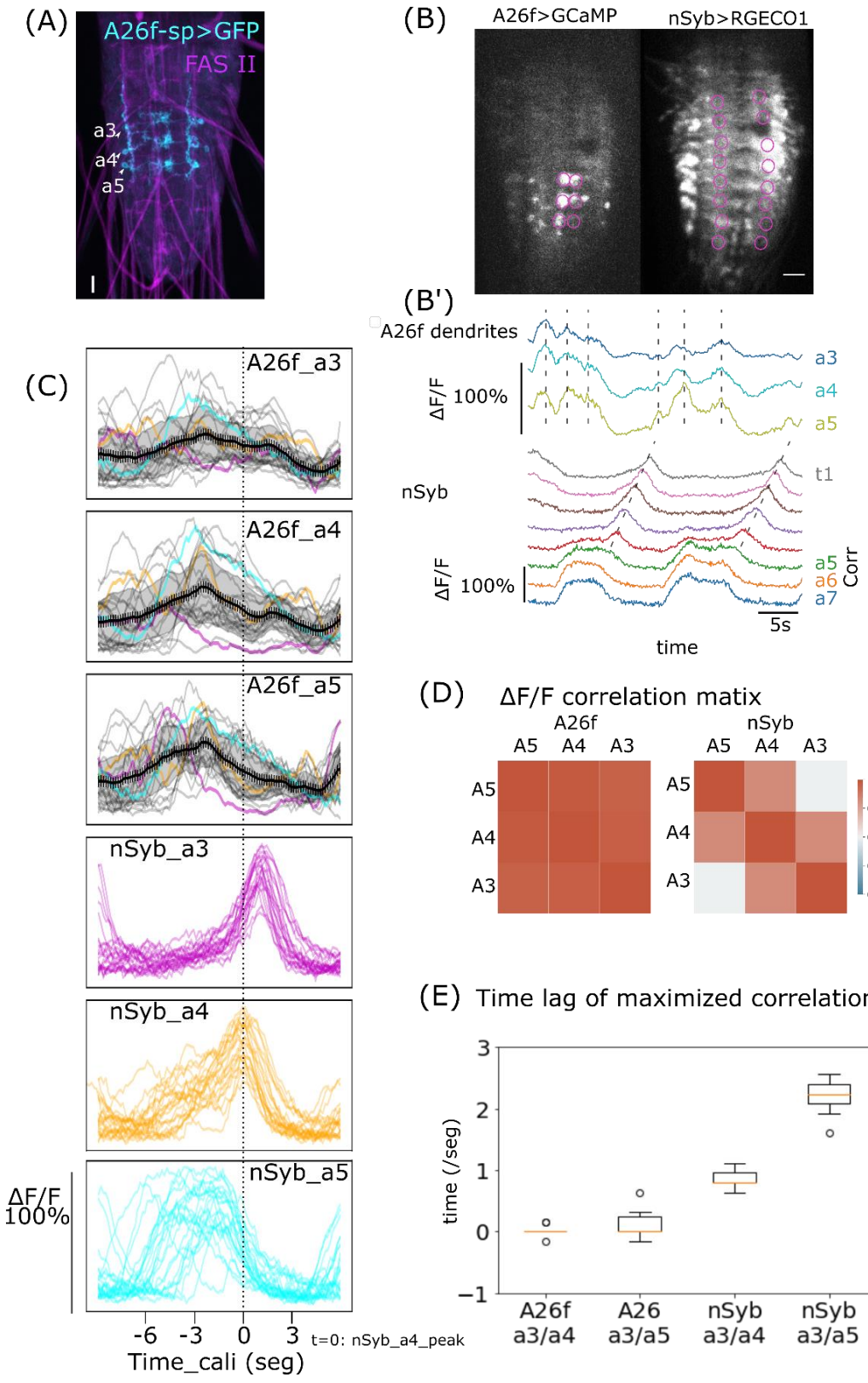
(A)
A26f-sp>GFP
FAS II
a3
a4
a5
(B)
A26f>GCaMP
nSyb>RGECO1
(B')
A26f dendrites
ΔF/F
100%
a3
a4
a5
nSyb
t1
ΔF/F
100%
a5
a6
a7
Corr
5s
time
(C)
A26f_a3
A26f_a4
A26f_a5
nSyb_a3
nSyb_a4
nSyb_a5
ΔF/F
100%
-6 -3 0 3
t=0: nSyb_a4_peak
Time_cali (seg)
(D)
ΔF/F correlation matix
A26f
A5 A4 A3
nSyb
A5 A4 A3
A5
A4
A3
1.00
0.75
0.50
0.25
0.00
(E)
Time lag of maximized correlation
time (/seg)
3
2
1
0
−1
A26f
a3/a4
A26
a3/a5
nSyb
a3/a4
nSyb
a3/a5

Figure 4.2 A26f neurons show synchronous activity across segments

(A) Confocal images of *A26-sp* > *GFP*. Scale bar: 20 μm. **(B-B')** Example activity of A26f neurons compared with neurons targeted by the pan-neuronal driver *nSyb-LexA* (nSyb-neurons). **(B)** A still image of the neuronal fluorescence during dual-color imaging. **Left**: A26f neurons. **Right**: nSyb-neurons. Scale bars: 20 μm. Pink circles: ROIs that are manually selected to analyze the fluorescence. **(B')** Simultaneous changes of fluorescence compared with the baseline ΔF/F of the dendrites of A26f neurons in neuromeres A3-A5 and the neurites of nSyb-neurons in neuromeres T1-A7. **(C)** The overlapped and averaged ΔF/F as described in (B') (n = 18 traces, 6 animals). Time is aligned to the two moments when the ΔF/F of nSyb-neurons maximizes at segment A4 and segment A1. In the upper three panels for A26f neurons, the black line and gray shading represent the average ΔF/F and the standard error of A26f neuronal ΔF/F, and the colored lines show three representative traces. **(D)** The correlation matrix of the ΔF/F of A26f neurons and the nSyb-neuron. **(E)** The time lag maximizes the correlation of ΔF/F between segments by moving the traces in panel C.

4-3. Identification of A31c, a GABAergic interneuron presynaptic with A26f neurons

To understand the neural circuit controlling the A26f – LTM system, I searched for the upstream neurons of A26f and identified a segmentally repeated interneuron A31c as a candidate. I first identified a GAL4 driver (*A31c-a8-GAL4*) targeting the A31c neuron in neuromere A8, which shows the potential to synapse with the A26f neurons from the location of its neurites (Figure 4.3 A). I then reviewed the images in the FlyLight database, a database showing the expression pattern of GAL4 lines in CNS, to search for genetic drivers that target A31c neurons in other neuromeres (Li et al., 2014). I identified several genetic drivers to target this neuron, including a split GAL4 driver (*A31c-a8-sp*) specifically targeting the A31c neuron in segment A8, a split GAL4 driver (*A31c-sp*) targeting the A31c neurons in neuromeres A2-A8, and a LexA driver (*A31c-LexA*) targets A31c neurons stochastically.

To characterize the morphology of A31c neurons, I used the Multi-Color FLP-Out system to label the single neurons stochastically (section 1.3.2, Fig 4.3 A), which revealed that the cell body is located at the dorsal cortex and sends the main branch into the dorsal neuropil. The dendritic-like processes are arborized at the ipsilateral side and extend along the DL tract mostly within the neuromere the cell body resides and shortly in the anterior neuromere. The main branch extends straight to the midline, where the boutons are formed locally along the DM tracts and dorsally.

I then used the DenMark and syt::GFP systems to label the pre-and postsynaptic sites (section 1.3.2). The postsynaptic sites were labeled along the DL tracts. The presynaptic site marker syt::GFP was mostly expressed at the medial side, while some lateral presynaptic sites

were also labeled along the main branch at the medial side of the DL tract (Figure 4.3 B). The syt::GFP had no expression near the DL tract in the A31c neuron in neuromere A8 and had expression in a few boutons near the DL tract in neuromere A6, which suggests a segmental difference in the location of the presynaptic sites. I identified A31c neurons as GABAergic neurons by co-staining the *A31 > GFP* with the antibody of small-molecule neurotransmitters (anti-ChAT, anti-VGlut, anti-GABA) (Figure 4.3 C).

Finally, I used *trans*-Tango, a genetic tool for tracing postsynaptic partners, to explore the downstream neurons of A31c. I used *A31c-sp-a8* to drive the expression of *trans*-Tango in downstream neurons. After one day of incubating at 30 °C, *trans*-Tango could be stochastically expressed in a small number of neurons, which enabled the identification of single neurons. In 24 samples with positive expression of the A31c-a8 neuron, I did not see any Tango expression in the peripheral nerves, suggesting that the A31c-a8 neuron is not likely to innervate MNs. I repeatedly identified Tango expression in A26f-like and A02l-like interneurons in segment A7 (four samples showing A26f-a7 neurons; four samples showing A02l neurons from 24 samples; Figure 4.4 A, B, C). I also found that ten samples had a dense expression of *trans*-Tango in the A9 neuromere, though I could not identify the identity of single neurons there. To inspect if the Tango signal is activated by other neurons, I reviewed the expression of Tango in samples that had the same genetics but did not target the A31c-a8 neuron due to the stochastic nature of the gene expression. I did not find the signal of *trans*-Tango in A26f neurons, A02l neurons, or A9 neuromere in those samples, which supported that the *trans*-Tango expression was driven by the A31c neuron. The connectivity between A31c neurons and A26f neurons was also confirmed in the EM reconstruction (Ohyama et al., 2015; Saalfeld et al., 2009).

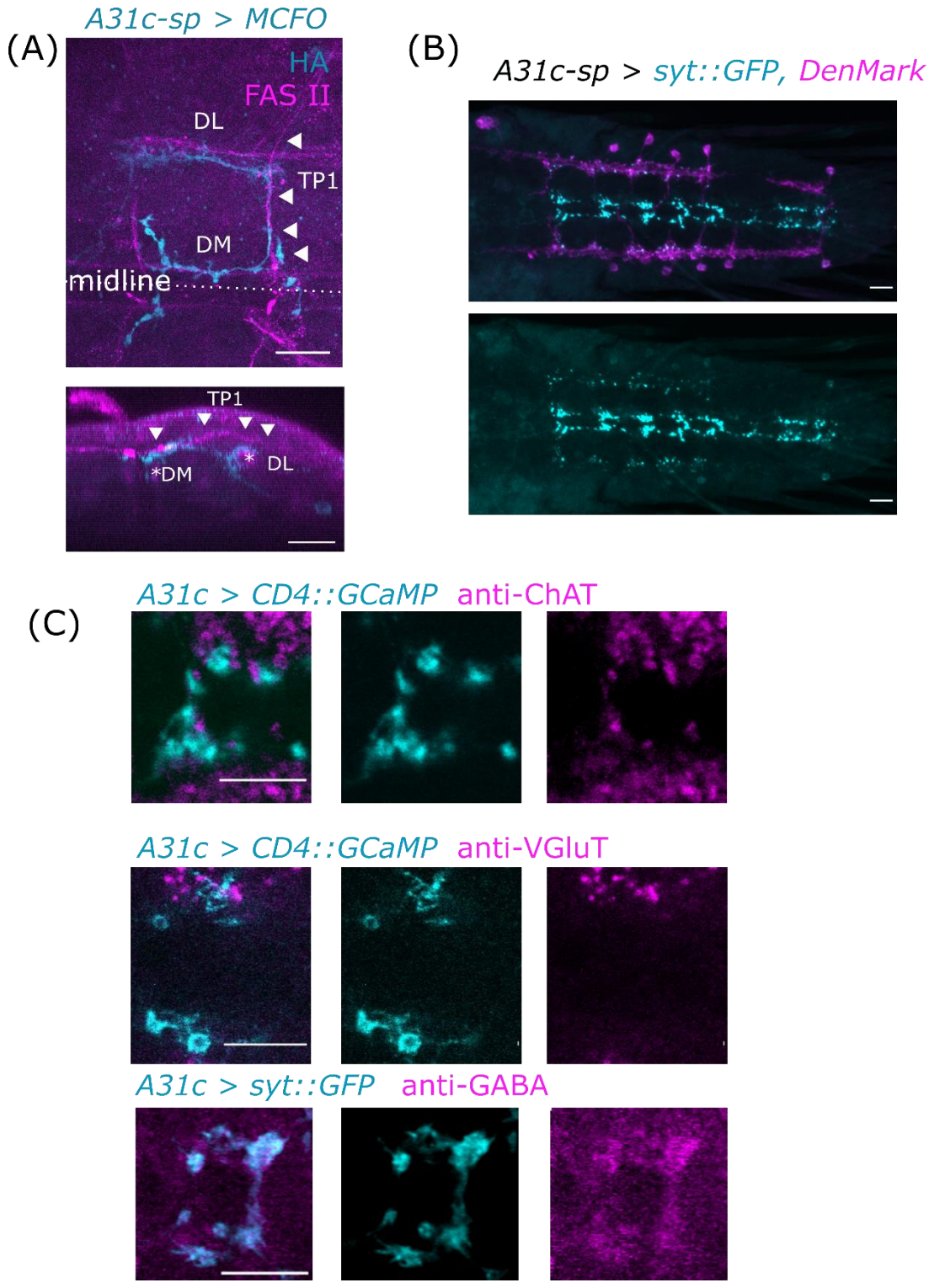
(A)
A31c-sp > MCFO
HA
FAS II
DL
TP1
DM
midline
TP1
*DM
* DL
(B)
A31c-sp > syt::GFP, DenMark
(C)
A31c > CD4::GCaMP anti-ChAT
A31c > CD4::GCaMP anti-VGluT
A31c > syt::GFP anti-GABA

Figure 4.3 Identification of A31c, a GABAergic interneuron sending axon locally along DM tract

(A) Confocal images of the immunostaining of the A31c-a2 neuron labeled by MCFO system and anti-FAS2. Upper: dorsal view. Lower: frontal view. Scale bars: 20 μm. **(B)** Confocal images of the staining of the DenMark and syt::GFP expressed in A31c neurons reveal the location of the pre- and post-synaptic sites. Scale bars: 20 μm. **(C)** Confocal images of the co-staining of A31c neurons and antibodies for neurotransmitters Scale bars: 10 μm.

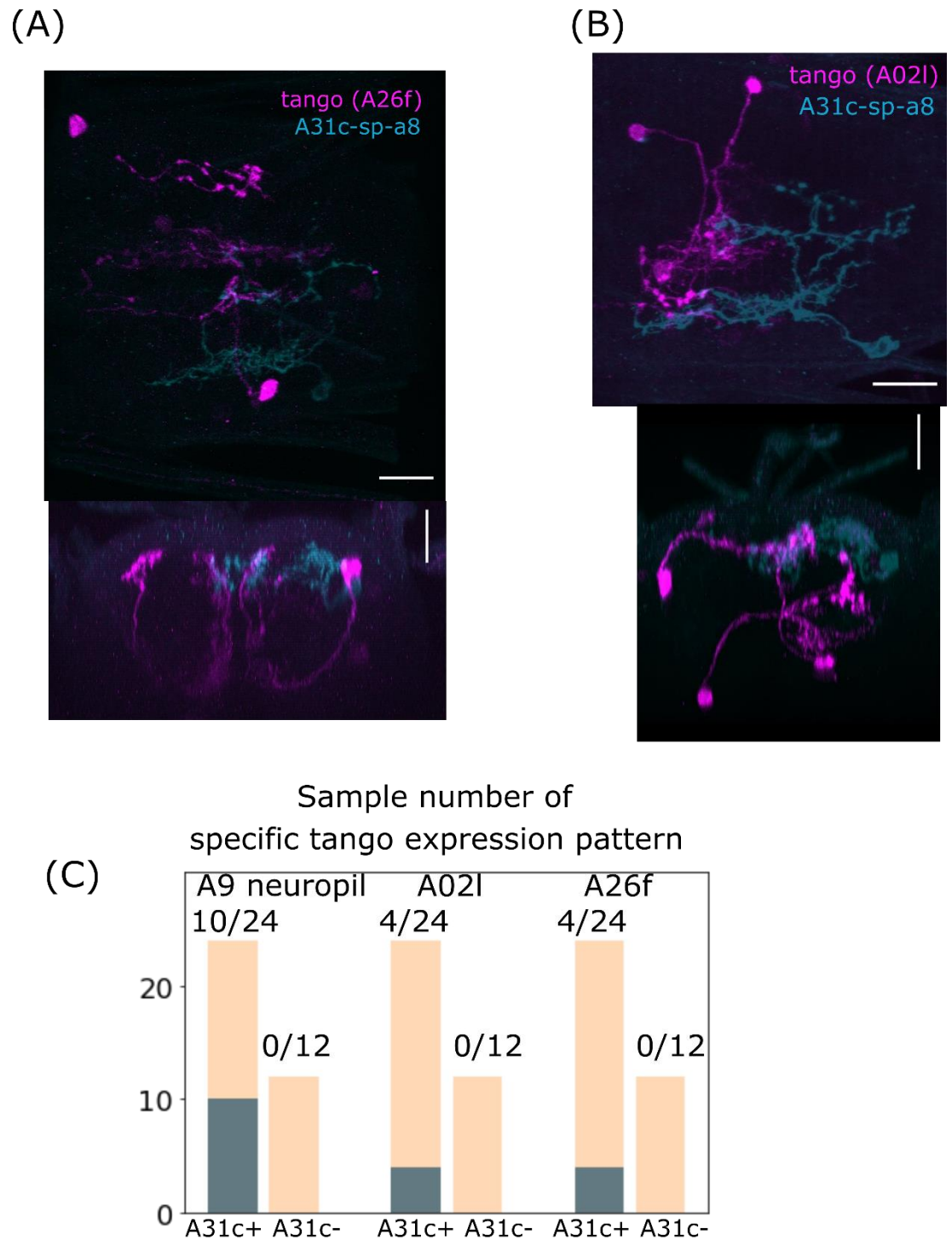

Figure 4.4 *A31c-sp-a8* drives tango expression in postsynaptic partners A26f and A02l

neurons

(A) *A31c-sp-a8* drives the expression of tango in the A26f-a7 neuron. Upper: dorsal view. Lower: frontal view. Scale bar: 20 μm**. (B)** *A31c-sp-a8* drives the expression of tango in the A02l-a7 neuron. Upper: dorsal view. Lower: frontal view. Scale bar: 20 μm**. (C)** The number of samples that show expression in the structures/neurons that are repeatedly identified. A31c+: samples show GFP expression in the A31c-a8 neuron targeted by GAL4. A31c-: samples do not show GFP expression in the A31c-a8 neuron due to the stochasticity of the GAL4 driver.

4-4. A31c neurons are coactivated during the initiation of forward wave

To examine the activity of A31c neurons, I used dual-color calcium imaging to monitor the activity of A31c neurons by *A31c-sp > CD4::GCAMP6f* and the pan-neural activity state by *nSyb-LexA > RGECO1*. I found that A31c neurons are mainly activated during the posterior synchronous activity (Psync) and the fictive forward wave (Figure 4.5 A). The activity during forward locomotion can be separated into two periods. At the initiation of forward locomotion, all abdominal A31c neurons show burst-like coactivation during the Psync preceding the forward wave (Figure 4.5 A, B; Pulver et al., 2015). During the forward wave following the Psync A31c neurons in posterior segments A6-A8 are silent but A31c neurons in anterior segments A2-A5 are re-activated in sync. The fluorescence starts to decay near the moment when the activity of the segmental neurons labeled with the pan-neuronal driver *nSyb-LexA* (nSyb-neurons) maximizes (Figure 4.5 B). The activity of A31c neurons in anterior and posterior segments has a higher correlation than that of the group activity of neurons labeled by nSyb-neurons, revealing that coactivation is an uncommon feature of A31c neurons (Figure 4.5 C). I also compared the activity of A31c neurons and nSyb-neurons when the activity of nSyb_a7 peaks at the Psync. I found a similar activity level in A31c neurons in anterior and posterior segments, whereas the activity of posterior nSyb-neurons is much higher than that of the anterior ones (Figure 4.5 E). During the BW, A31c neurons can show weak wave-like activity, but the peak amplitude of the wave-like activity in the A31c_a4 neuron during the BW was lower than the peak during the FW or at the initiation phase of the FW (Figure 4.5 D).

As both A26f neurons and A31c neurons are showing robust synchronous activity at

the initiation of FW, to know the sequence of activation in detail, I then monitored the activity of the two neurons simultaneously by using *A31c-LexA* to drive the expression of jRGECO1b and *A26f-GAL4* to drive the expression of GCaMP. I found that the synchronous peak of A31c neurons was earlier than the synchronous peak of A26f neurons. The peak of A26f neurons has similar timing to the reactivation of A31c neurons in anterior segments (Figure 4.5 F).

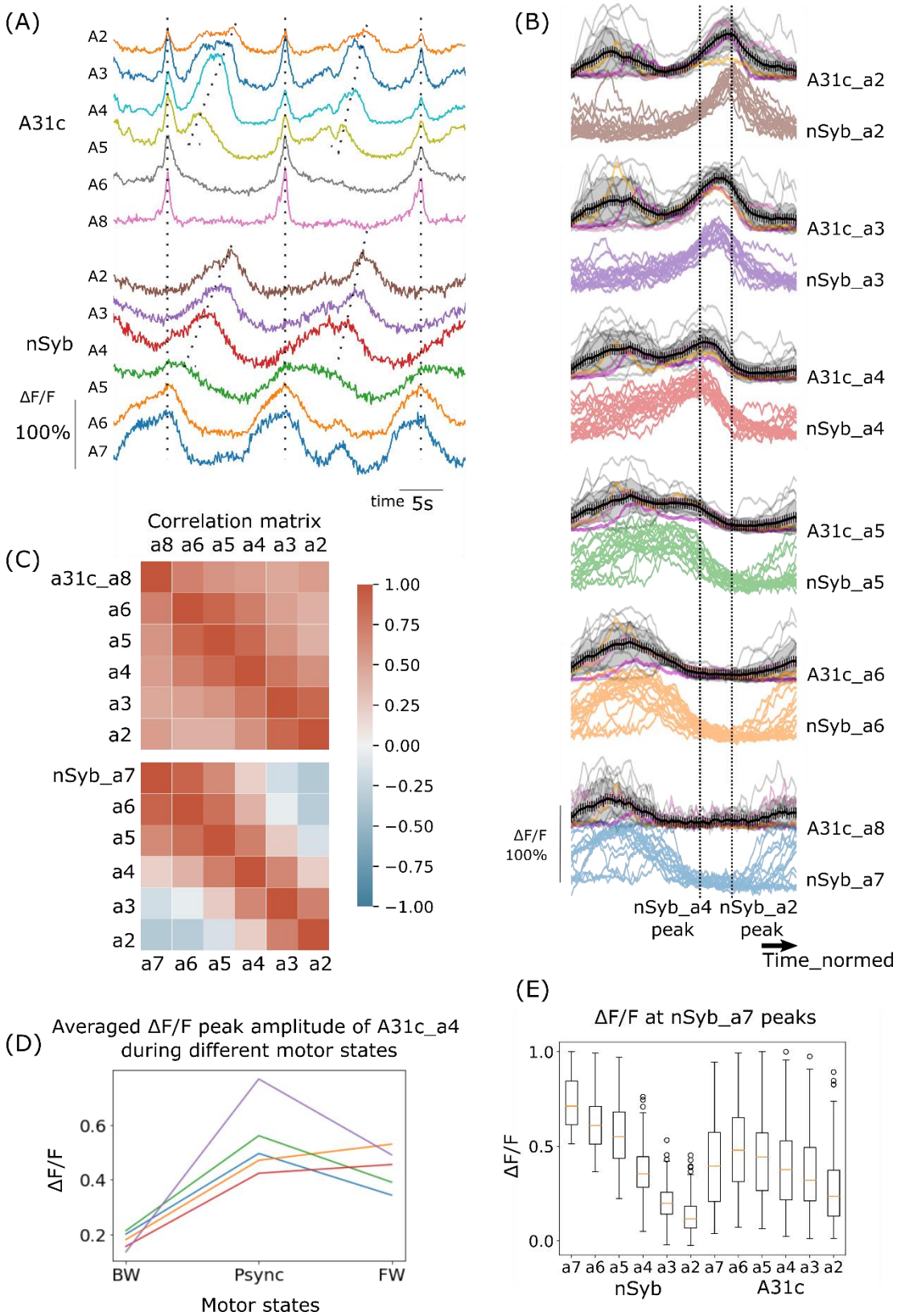
(A)
A31c
A2
A3
A4
A5
A6
A8
nSyb
A2
A3
A4
A5
A6
A7
ΔF/F
100%
time 5s
(B)
A31c_a2
nSyb_a2
A31c_a3
nSyb_a3
A31c_a4
nSyb_a4
A31c_a5
nSyb_a5
A31c_a6
nSyb_a6
A31c_a8
nSyb_a7
ΔF/F
100%
nSyb_a4 peak
nSyb_a2 peak
Time_normed
(C)
Correlation matrix
a8 a6 a5 a4 a3 a2
a31c_a8
a6
a5
a4
a3
a2
nSyb_a7
a6
a5
a4
a3
a2
a7 a6 a5 a4 a3 a2
1.00
0.75
0.50
0.25
0.00
−0.25
−0.50
−0.75
−1.00
(D)
Averaged ΔF/F peak amplitude of A31c_a4
during different motor states
ΔF/F
0.6
0.4
0.2
BW
Psync
FW
Motor states
(E)
ΔF/F at nSyb_a7 peaks
ΔF/F
1.0
0.5
0.0
a7 a6 a5 a4 a3 a2 a7 a6 a5 a4 a3 a2
nSyb
A31c

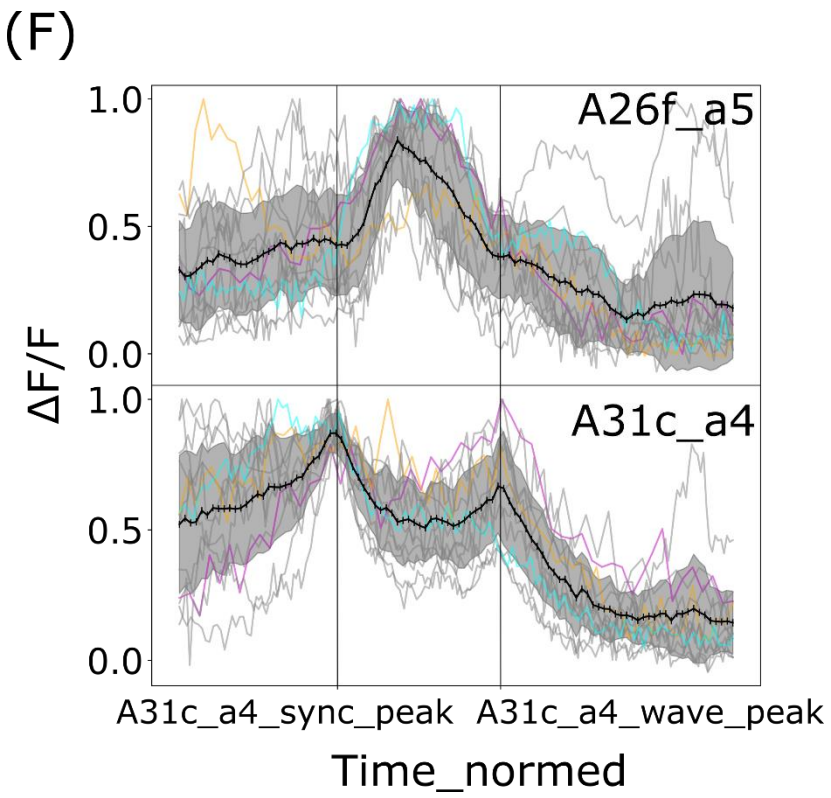

Figure 4.5 A31c neurons exhibit synchronous activity across segments and wave-like decay

(A) Example fluorescence of A31c neurons and neurons targeted by the pan-neuronal driver *nSyb-LexA* (nSyb-neurons) during forward waves. **(B)** The fluorescence change compared with the baseline (ΔF/F) of A31c neurons and nSyb-neurons during the forward wave (n = 15 traces, 5 animals). Time is aligned to the two moments when ΔF/F of nSyb-neurons maximizes at segment A4 and segment A2. In each panel, the upper side shows the ΔF/F of A31c neurons, and the lower side shows the ΔF/F of nSyb-neurons. On the upper side, the black line and gray shading represent the average activity and standard error of the ΔF/F of A31c neurons, while the colored lines show three representative traces. On the lower side, the colored lines are the traces of nSyb-neurons segmental ΔF/F. **(C)** Correlation matrix of the ΔF/F of different segments of A31c neurons and

nSyb-neurons. **(D)** Comparison of the averaged peak amplitude of ΔF/F of the A31c neuron in segment A4 in the different motor states. BW: backward wave state. Psync: Posterior synchronous activity state before a forward wave. FW: forward wave state. (5 animals; for each animal, n_BW ≥ 1, n_FW and n_Psync ≥ 4) **(E)** Comparison of ΔF/F in each segment of nSyb-neurons and A31c neurons when the ΔF/F of the A7 segment of nSyb-neurons maximizes during posterior synchronous activity. **(F)** Example ΔF/F of the A31c_a4 neuron expressing jRCaMP1b and the A26f_a5 neuron expressing GCaMP during forward waves. (n = 13 traces, 7 animals) Time is aligned at the two moments when the ΔF/F of the A31c_a4 neuron maximizes during the synchronous activity and the wave-like activity. The black line and gray shading represent the average activity and standard error. Colored lines show three representative traces.

PART II: Perturbational analysis

4-5. Optogenetic activation of A26f neurons causes the reduced contraction of LTM during forward cycles in the Cartesian preparation

Based on the previous results, A26f neurons should give inhibitory outputs to MNs innervating LTM. To assess the response of LTM to the activation of A26f neurons, I optogenetically activated A26f neurons with muscular imaging in a preparation called Cartesian preparation that allows the peristaltic movement (Figure 4.6 A, B; section 2.2.6). I combined the usage of the optogenetic activator *UAS-CsChrimson* (section 1.3.5) to activate the A26f neurons targeted by *A26f-sp* and the genetic marker *mhc-GFP* expressing GFP in muscular cells to visualize the body wall muscles. I used the animals that have a similar genetic background but have no *A26f-sp* as a control (*yw* > *CsCh*rimson). Because of the spectral overlap between the light to activate CsChrimson and that to stimulate GFP, I used a confocal microscopy system that separates the light for optogenetics and imaging to perform both tasks simultaneously (section 2.2.6; Takagi et al., 2017). To constraint the movement of larva without impairing the peristaltic behavior, I devised a new preparation named Cartesian preparation, in which the larva is fixed by two pins and oriented the lateral side up to visualize the LTM (Figure 4.6 A, B; section 2.2.6). The larva can show spontaneous forward and backward peristalsis-like behavior in this preparation. The larva can contract the LTM remarkably at the initiation of FWs.

I used a green laser beam (559 nm) scanned in a rectangular region at the ventral side of the thoracic segments to activate the A26f neurons (Figure 4.6 B). I carefully set the ROI to

avoid shining the Bolwig's organ directly. I used DeepLabCut to track the muscular length change in several animals (Mathis et al., 2018). As a typical pattern, the LT muscles were contracted before the initiation of FWs (Figure 4.6 C, D). Activation of the A26f neurons caused less contraction of LTM in segment A5 (Figure 4.6 D), while the contraction of VL and DL muscles was almost unchanged. To quantify the change of muscular contraction of LTM, I measured the minimum length of the LT2 muscle in segment A5 manually during each forward cycle. The minimum length significantly increases after the optogenetic stimulation (Figure 4.6 E). This result supports the hypothesis that A26f neurons give inhibitory inputs to motor neurons innervating the LT muscles.

4-6. Optogenetic activation of A26f neurons causes the reduction of tail lag and the increase of locomotion speed in free-crawling larvae

In free crawling larvae, the over-activation of A26f neurons should reduce the tail lag, especially when the LTMs are activated at a high level to generate a long tail lag. To test this hypothesis, I activated A26f neurons in free crawling larvae optogenetically. I used a red LED (660 nm) to activate A26f neurons when the larva showed successive forward cycles (Figure 4.7 A). I used *A26f-sp* to drive the expression of CsChrimson in the A26f neurons in neuromeres A3-A5. I used the animal that has similar genetic insertions but no *A26f.DBD* as a control (*A26f.AD* > *CsCh*rimson). I used the low-concentration agarose plate (0.7 %) as the substrate. After activating A26f neurons, I found a clear transition of the crawling from longer tail lags to shorter ones (Figure 4.7 B). I analyzed the larvae in which the expression of CsChrimson was

confirmed in more than four A26f neurons. I first measured the temporal parameters (the tail lag, the wave duration, and the stride duration) before and after the optogenetic stimulation (Figure 4.7 C). The tail lag was significantly decreased, while the wave duration was increased significantly but with a smaller amplitude. The stride duration was significantly decreased. I then measured the stride length (Figure 4.7 C). Interestingly, the stride length was significantly increased after the stimulation. The speed was increased significantly since both the stride frequency and the stride length were increased.

These results suggest that the activation of A26f neurons can reduce the tail lag but not the wave duration, which results in a shorter stride duration. The increase of the stride length caused by activation of A26f neurons implies an unexpected function of A26f neurons. One hypothesis is that the over-inhibition of LTM led to more contraction of the posterior segments than usual to generate the required extension of the head, which led to a longer stride length. Another interesting finding is that the tail lag is likely to be dependent on the substrate's stiffness and moisture. Initially, I used the agarose plates of about 1.5% agarose as substrates, which is generally used to assay the larval behavior. However, larvae were not likely to show successive crawling of long-tail lags under this condition, which made it difficult to understand if the tail lag is reduced by the optogenetic perturbation (data not shown). I then switched to using the agarose plates with a lower concentration (0.7% agarose), which makes the substrate softer and moister. Larvae are more sunk in the substrate and kept moist during crawling when placed on this plate. The crawling gait seems to be affected. Forward peristalses of long-tail lag become more frequent.

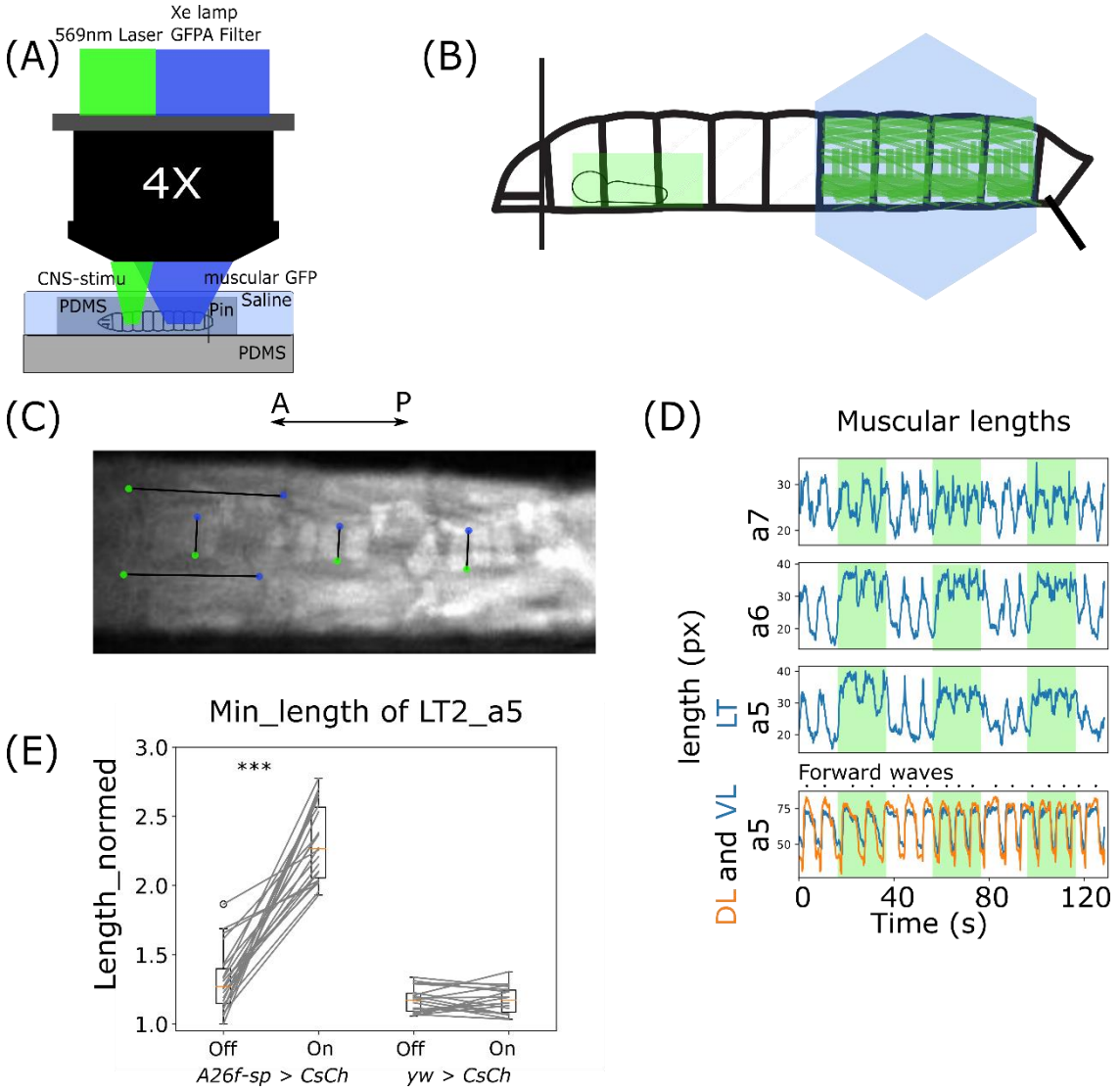

Figure 4.6 Activation of A26f neurons causes the reduced level of contraction in forward cycles in the Cartesian preparation

(A) Schematic drawing of the Cartesian preparation to combine optogenetics and muscular imaging (section 2.2.5). **(B)** Schematic drawing of the setup from the top view. Green rectangular: CNS is illuminated by the 559 nm laser. Blue hexagon: muscles expressing *mhc-GFP* are

illuminated by blue light from a Xe lamp. **(C)** Example view of muscles in the Cartesian preparation. Lines and dots represent the muscles tracked by DeepLabCut (Mathis et al., 2018). **(D)** Example tracking of the LT2 muscle in segments A5-A7 and DL/VL in segment A5. Green shading: periods of optogenetic stimulation. **(E)** Quantification of the minimum length during forward peristalsis (n = 22 trials, 4 animals for *A26f-sp > CsCh*; n = 18 trials, 4 animals for *yw > CsCh;* ***p < 0.0005, paired t-test). p-values in **(E)** are shown in the following table.

p-values in Figure 4.6

	p-values of *A26f-sp > CsCh* group	p-values of *yw > CsCh* group
min_length	<1e-7	0.59718

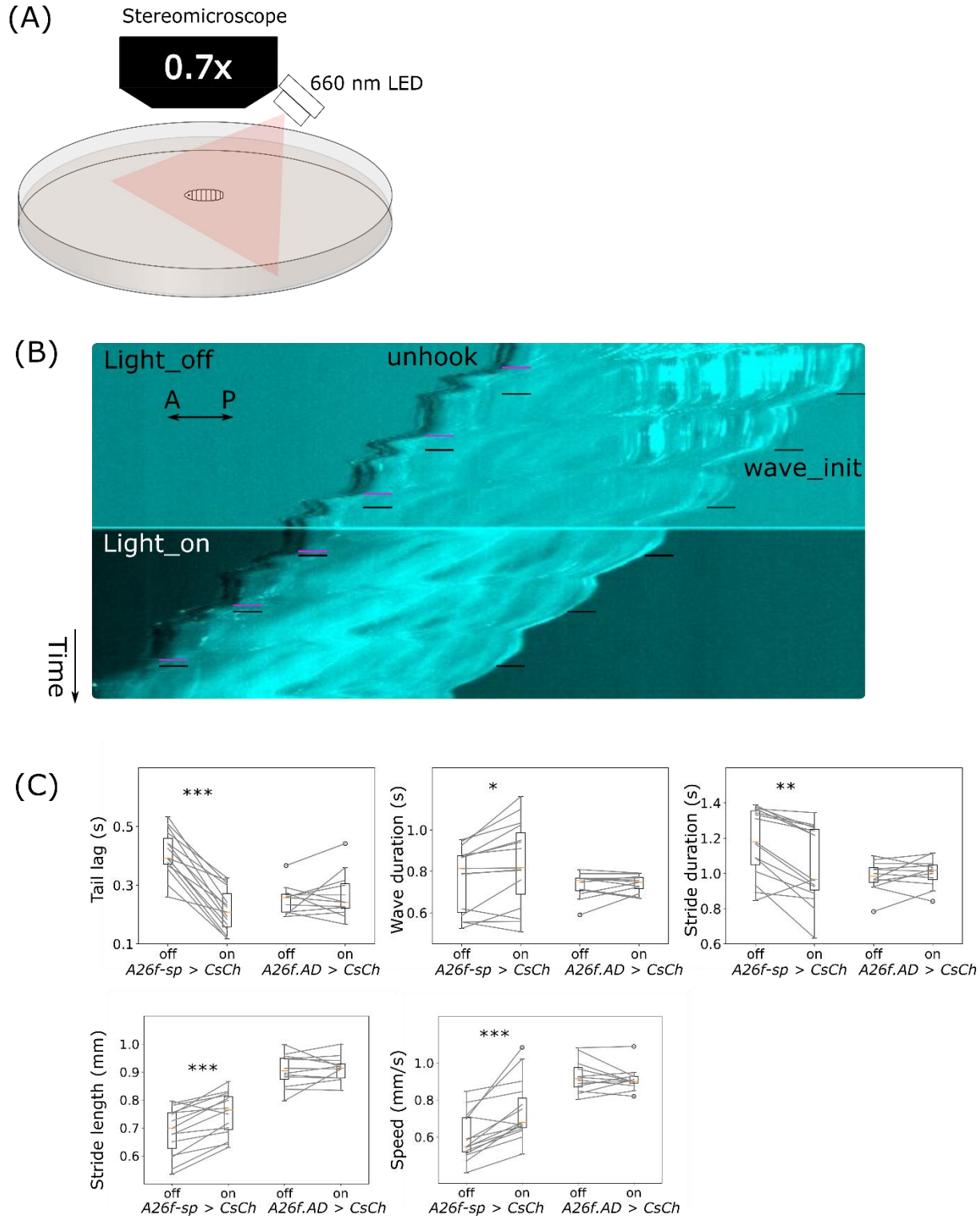
(A)
Stereomicroscope
0.7x
660 nm LED
(B)
Light_off
A
P
unhook
wave_init
Light_on
Time
(C)
Tail lag (s)
Wave duration (s)
Stride duration (s)
Stride length (mm)
Speed (mm/s)
***
*
**
off
on
A26f-sp > CsCh
A26f.AD > CsCh

Figure 4.7 Activation of A26f neurons causes the reduction of the tail lag and the increase of crawling speed

(A) Schematic drawing of the experimental setup for the optogenetic assay in free-crawling larvae. **(B)** Kymograph showing the movement of head and tail during the forward cycles before and after optogenetic stimulation. Magenta line: timing of unhooking. Blackline: timing of wave initiation. **(C)** Quantification of the temporal parameters (tail lag, wave duration, stride duration), stride length, and speed in the successive forward cycles before and after the light stimulation (n = 15 trials, 5 animals for *A26f-sp* > *CsCh*; n = 12 trials, 4 animals for *A26f.AD* > *CsCh*; ***p < 0.0005, **p < 0.005, *p < 0.05 paired t-test). p-values in **(C)** are shown in the following table.

p-values in Figure 4.7

	p-value of *A26f-sp* > *CsCh* group	p-value of *A26f.AD* > *CsCh* group
Tail lag	<1e-7	0.46624
Wave duration	0.0066	0.59693
Stride duration	0.00051	0.32883
Stride length	0.00013	0.65693
Speed	0.00016	0.44620

4-7. Optogenetic activation of A31c neurons causes the contraction of LTM in the fillet preparation

As the previous results suggest, A26f neurons should receive inhibitory inputs from A31c neurons. It leads to the hypothesis that activation of A31c neurons can upregulate the LTM's activity. To test that, I optogenetically activated A31c neurons and monitored the muscular lengths of the LTM in the fillet preparation (Figure 4.8 A). I used an optogenetic activator Channelrhodopsin 2 T159C (Chr2.T159C), a variant of Channelrhodopsin 2, to activate A26f neurons targeted by *A26f-sp*. I used the animal that only carries the *UAS-Chr2.T159C* as the control group (*yw > Chr2.T159C*). As the *A31c-sp* driver can target neurons out of VNC, the laser was scanned at the abdominal neuromeres to avoid activating the SEG or brain neurons. After the dissection, I waited for about 10 minutes when the larva stopped the frequent spontaneous axial waves. The optogenetic stimuli caused LTM's contraction in abdominal neuromeres (Fig. 4.8 B, C). I observed that the contraction could happen in all the visualized segments in segments A3-A8. I measured the minimum length of muscles in the A5 segment at the start and the end of the stimulation. The muscular length was significantly reduced (Fig. 4.8 D).

These results suggest that the activation of A31c neurons is sufficient to activate the LTM. As no apparent contraction of other muscles was confirmed, I assume that the A31c neurons mainly regulate the activity of the LT muscles.

4-8. Optogenetic activation of A31c neurons causes the increase of tail lag in free-crawling

larvae

As the activation of A31c neurons causes the over-contraction of LTM, the tail lag might be extended to avoid over-pressurizing the larva. To test this hypothesis, I activated A31c neurons in free crawling larvae optogenetically. I used a similar setup when activating A26f neurons (Figure 4.7 A). To avoid targeting the neurons in the brain, I used a genetic system *VNC-CsChrimson* that refines the expression of CsChrimson to neurons in VNC targeted by the *A31c-sp*. The resulting expression of the CsChrimson can be seen in A31c neurons in neuromeres A2-A8. I used the animal that has similar genetic insertions but no GAL4 driver as a control (*yw > VNC-CsCh*rimson). I used a setup similar to the one used in section 4.6 except that the 1.5% concentration agarose plate was used as the substrate. The optogenetic stimuli can induce instant turning or stopping responses that halt the successive crawling.

To assess the change of tail lag responding to the stimulation, I analyzed the strides if the forward cycles were not halted, or the forward cycles were reinitiated. Similar to the behavior assay when activating A26f neurons, I measured the tail lag, the wave duration, the stride duration, the stride length, and the speed (Figure 4.9 A-E). The tail lag was significantly increased. The wave duration was slightly increased with no statistical significance. The stride duration was significantly increased. The stride length was not significantly increased in the *A31c-sp > VNC-CsChrimson*, but the stride length was significantly increased in the control group (Figure 4.9 D). The speed decreased significantly for both the experimental and control groups.

These results suggest that the activation of A31c neurons is sufficient to increase the

tail lag and stride duration, thus decreasing the speed. However, the relationship in stride length is not likely to be differentiated since the unexpected decrease of the stride length in the control group. Further experiments might be required to obtain some more conclusive results. Also, though the expression of *A31c-sp* is confined to A31c neurons in abdominal neuromeres for most markers, combination usage with *VNC-CsChrimson* can label other neurons in abdominal segments. A sparser genetic targeting is required to understand further the larval behavior upon the activation of A31c neurons.

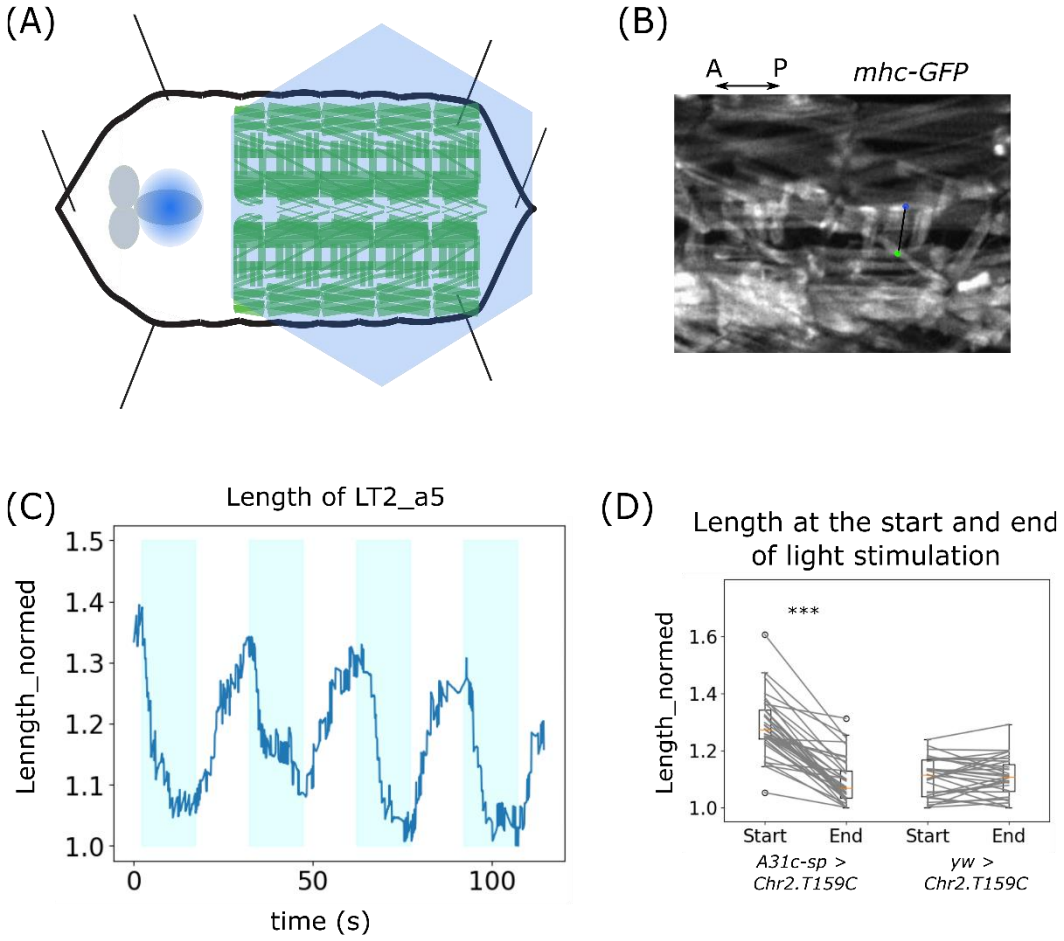

Figure 4.8 Activation of A31c neurons causes the contraction of LT muscles in the fillet preparation

(A) Schematic drawing of the setup for combining optogenetics and muscular imaging in the fillet preparation. Blue circle: the 488nm laser stimulation focusing on the VNC to activate the VNC neurons. Hexagon: the blue Xe lamp illumination to visualize the muscles. **(B)** Example view of muscles in the Cartesian preparation. Lines and dots represent the tracked muscles. **(C)** Example tracking of the LT2 muscle in segments A5-A7. Shading: periods of optogenetic stimulation. **(D)** Quantification of the muscular length at the start and end of the light stimulation (4 animals for

both groups; ***p < 0.0005, paired t-test). P-values in **(D)** are shown in the following table.

p-values in Figure 4.8

	p-value of *A31c-sp* > *Chr2.T159C* group	p-value of *yw* > *Ch2.T159C* group
min_length	<1e-7	0.59718

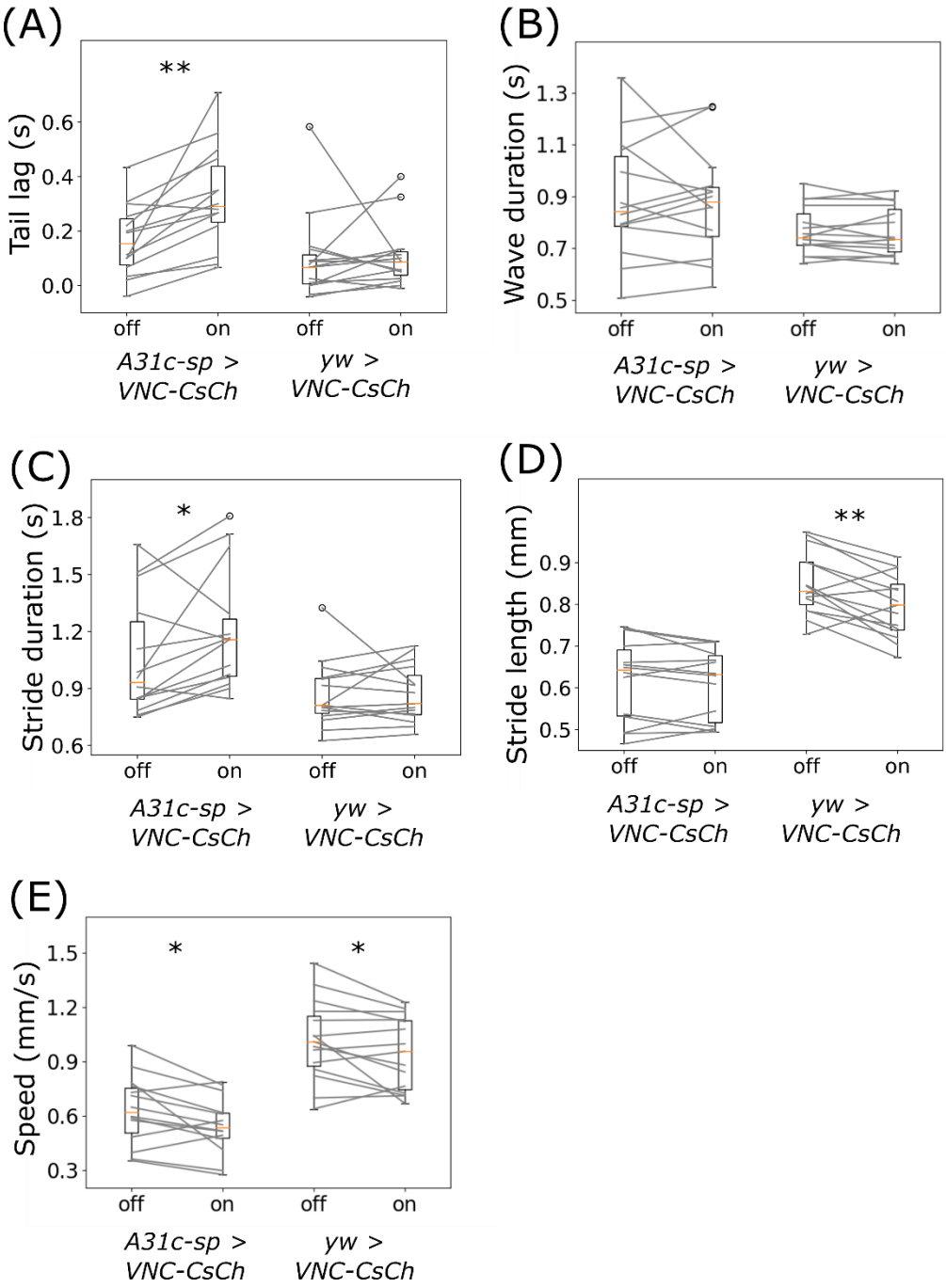

Figure 4.9 Activation of A31c neurons increase the tail lag and reduce the speed

(A-E) Quantification of the crawling parameters before and after the light stimulation in successive forward cycles (n = 15 trials, 5 animals for *A31c-sp > VNC-CsCh*; n = 15 trails, 5 animals for *yw > VNC-CsCh*; ***p < 0.0005, **p < 0.005, *p < 0.05 paired t-test). **(A)** Tail lag. **(B)** Wave duration. **(C)** Stride duration. **(D)** Stride length. **I** Speed. p-values in **(A-E)** are shown in the following table.

p-values in Figure 4.9

	p-values of *A31c-sp > VNC-CsCh* group	p-values of *yw > VNC-CsCh* group
Tail lag	0.00168	0.88724
Wave duration	0.69820	0.71727
Stride duration	0.04502	0.95159
Stride length	0.35982	0.00419
Speed	0.01888	0.04847

4-9. LTM are contracted at an undesired level upon optogenetic inhibition of A31c or A26f neurons

Next, I examined if the interneurons of interest were required to generate the desired contraction of LTM. Although it was supposed that the interneurons A31c and A26f are mainly regulating the inhibitory inputs to MNs innervating LTM, I supposed the level of contraction should be affected by an inappropriate timing or level of inhibitory inputs. To test that, I used optogenetic silencing with muscular imaging in the Cartesian preparation (as described in section 2.2.5; Figure 4.5).

First, I inhibited A26f neurons by expressing GtACR1, an optogenetic silencing tool (introduced in section 1.3.5). I used the animal that only carries *UAS-GtACR1* as a control (*yw > GtACR1*). I measured the minimum length of the LT2 muscle in segment A5 in each forward cycle. I found that the minimum length decreased when A26f neurons were inhibited optogenetically (Figure 4.10 A, B). Thus, the activation of A26f neurons is not only sufficient to inhibit the contraction of LTM but also is required to generate the desired level of contraction during forward cycles. Then, I optogenetically inhibited A31c neurons by using a similar setup. The optogenetic inhibition caused the increase of the minimum length of the LT2 muscle in segment A5 during forward cycles (Figure 4.10 A, B).

These results suggest that A26f neurons downregulate the activity of LTM, while A31c neurons upregulate. Therefore, optogenetic inhibiting A26f neurons or A31c neurons can cause a deficit in the modulation of the motor output to LTM.

4-10. Optogenetic inhibition of A26f neurons causes the increase of tail lag and reduction of speed

Next, I asked if A26f neurons are required to regulate the tail lag and thereby the speed in free crawling. To this end, I optogenetically inhibited A26f neurons during successive forward strides. I used *A26f-sp > GtACR1* for optogenetic inhibition and the animal that only carries heterogenous *UAS-GtACR1* as a control (*yw > GtACR1*). The setup was similar to the optogenetic activation experiment in section 4.7**,** except that the wavelength for optogenetic stimulation was different. I used a 590 nm LED to activate GtACR1 with a power of about 150 μW/mm2. The larvae have innate light avoidance behavior in response to the light. In some trials, the larvae showed turning behavior when the light was turned on. However, larvae can show continuous forward cycles in many trials. I then optogenetically inhibited the A26f neurons and analyzed those trials that the forward cycles were not interrupted.

I found that inhibiting the A26f neurons increased the tail lag and stride duration but had no significant effect on the wave duration (Figure 4.11 A, B, C). The optogenetic inhibition also significantly reduced the stride length but had a less significant effect (Figure 4.11 D). The speed decreased, mainly due to the increased stride duration (Figure 4.11 E). These results suggest that the co-activation of A26f neurons was required to regulate tail lag and speed. Combined with previous analyses on the muscular response to the manipulation of A26f neurons, these results indicate that the A26f neurons are functionally required to produce the appropriate tail lag by modulating the contraction of LTM.

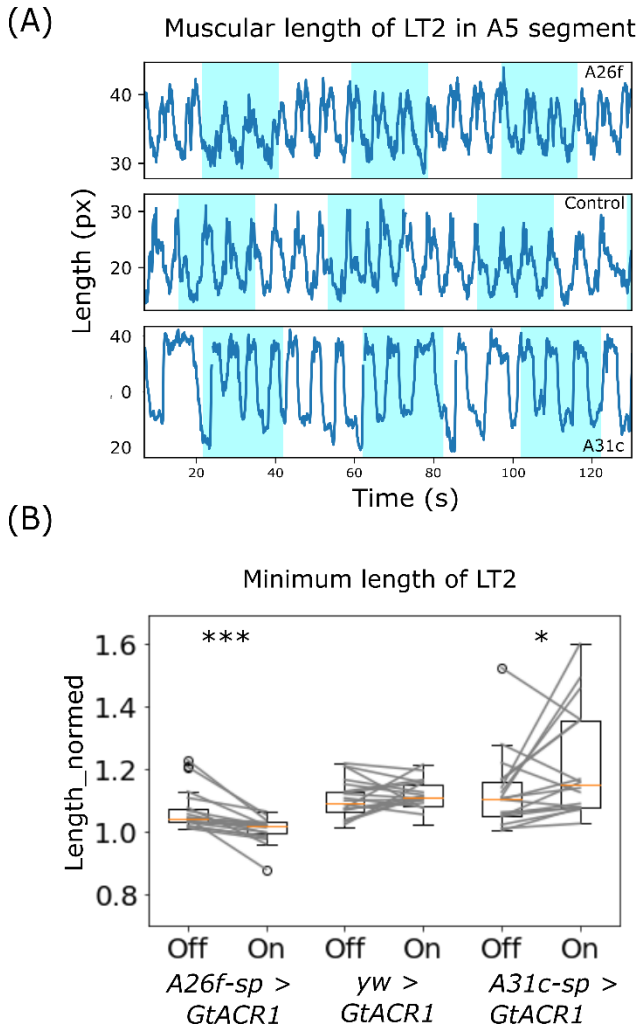

Figure 4.10 Desired contraction of the LT2 muscle requires the modulation input from A31c neurons and A26f neurons

(A) Muscular contraction responses to optogenetic inhibition. Shading: periods of optogenetic stimulation. **(B)** Quantification of the averaged minimum length of the LT2 muscle in segment

A5 during the periods before and after the optogenetic inhibition (6 animals for *A26f-sp* > *GtACR1*; 6 animals for *yw* > *GtACR1*; 5 animals for *A31c-sp* > *GtACR1*; ***p < 0.0005, **p < 0.005, *p < 0.05 paired t-test). p-values in **(B)** are shown in the following table.

p-values in Figure 4.10

	p-value of *A26f-sp* > *GtACR1* group	p-value of *yw* > *GtACR1* group	p-value of *A31c-sp* > *GtACR1* group
Minimum length of LT2	0.00014	0.39067	0.04172

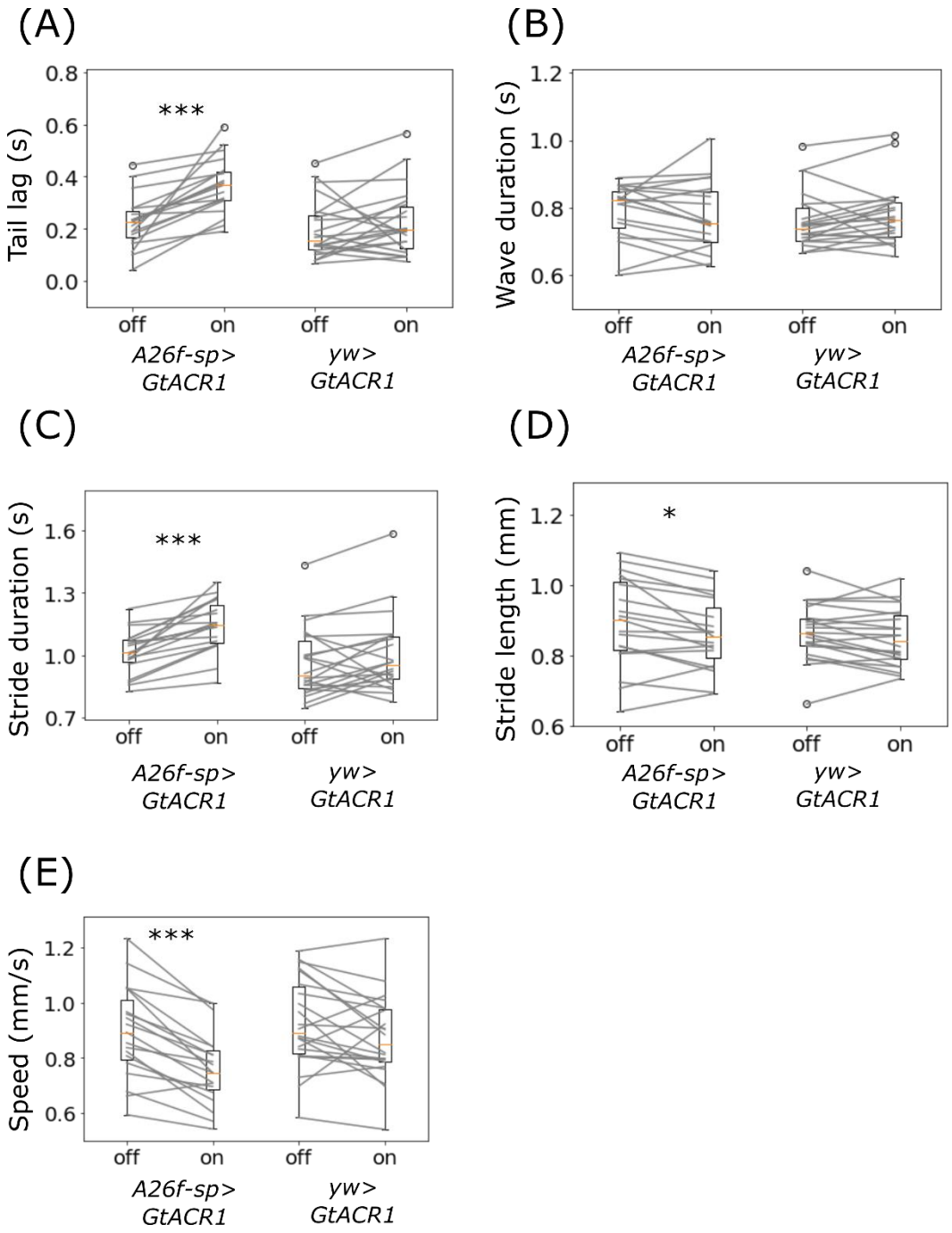

Figure 4.11 Optogenetic inhibition of A26f neurons caused the increase of tail lag and the

reduction of speed

(A-E) Quantification of the crawling parameters before and after the light stimulation in successive forward cycles (n = 19 trials, 7 animals, for *A26f-sp* > *CsCh*; n = 21 trials, 7 animals for *yw* > *CsCh*; ***p < 0.0005, **p < 0.005, *p < 0.05 paired t-test). **(A)** Tail lag. **(B)** Wave duration. **(C)** Stride duration. **(D)** Stride length. **(E)** Speed. p-values in **(A-E)** are shown in the following table.

p-values in Figure 4.11

	p-values of *A26f-sp* > *GtACR1* group	p-values of *yw* > *GtACR1* group
Tail lag	2.7e-05	0.47289
Wave duration	0.69820	0.26956
Stride duration	<1e-5	0.14308
Stride length	0.00769	0.10205
Speed	<1e-5	0.05362

Chapter 5. Conclusion and discussion

Part I: Conclusion

In this study, I investigated the neural circuit to regulate locomotion speed in *Drosophila* larvae. In chapter 3, I demonstrated the change of kinematic parameters and muscular patterns under different speeds. Similar to the walking speed can be modulated by the fraction of time spent in the stance phase, the larva can crawl faster by adjusting the fraction of time spent in the tail lag, a period between the consecutive peristaltic waves. The tail lag is increased differently with the wave duration and is preferably adapted to speed. At the muscular level, the lateral transverse muscles (LTM) in abdominal segments are identified to be crucially involved in the regulation of tail lag. The LTM is contracted together with a duration scaled with the tail lag.

In chapter 4, I demonstrated the identification of two upstream interneurons of the LTM controlling the locomotion speed: the GABAergic interneuron A26f, a premotor neuron specifically innervating the MNs for LTM, and the GABAergic interneuron A31c, a presynaptic partner of A26f. The two interneurons showed synchronous activity respectively across segments preceding the forward wave. Both of them are required for the generation of appropriate activity of LTM. Furthermore, the tail lag but not wave duration are influenced when A26 neurons are inhibited or activated, which leads to speed change. Connectivity

analysis further revealed that the A31c neurons give output to A26f neurons locally and via ascending neurons to communicate with anterior A26f neurons (see the following section 5.1 for details). These results collectively reveal that the synchronous activity of A26f neurons is crucial to the regulation of the speed by adjusting the tail lag.

In the following discussion (section 5.2), the EM reconstruction by Dr. Maarten Zwart confirmed the connectivity from A31c neurons to A26f neurons. Furthermore, the A31c neurons are predominantly innervated by descending neurons. Posterior A31c neurons innervate ascending neurons which can further innervate the anterior A26f neurons. These results further support that the A31c-A26f pathway has an essential role in the control of LTM to regulate the tail lag (Figure 5.2).

In summary, although the peristalsis can be generally described as the sequential wave-like contraction from one end to the other, I find that the duration out of the contraction wave is an essential factor impacting the speed. I demonstrate the mechanism from the muscles to the interneurons. Further work is needed to unravel the descending pathways from the higher control center. These findings revealed a novel speed regulation mechanism in *Drosophila* larvae at the organism, muscular, and neural levels (Figure 5.1). I believe the mechanisms can be applied to a broader range of crawling species.

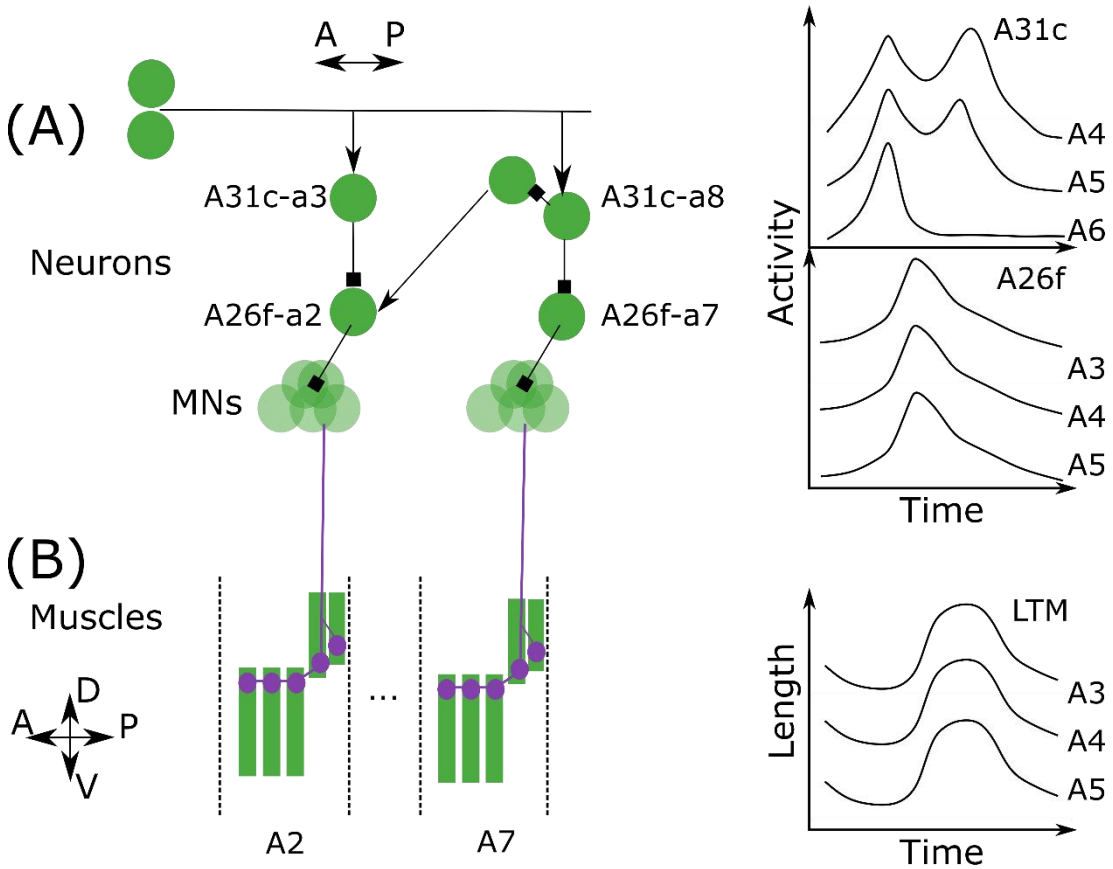
(A)
A
P
A31c-a3
A31c-a8
Neurons
A26f-a2
A26f-a7
MNs
A31c
A4
A5
A6
Activity
A26f
A3
A4
A5
Time
(B)
Muscles
D
A
P
V
A2
A7
LTM
A3
A4
A5
Length
Time

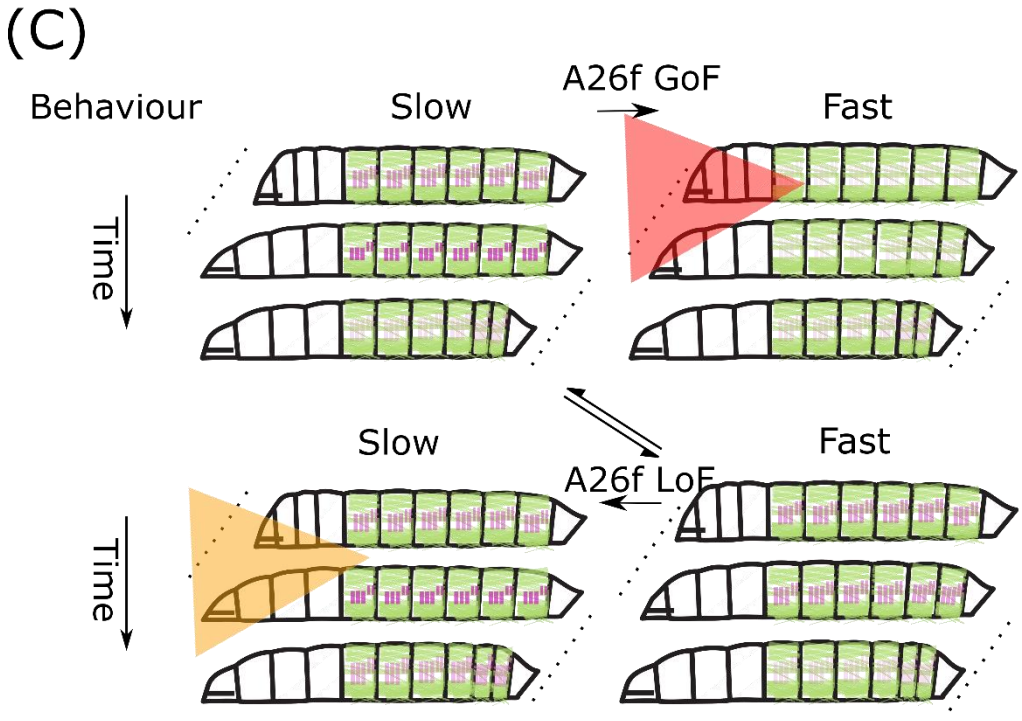
(C)
Behaviour
Slow
A26f GoF
Fast
Time
Slow
Fast
A26f LoF
Time

Figure 5.1 Schematics show the A31c-A26f circuit that controls the activity of LTM and the speed.

(A) Schematic drawing of the architecture of the neural circuit and the activity of component interneurons. **Left**: Circuit diagram. Descending neurons innervate A31c neurons. A31c neurons give inhibitory output to A26f neurons via direct synaptic connection or an ascending neuron. A26f neurons innervate MN that innervates LTM. **Right**: Activity of A31c neurons and A26f neurons. Traces represent activity of A31c neurons (A31c-a4, A31c-a5, A31c-a6) and A26f neurons (A26f-a3, A26f-a4, A26f-a5) from up to bottom. **(B)** Schematic drawing of the arrangement of LT muscles and their activity pattern. **Left**: Layout of LTM in segments A2 and A7. **Right**: LTM contraction in segment A3-A5 from up to bottom. **(C)** Schematic drawing shows the change of behavior in response to optogenetic stimulation. Movement state can also transit between the upper left to the lower right in free crawling larvae. Contraction of muscles is speculated from the GoF/LoF in Cartesian preparation. **Upper**: optogenetic GoF of A26f by CsChrimson causes faster locomotion. **Lower**: optogenetic LoF by GtACR1 causes slower locomotion. The darker purple color represents more contraction.

Part II. Discussion

5-1. EM reconstruction reveals that A26f neurons receive inputs from A31c neurons across segments

To understand the details of the connectivity of this circuit, my collaborator Dr. Maarten Zwart reconstructed the connections from A31c neurons in CATMAID (Saalfeld et al., 2009). He identified A31c neurons in neuromeres A2-A8 in CATMAID (Figure 5.2 A), reconstructed the pre- and post-synaptic partners (Figure 5.2 D and Figure 5.3), and analyzed the connectivity (Figure 5.2 D). He separately analyzed the connectivity of A31c neurons in anterior segments (segments A2 and A3) and posterior segments (segments A7 and A8; Figure 5.3). He found that several descending neurons innervate A31c neurons across segments (Figure 5.3 A). A31c neurons receive most synaptic inputs from the same SEG descending neuron S10. On the other hand, the synaptic output differed for the anterior and posterior A31c neurons (Figure 5.3 A). However, he found that the A26f neurons are among the top three postsynaptic partners of A31c neurons. A26f neurons also receive the synaptic inputs from a descending neuron A19f, one of the top postsynaptic partners of A31c neurons.

The reconstruction of connectivity from EM reconstruction supports my finding that A26f neurons are postsynaptic partners of A31c neurons. It also suggests that the synaptic output of A31c neurons across segments can converge to the anterior A26f neurons via the direct synaptic contact by the anterior A31c neurons or the downstream ascending neurons presynaptic to anterior A26f neurons.

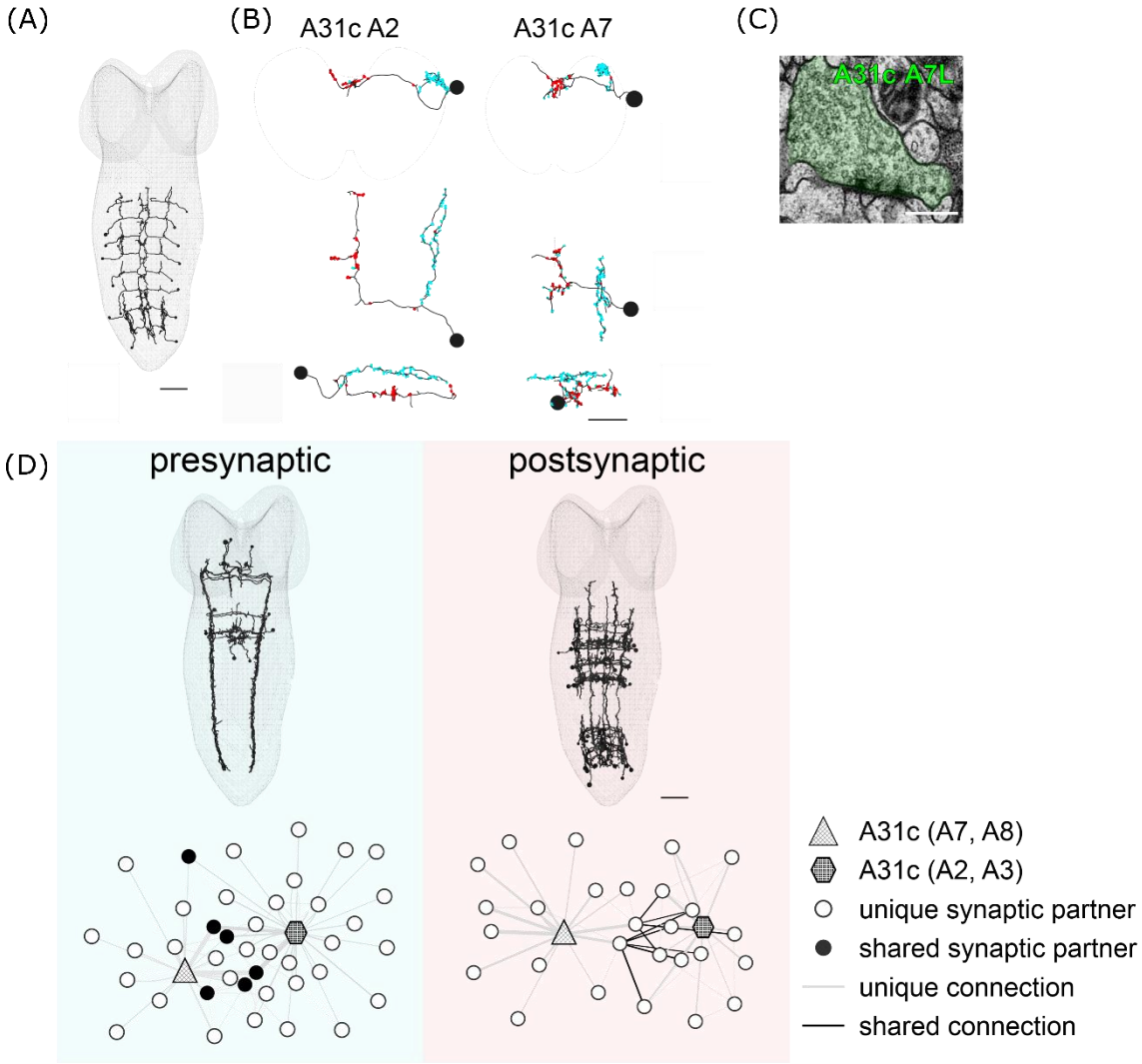

Figure 5.2 EM reconstruction of synaptic partners of A31c neurons

(A) Reconstructed A31c neurons in L1 larval CNS. Scale bar: 20 µm. **(B)** Reconstruction A31c neurons in segments A2 and A7. Scale bar: 10 µm. **(C)** Representative EM volume shows a synaptic contact. Scale bar: 0.5 µm. **(D)** Reconstructed presynaptic partners and postsynaptic partners. **Left**: presynaptic partners of A31c neurons. Descending neurons give synaptic outputs to the A31c across segments. **Right**: postsynaptic partners of A31c neurons. Synaptic outputs of

A31c neurons and their postsynaptic partners converge to the same neurons. This figure is a courtesy of Dr. Maarten Zwart.

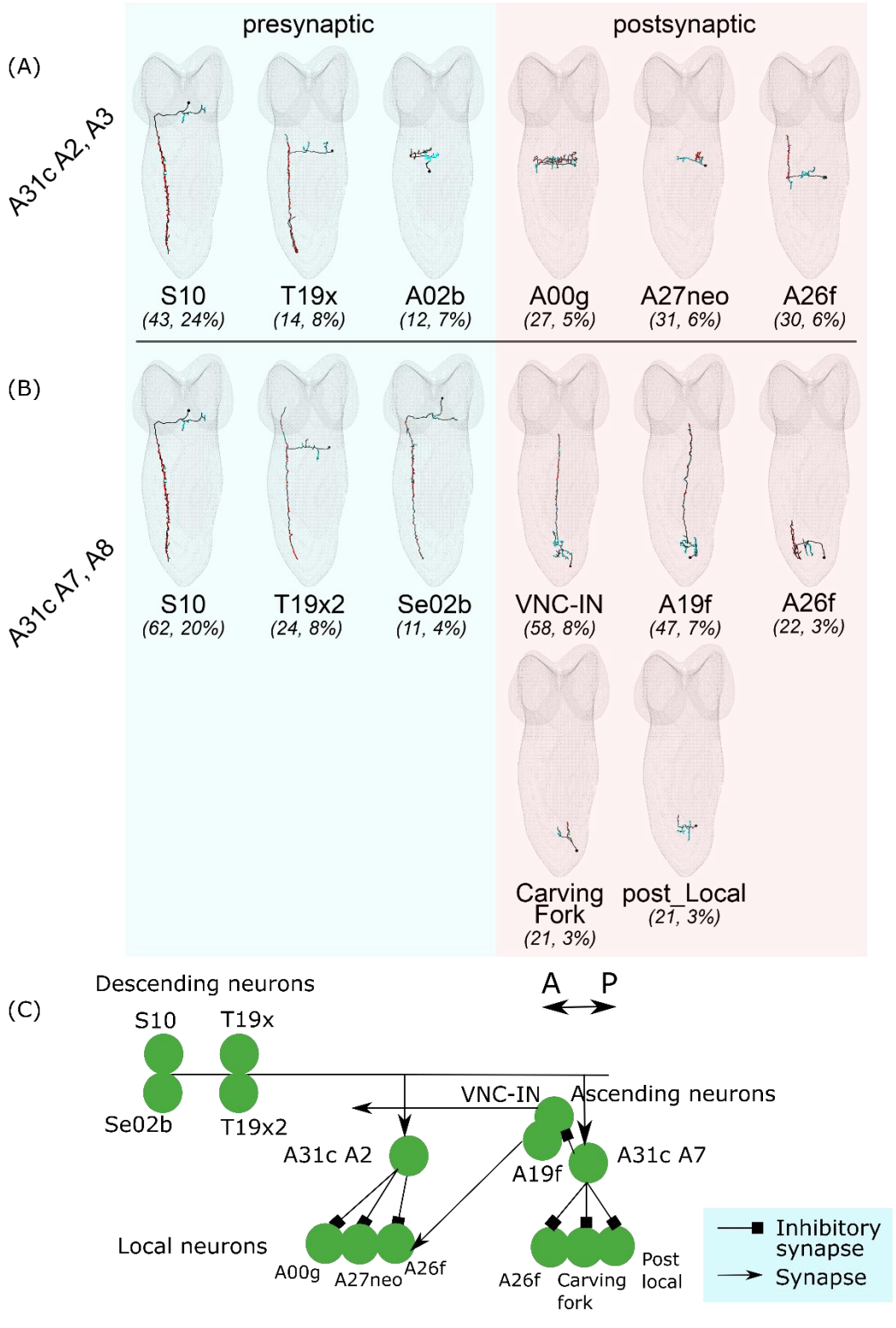
(A)
A31c A2, A3
presynaptic
postsynaptic
S10
(43, 24%)
T19x
(14, 8%)
A02b
(12, 7%)
A00g
(27, 5%)
A27neo
(31, 6%)
A26f
(30, 6%)
(B)
A31c A7, A8
S10
(62, 20%)
T19x2
(24, 8%)
Se02b
(11, 4%)
VNC-IN
(58, 8%)
A19f
(47, 7%)
A26f
(22, 3%)
Carving Fork
(21, 3%)
post_Local
(21, 3%)
(C)
Descending neurons
A P
S10
T19x
Se02b
T19x2
VNC-IN
Ascending neurons
A31c A2
A19f
A31c A7
Local neurons
A00g
A27neo
A26f
A26f
Carving fork
Post local
Inhibitory synapse
Synapse

Figure 5.3 EM reconstruction of synaptic partners of A31c neurons

(A) Reconstructed top postsynaptic partners of A31c neurons in anterior segments. **(B)** Reconstructed top postsynaptic partners of A31c neurons in posterior segments. Panels **(A-B)** are courtesies of Dr. Maarten Zwart. (C) Schematic diagram of the connectivity result from EM reconstruction.

5-2. Heterogenous activity patterns of LTM during *Drosophila* larval locomotion

Although the LTM activity is highly synchronized across abdominal segments during free crawling on the agarose plate, other activity patterns of LTM were reported during larval locomotion in previous studies. It has been shown that the LTM or the motor neurons innervating it exhibit wave-like contraction in multiple other preparations (Kohsaka et al., 2019; Pulver et al., 2015; Zarin et al., 2019; Zwart et al., 2016). First instar larvae use wave-like contraction of LTM when crawling in a linear channel (Heckscher et al., 2012). The LT muscles are contracted about the same time when the longitudinal muscles are contracted in the next segment of the moving direction (section 1-2). Other studies have confirmed the existence of the delayed wave-like activity of the LTM or the upstream motor neurons of multiple preparations, including the fictive activity of SNa motor neurons in the isolated CNS, the LTM's calcium activity of second instars contained in a cage, and the LTM's contraction in the fillet preparation (Kohsaka et al., 2019; Pulver et al., 2015; Zarin et al., 2019; Zwart et al., 2016). Zwart et al. and Kohsaka et al. have studied the neural circuits underlying the generation of the delayed recruitment of LT muscles (Kohsaka et al., 2019; Zwart et al., 2016).

Although I did not notice an apparent wave-like motor pattern in the free crawling on the agarose plate of the third instar, I did notice a wave-like contraction of the LTM when the third instar larva was tunneling in a narrow linear channel (data not shown). Under all these conditions where LTM shows wave-like activity, the wave duration of the peristaltic waves is longer (about 5 s – 20 s) than that in the free crawling (about 1 s) (Heckscher et al., 2012; Pulver et al., 2015; Zarin et al., 2019). Therefore, I assume that the motor output can be

modulated differently when larvae perform peristalses in a much lower speed range.

I assume that the lack of the wave-like pattern in the fast rhythms may be a result of the slow kinetics of the muscles. The somatic muscles of *Drosophila* larvae are assumed to be super-contractile but have slow kinetics (Peron et al., 2009). The contraction and relaxation of transverse muscles might not be fast enough to follow the wave-like rhythm. Specifically, unlike that the relaxation of longitudinal muscles can be aided by the stretching force from the contraction of longitudinal muscles of adjacent segments, the relaxation of the transverse muscles is not likely to be aided by other muscles, which could lead to longer relaxation durations.

5-3. Why regulating tail lag is an efficient strategy for speed regulation?

Our study has denoted that speed can be regulated by the tail lag by varying the contraction duration of LTM. However, the extension of tail lag seems to have a high energy cost and a low mobility performance. I considered several possible reasons for the larva to use this strategy: (1) A simpler control strategy. Separating the control of the unhooking/head extension and the wave initiation reduces the complexity of the motor control. (2) Increase the flexibility of the head and tail. The two ends can be separately moved, allowing more flexibility of the head and tail. (3) Energy efficiency. Though the separate movement of the head and tail seem to cause more energy dissipation during the contraction/extension of LTM, the total energy cost might be quite efficient. One reason is the energy cost in moving the center of mass (CoM) might be reduced. The CoM is mainly moved in the pistoning phase during the head extension and the tail contraction (Heckscher et al., 2012). With a long tail lag, the CoM can be moved slowly,

reducing the energy dissipation during the acceleration/deceleration.

5-4. Functional role of the distributed control of synchronized movement

Our findings suggest that these local interneurons are recruited for the control of the synchronous movement of LTM. What is the design principle under the distributed neural networks for synchronized control?

First, the local projection pattern of A26f neurons may allow smooth control of muscular activity across segments. A26f neurons project across multiple segments (Figure 4.1). In addition, A26f neurons are likely to have multiple axonal arbors with more presynaptic sites in the local segment than in the distant segments (Figure 4.1). I assume that this projection pattern enables a graded control of LTM across segments, which allows a smooth variation of muscular activity across segments similar to the Gaussian filter in image processing.

Second, although a centralized motor control may be enough to determine the timing of the transition from tail lag to wave phase, the synergistic muscular pattern should be regulated by the local pattern generator. As to the control of the activity of LTM, one simple hypothesis is when the wave is initiated, the pattern generator in the posterior neuromeres could dominate the control to coordinate the initiation of wave and the relaxation of the LTM. Before that, the pattern generator in the anterior neuromeres could dominate the control to coordinate the extension of the head and the contraction of LTM. As A31c neurons predominantly receive inputs from descending neurons but inhibit ascending neurons, these interneurons possibly delay the “take-over” of the control of LTM from anterior segments to the posterior segments. As those neurons are segmentally divided, their activity level can be regulated separately, which

allows finer timing control of the “take-over” in each segment.

5-5. Generation of speed-dependent locomotion patterns in pedestrian vertebrates and *Drosophila* larvae

Motor control of speed requires the modulation of muscular output to generate the desired movement of body parts. In pedestrian animals, it has been well established that the movement of limbs is mainly varied during the stance phase, while the movement during the swing phase is almost unchanged (section 1.1). It suggests that the coordination of flexor-extensor muscles is speed-dependent as the flexor muscles are mainly contracted during the swing phase while the extensor muscles are mainly contracted during the stance phase (Figure 5.4). In *Drosophila* larvae and other crawling animals, speed-dependent variations of locomotion patterns have not been well understood. Our study has first shown that the variation of the tail lag phase contributes more to the speed change similar to the stance phase while the wave phase varies less which is similar to the swing phase. Analogous to the flexor-extensor antagonists, The transverse muscles across segments as a whole function antagonist with the longitudinal muscles. The transverse muscles are mainly contracted during the tail lag phase while the longitudinal muscles are mainly contracted during the wave phase. These results suggest a shared strategy is used by the pedestrian animals and *Drosophila* larvae to change the speed by modulating the motor output of a subset of muscles corresponding to the “variable phase”, which implies the possible conservation of the neural architecture for the speed-dependent rhythm generation.

However, no experimental evidence was given about the identity of neurons that generate the speed-dependent rhythm in vertebrate pedestrian animals (Kiehn, 2016). Modeling studies have suggested a higher layer called the rhythmic generation layer generating the speed-dependent rhythm, which is above the pattern generation layer (Kiehn, 2016). The endogenous difference in the bursting of the flexor centre and that of the extensor centre of the rhythmic generating layer might explain the speed-dependent neuronal modulation (Figure 5.4). In *Drosophila* larvae, our study has identified the interneurons corresponding to the modulation of neural output to the transverse muscles, while how the coordination of the longitudinal-transverse muscles was achieved is still unknown. As the A31c neurons receive synaptic input from descending neurons in the SEG and give synaptic output to the ascending neurons in the posterior abdominal segments, these projection neurons might be used to coordinate the activity of the transverse muscles in abdominal segments and the longitudinal muscles in the head and tail (Fig 5.4). Investigating the connectivity and function of these neurons might help understand how the CNS generates the coordinated muscular patterns for different speeds.

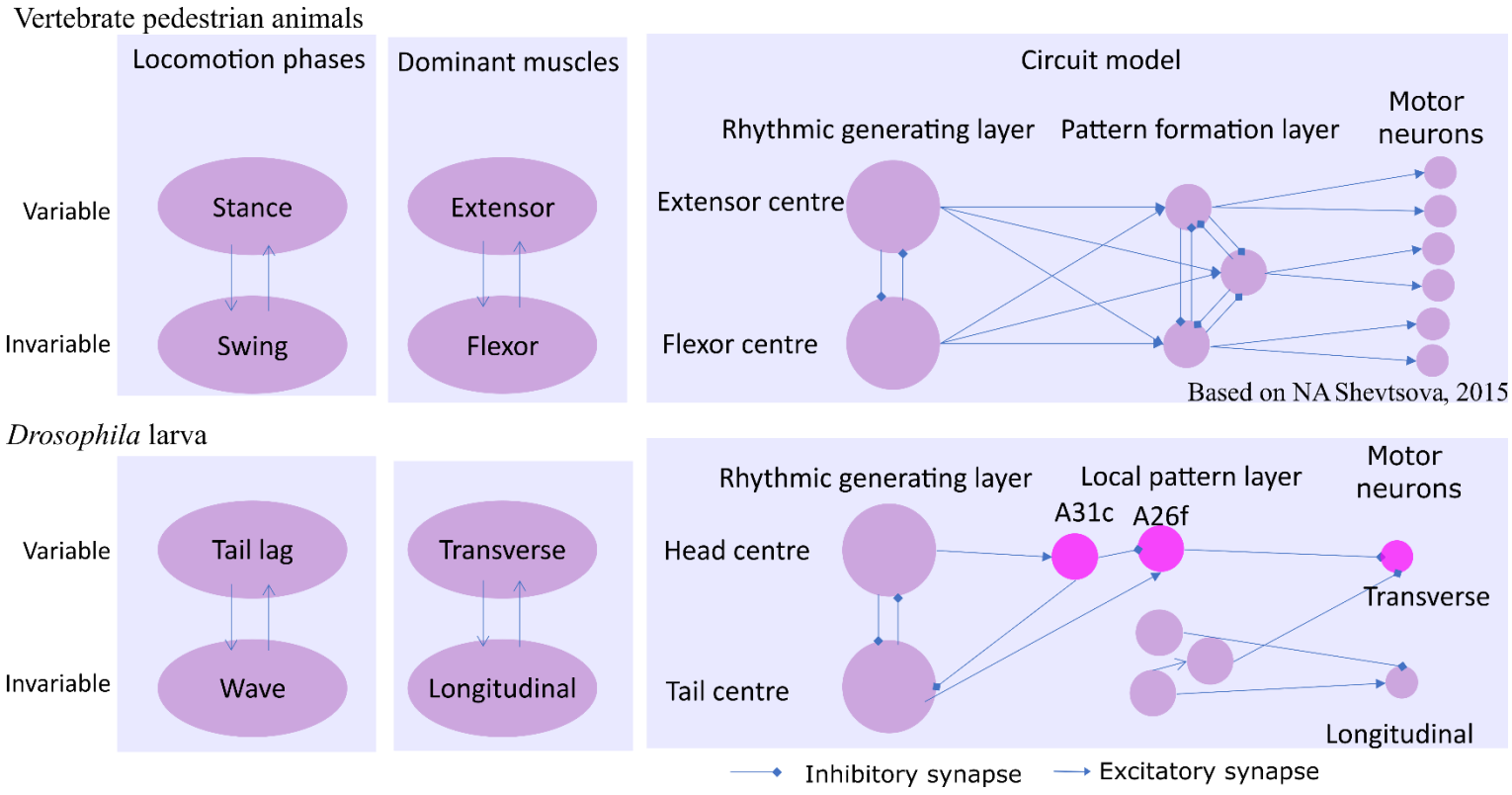
Vertebrate pedestrian animals
Locomotion phases
Dominant muscles
Circuit model
Variable
Invariable
Stance
Swing
Extensor
Flexor
Rhythmic generating layer
Pattern formation layer
Motor neurons
Extensor centre
Flexor centre
Based on NA Shevtsova, 2015
Drosophila larva
Variable
Invariable
Tail lag
Wave
Transverse
Longitudinal
Rhythmic generating layer
Local pattern layer
Motor neurons
A31c
A26f
Head centre
Tail centre
Transverse
Longitudinal
Inhibitory synapse
Excitatory synapse

Figure 5.4 Comparison of the generation of the speed-dependent pattern at the behavioral, muscular, and neuronal levels in vertebrate pedestrian animals and the *Drosophila* larvae.

The diagram of the circuit model of pedestrian animals is created based on (Shevtsova et al., 2015).

Acknowledgments

I would like to first express my most gratitude to Dr. Akinao Nose, Dr. Hiroshi Kohsaka, and Dr. Maarten Zwart who supervised me and helped accomplish this work. Many thanks to Dr. Akinao Nose for his support throughout the work. Without his generosity, I would not be able to start neuroscience research in the middle of my doctoral course. Most thanks to Dr. Hiroshi Kohsaka for his greatest support and invaluable advice. Without his guidance and supervision, I might be lost in the universe of the larval nervous system. Special thanks to Dr. Maarten Zwart, a white knight from Scotland who brought precious advice and constant encouragement. It was not a coincidence that those sparkling natural beauties turned out one by one after his engagement in our study.

I would like to thank the senior students Dr. Young-taek Yoon, Dr. Dohjin Miyamoto, Dr. Suguru Takagi, Dr. Atsuki Hiramoto, Dr. Xiangsunze Zeng, Jeonghyuk Park, Shoya Ohura, and Yuji Matsuo. I would express my gratitude to them here for their teaching and help. Thanks to those lab members Dr. Xiyang Sun, Xu Zhang, Kazushi Fukumasu, Kazuki Tomatsu, Miho Manaka, Hiroto Nakabayashi, Shinsuke Inaba, Shu Morise, Kento Kawasaki, Li Ziyuan, Date Takahisa, Komanome Yuko, Takano Shiina, Osnato Nicodemo, Hashimoto Yusaku, and Okado Yuki. I will remember the days spent with them. Thanks to Ms. Kasumi Shibahara for her assistance.

I would like to thank Dr. Seiji Kawamura who guided me to the world of curiosity and discovery.

I would like to thank Drs. Aref Arzan Zarin, Chris Doe, Eri Hasegawa, Gregory Jefferis, James Truman, and Sebastian Cachero for their communication or generous gift of invaluable resources to this study.

Finally, I would like to thank my family. They always accepted my decisions and supported me wordlessly. I dedicate this work to them.

References

Aleman-Meza B, Jung S-K, Zhong W. 2015. An automated system for quantitative analysis of Drosophila larval locomotion. *BMC Dev Biol* **15**:11.

Alexander RM. 1989. Optimization and gaits in the locomotion of vertebrates. *Physiol Rev* **69**:1199–1227.

Ampatzis K, Song J, Ausborn J, El Manira A. 2014. Separate microcircuit modules of distinct v2a interneurons and motoneurons control the speed of locomotion. *Neuron* **83**:934–943.

Ayali A, Borgmann A, Büschges A, Couzin-Fuchs E, Daun-Gruhn S, Holmes P. 2015. The comparative investigation of the stick insect and cockroach models in the study of insect locomotion. *Current Opinion in Insect Science* **12**:1–10.

Bate M, Arias AM. 1993. The development of Drosophila melanogaster. Cold Spring Harbor Laboratory Press.

Bellardita C, Kiehn O. 2015. Phenotypic characterization of speed-associated gait changes in mice reveals modular organization of locomotor networks. *Curr Biol* **25**:1426–1436.

Berni J. 2015. Genetic dissection of a regionally differentiated network for exploratory behavior in Drosophila larvae. *Curr Biol* **25**:1319–1326.

Berrigan D, Pepin DJ. 1995. How maggots move: Allometry and kinematics of crawling in larval Diptera. *J Insect Physiol* **41**:329–337.

Betley JN, Wright CVE, Kawaguchi Y, Erdélyi F, Szabó G, Jessell TM, Kaltschmidt JA. 2009. Stringent specificity in the construction of a GABAergic presynaptic inhibitory circuit. *Cell* **139**:161–174.

Brand AH, Perrimon N. 1993. Targeted gene expression as a means of altering cell fates and generating dominant phenotypes. *Development* **118**:401–415.

Burnham KP, Anderson DR. 2004. Multimodel Inference: Understanding AIC and BIC in Model Selection. *Sociol Methods Res* **33**:261–304.

Büschges A. 1995. Role of local nonspiking interneurons in the generation of rhythmic motor activity in the stick insect. *J Neurobiol* **27**:488–512.

Caldwell JC, Miller MM, Wing S, Soll DR, Eberl DF. 2003. Dynamic analysis of larval locomotion in Drosophila chordotonal organ mutants. *Proc Natl Acad Sci U S A* **100**:16053–16058.

Chen T-W, Wardill TJ, Sun Y, Pulver SR, Renninger SL, Baohan A, Schreiter ER, Kerr RA, Orger MB, Jayaraman V, Looger LL, Svoboda K, Kim DS. 2013. Ultrasensitive fluorescent proteins for imaging neuronal activity. *Nature* **499**:295–300.

Crone SA, Zhong G, Harris-Warrick R, Sharma K. 2009. In mice lacking V2a interneurons, gait depends on speed of locomotion. *J Neurosci* **29**:7098–7109.

DeAngelis BD, Zavatone-Veth JA, Clark DA. 2019. The manifold structure of limb coordination in walking Drosophila. *Elife* **8**:e46409.

Frigon A, D'Angelo G, Thibaudier Y, Hurteau M-F, Telonio A, Kuczynski V, Dambreville C. 2014. Speed-dependent modulation of phase variations on a step-by-step basis and its impact on the consistency of interlimb coordination during quadrupedal locomotion in intact adult cats. *J Neurophysiol* **111**:1885–1902.

Grillner S, Halbertsma J, Nilsson J, Thorstensson A. 1979. The adaptation to speed in human locomotion. *Brain Res* **165**:177–182.

Guarente L, Yocum RR, Gifford P. 1982. A GAL10-CYC1 hybrid yeast promoter identifies the GAL4 regulatory region as an upstream site. *Proc Natl Acad Sci U S A* **79**:7410–7414.

Han C, Jan LY, Jan Y-N. 2011. Enhancer-driven membrane markers for analysis of nonautonomous mechanisms reveal neuron–glia interactions in Drosophila. *Proc Natl Acad Sci U S A* **108**:9673–9678.

Heckscher ES, Lockery SR, Doe CQ. 2012. Characterization of Drosophila larval crawling at the level of organism, segment, and somatic body wall musculature. *J Neurosci* **32**:12460–12471.

Hooper SL. 2017. Neurobiology of Motor Control: Fundamental Concepts and New Directions. Wiley-Blackwell.

Hughes CL, Thomas JB. 2007. A sensory feedback circuit coordinates muscle activity in Drosophila. *Mol Cell Neurosci* **35**:383–396.

Inoue M, Takeuchi A, Manita S, Horigane S-I, Sakamoto M, Kawakami R, Yamaguchi K, Otomo K, Yokoyama H, Kim R, Yokoyama T, Takemoto-Kimura S, Abe M, Okamura M, Kondo Y, Quirin S, Ramakrishnan C, Imamura T, Sakimura K, Nemoto T, Kano M,

Fujii H, Deisseroth K, Kitamura K, Bito H. 2019. Rational Engineering of XCaMPs, a Multicolor GECI Suite for In Vivo Imaging of Complex Brain Circuit Dynamics. *Cell* **177**:1346-1360.e24.

Jacobson RD, Hollyday M. 1982. A behavioral and electromyographic study of walking in the chick. *J Neurophysiol* **48**:238–256.

Kiehn O. 2016. Decoding the organization of spinal circuits that control locomotion. *Nat Rev Neurosci* **17**:224–238.

Klapoetke NC, Murata Y, Kim SS, Pulver SR, Birdsey-Benson A, Cho YK, Morimoto TK, Chuong AS, Carpenter EJ, Tian Z, Wang J, Xie Y, Yan Z, Zhang Y, Chow BY, Surek B, Melkonian M, Jayaraman V, Constantine-Paton M, Wong GK-S, Boyden ES. 2014. Independent optical excitation of distinct neural populations. *Nat Methods* **11**:338–346.

Knöpfel T, Song C. 2019. Optical voltage imaging in neurons: moving from technology development to practical tool. *Nat Rev Neurosci* **20**:719–727.

Kohsaka H, Takasu E, Morimoto T, Nose A. 2014. A group of segmental premotor interneurons regulates the speed of axial locomotion in Drosophila larvae. *Curr Biol* **24**:2632–2642.

Kohsaka H, Zwart MF, Fushiki A, Fetter RD, Truman JW, Cardona A, Nose A. 2019. Regulation of forward and backward locomotion through intersegmental feedback circuits in Drosophila larvae. *Nat Commun* **10**:2654.

Koon AC, Ashley J, Barria R, DasGupta S, Brain R, Waddell S, Alkema MJ, Budnik V. 2010. Autoregulatory and paracrine control of synaptic and behavioral plasticity by octopaminergic signaling. *Nat Neurosci* **14**:190–199.

Lahiri S, Shen K, Klein M, Tang A, Kane E, Gershow M, Garrity P, Samuel ADT. 2011. Two alternating motor programs drive navigation in Drosophila larva. *PLoS One* **6**:e23180.

Lai S-L, Lee T. 2006. Genetic mosaic with dual binary transcriptional systems in Drosophila. *Nat Neurosci* **9**:703–709.

Landgraf M, Sánchez-Soriano N, Technau GM, Urban J, Prokop A. 2003. Charting the Drosophila neuropile: a strategy for the standardised characterisation of genetically amenable neurites. *Dev Biol* **260**:207–225.

Landgraf M, Thor S. 2006. Development and structure of motoneurons. *Int Rev Neurobiol* **75**:33–53.

Li H-H, Kroll JR, Lennox SM, Ogundeyi O, Jeter J, Depasquale G, Truman JW. 2014. A GAL4 driver resource for developmental and behavioral studies on the larval CNS of Drosophila. *Cell Rep* **8**:897–908.

Lin H-T, Trimmer B. 2010. Caterpillars use the substrate as their external skeleton: A behavior confirmation. *Commun Integr Biol* **3**:471–474.

Luan H, Peabody NC, Vinson CR, White BH. 2006. Refined Spatial Manipulation of Neuronal Function by Combinatorial Restriction of Transgene Expression. *Neuron* **52**:425–436.

Maes L, Abourachid A. 2013. Gait transitions and modular organization of mammal locomotion. *J Exp Biol* **216**:2257–2265.

Mantziaris C, Bockemühl T, Büschges A. 2020. Central pattern generating networks in insect locomotion. *Dev Neurobiol* **80**:16–30.

Marder E, Bucher D. 2001. Central pattern generators and the control of rhythmic movements. *Curr Biol* **11**:R986-96.

Mathis A, Mamidanna P, Cury KM, Abe T, Murthy VN, Mathis MW, Bethge M. 2018. DeepLabCut: markerless pose estimation of user-defined body parts with deep learning. *Nat Neurosci* **21**:1281–1289.

Mohammad F, Stewart JC, Ott S, Chlebikova K, Chua JY, Koh T-W, Ho J, Claridge-Chang A. 2017. Optogenetic inhibition of behavior with anion channelrhodopsins. *Nat Methods* **14**:271–274.

Monastirioti M, Gorczyca M, Rapus J, Eckert M, White K, Budnik V. 1995. Octopamine immunoreactivity in the fruit fly Drosophila melanogaster. *J Comp Neurol* **356**:275–287.

Nagel G, Szellas T, Huhn W, Kateriya S, Adeishvili N, Berthold P, Ollig D, Hegemann P, Bamberg E. 2003. Channelrhodopsin-2, a directly light-gated cation-selective membrane channel. *Proc Natl Acad Sci U S A* **100**:13940–13945.

Nakai J, Ohkura M, Imoto K. 2001. A high signal-to-noise Ca2+ probe composed of a single green fluorescent protein. *Nat Biotechnol* **19**:137–141.

Nern A, Pfeiffer BD, Rubin GM. 2015. Optimized tools for multicolor stochastic labeling reveal diverse stereotyped cell arrangements in the fly visual system. *Proc Natl Acad Sci U S A* **112**:E2967-76.

Nicolaï LJJ, Ramaekers A, Raemaekers T, Drozdzecki A, Mauss AS, Yan J, Landgraf M, Annaert W, Hassan BA. 2010. Genetically encoded dendritic marker sheds light on neuronal connectivity in Drosophila. *Proc Natl Acad Sci U S A* **107**:20553–20558.

Nirody JA, Duran LA, Johnston D, Cohen DJ. 2021. Tardigrades exhibit robust interlimb coordination across walking speeds and terrains. *Proc Natl Acad Sci U S A* **118**. doi:10.1073/pnas.2107289118

Ohyama T, Schneider-Mizell CM, Fetter RD, Aleman JV, Franconville R, Rivera-Alba M, Mensh BD, Branson KM, Simpson JH, Truman JW, Cardona A, Zlatic M. 2015. A multilevel multimodal circuit enhances action selection in Drosophila. *Nature* **520**:633–639.

Peron S, Zordan MA, Magnabosco A, Reggiani C, Megighian A. 2009. From action potential to contraction: Neural control and excitation–contraction coupling in larval muscles of Drosophila. *Comp Biochem Physiol A Mol Integr Physiol* **154**:173–183.

Pfeiffer BD, Ngo T-TB, Hibbard KL, Murphy C, Jenett A, Truman JW, Rubin GM. 2010. Refinement of tools for targeted gene expression in Drosophila. *Genetics* **186**:735–755.

Pfeiffer BD, Truman JW, Rubin GM. 2012. Using translational enhancers to increase transgene expression in Drosophila. *Proc Natl Acad Sci U S A* **109**:6626–6631.

Potter CJ, Tasic B, Russler EV, Liang L, Luo L. 2010. The Q system: a repressible binary system for transgene expression, lineage tracing, and mosaic analysis. *Cell* **141**:536–548.

Price GD, Trussell LO. 2006. Estimate of the chloride concentration in a central glutamatergic terminal: a gramicidin perforated-patch study on the calyx of Held. *J Neurosci* **26**:11432–11436.

Pulver SR, Bayley TG, Taylor AL, Berni J, Bate M, Hedwig B. 2015. Imaging fictive locomotor patterns in larval Drosophila. *J Neurophysiol* **114**:2564–2577.

Rickert C, Kunz T, Harris K-L, Whitington PM, Technau GM. 2011. Morphological characterization of the entire interneuron population reveals principles of neuromere organization in the ventral nerve cord of Drosophila. *J Neurosci* **31**:15870–15883.

Saalfeld S, Cardona A, Hartenstein V, Tomancak P. 2009. CATMAID: collaborative annotation toolkit for massive amounts of image data. *Bioinformatics* **25**:1984–1986.

Santos JG, Vömel M, Struck R, Homberg U, Nässel DR, Wegener C. 2007. Neuroarchitecture of peptidergic systems in the larval ventral ganglion of Drosophila melanogaster. *PLoS One* **2**:e695.

Schützler N, Girwert C, Hügli I, Mohana G, Roignant J-Y, Ryglewski S, Duch C. 2019. Tyramine action on motoneuron excitability and adaptable tyramine/octopamine ratios adjust Drosophila locomotion to nutritional state. *Proc Natl Acad Sci U S A* **116**:3805–3810.

Shevtsova NA, Talpalar AE, Markin SN, Harris-Warrick RM, Kiehn O, Rybak IA. 2015. Organization of left-right coordination of neuronal activity in the mammalian spinal cord: Insights from computational modelling. *J Physiol* **593**:2403–2426.

Simpson JH. 2016. Rationally subdividing the fly nervous system with versatile expression reagents. *J Neurogenet* **30**:185–194.

Sink H. 2006. Muscle Development in Drosophila. Springer, New York, NY.

Song W, Onishi M, Jan LY, Jan YN. 2007. Peripheral multidendritic sensory neurons are necessary for rhythmic locomotion behavior in Drosophila larvae. *Proc Natl Acad Sci U S A* **104**:5199–5204.

Squire LR. 2009. Encyclopedia of Neuroscience, Volume 1. Academic Press.

Takagi S, Cocanougher BT, Niki S, Miyamoto D, Kohsaka H, Kazama H, Fetter RD, Truman JW, Zlatic M, Cardona A, Nose A. 2017. Divergent Connectivity of Homologous Command-like Neurons Mediates Segment-Specific Touch Responses in Drosophila. *Neuron* **96**:1373-1387.e6.

Talay M, Richman EB, Snell NJ, Hartmann GG, Fisher JD, Sorkaç A, Santoyo JF, Chou-Freed C, Nair N, Johnson M, Szymanski JR, Barnea G. 2017. Transsynaptic Mapping of Second-Order Taste Neurons in Flies by trans-Tango. *Neuron* **96**:783-795.e4.

Talpalar AE, Kiehn O. 2010. Glutamatergic mechanisms for speed control and network operation in the rodent locomotor CpG. *Front Neural Circuits* **4**. doi:10.3389/fncir.2010.00019

Trimmer BA, Lin H-T. 2014. Bone-free: soft mechanics for adaptive locomotion. *Integr Comp Biol* **54**:1122–1135.

Vaadia RD, Li W, Voleti V, Singhania A, Hillman EMC, Grueber WB. 2019. Characterization of Proprioceptive System Dynamics in Behaving Drosophila Larvae Using High-Speed Volumetric Microscopy. *Curr Biol* **29**:935-944.e4.

Wiegert JS, Mahn M, Prigge M, Printz Y, Yizhar O. 2017. Silencing Neurons: Tools, Applications, and Experimental Constraints. *Neuron* **95**:504–529.

Wigglesworth VB. 2012. The Principles of Insect Physiology. Springer Science & Business Media.

Wilson DM. 1961. The Central Nervous Control of Flight in a Locust. *J Exp Biol* **38**:471–490.

Zarin AA, Mark B, Cardona A, Litwin-Kumar A, Doe CQ. 2019. A multilayer circuit architecture for the generation of distinct locomotor behaviors in Drosophila. *Elife* **8**. doi:10.7554/eLife.51781

Zhang YQ, Rodesch CK, Broadie K. 2002. Living synaptic vesicle marker: synaptotagmin-GFP. *Genesis* **34**:142–145.

Zwart MF, Pulver SR, Truman JW, Fushiki A, Fetter RD, Cardona A, Landgraf M. 2016. Selective Inhibition Mediates the Sequential Recruitment of Motor Pools. *Neuron* **91**:944.